Thermally Activated Delayed Fluorescence Based on Heptazine Derivatives and Its Application to Organic Light-Emitting Diodes

李, 杰

https://doi.org/10.15017/1470578

出版情報：九州大学, 2014, 博士（工学）, 課程博士
バージョン：
権利関係：全文ファイル公表済

2014

Doctor Thesis

Thermally Activated Delayed Fluorescence Based on Heptazine Derivatives and Its Application to Organic Light-Emitting Diodes

Jie Li

Department of Chemistry and Biochemistry,

Graduate School of Engineering,

Kyushu University

Table of Contents

Chapter 1

General Introduction

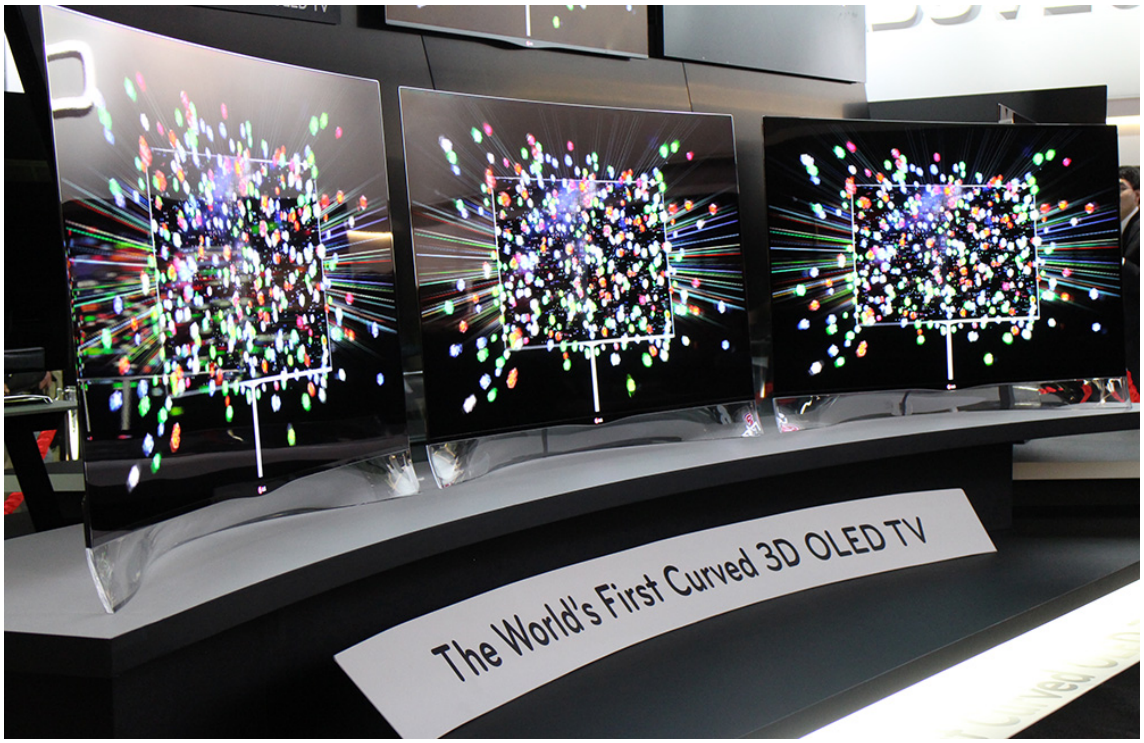

1-1. Introduction

Organic light-emitting diodes (OLEDs) have attracted tremendous interest from academia and industries over the last three decades because of their promise in next generation optoelectronic devices, especially flat-panel displays and general lighting.[1-4] As compared to liquid crystal displays (LCDs), OLEDs have a large number of merits, such as brighter and higher contrast images, self-emissive (no backlight), wider viewing angles, faster response, thinner and lighter, and potential flexible displays. However, there are still some shortcomings that need to overcome in order to kick off the large-scale commercialization of OLEDs, especially, the high cost and low efficiencies. Particularly, to obtain organic light-emitting materials with high efficiencies and low cost has been one of the most important prerequisites to achieve this goal.

Generally speaking, organic light-emitting materials for OLED applications can be classified into two categories according to the radiative decay occurring from singlet (S_1) or triplet (T_1) excited state: fluorescent and phosphorescent materials. OLEDs based on fluorescent materials usually show low efficiencies because they can only harvest singlet excitons under electrical excitation.[5-6] In contrast, phosphorescent OLEDs exhibit relatively high electroluminescence (EL) efficiencies due to sufficient utilization of both singlet and triplet excitons.[7-8] Nevertheless, phosphorescent materials usually contain transition metal complexes that greatly increase the cost and seem unsustainable. Therefore, it is necessary to develop novel organic light-emitting materials with both high efficiencies and low cost. Based on the requirement, organic light-emitting materials through triplet-triplet annihilation (TTA) and thermally activated delayed fluorescence (TADF) have been exploited to enhance the EL efficiencies of OLEDs.[9-11] However, the theoretical maximum internal quantum

efficiencies (IQEs) of OLEDs based on TTA materials are limited to 62.5%, which are not comparable with those of OLEDs employing TADF materials. Therefore, the development of highly efficient TADF materials and the study of approaches to realize TADF are of highly importance to improve the EL efficiencies and decrease the cost of OLEDs.

1-2. Organic light-emitting diodes (OLEDs)

1-2-1. History of OLEDs

Organic electroluminescence (EL) from a small-molecule material was first observed in single crystals of anthracene sandwiched between cathode and anode electrodes in the 1960s.[12-13] However, the high operating voltage (> 400 V) limited its practical application. After that, vacuum deposition technique was introduced to reduce the driving voltage.[14] Subsequently, organic EL from a polymer, poly(*N*-vinylcarbazole), (PVK) was reported.[15-16] In 1987, Tang and VanSlyke reported the first practical organic light-emitting diodes (OLEDs).[1] They introduced effective heterojunction devices based on small-molecule materials which were fabricated by thermal vacuum evaporation and gave low operating voltage (< 10 V) and attractive device efficiency (~1% photo/electron). The device structure is ITO/TAPC (50 nm)/Alq_3 (60 nm)/MgAg/Ag, where transparent indium tin oxide (ITO) is the anode, an alloy of magnesium (Mg) and silver (Ag) acts as the cathode, 1,1-bis(4-bis(4-methyl-phenyl)-amino-phenyl)-cyclohexane (TAPC) and tris(8-quinolinolato)aluminum (Alq_3) are a hole-transporting material and a light-emitting material, respectively. Subsequently, based on the Tang's report, advanced polymer OLEDs (PLEDs) were reported using poly(p-phenylenevinylene) (PPV) in 1990.[2] In contrast with vacuum deposition of small-molecule OLEDs, the polymer layers of PLEDs can be fabricated by spin-coating or other solution-casting processes.

These two reports have triggered extensive research and development of OLEDs from the standpoints of both fundamental science and practical applications. Furthermore, the groundbreaking work of development of phosphorescent materials has led to remarkable improvements in the EL efficiencies in the late 1990s and early

2000s.[3,7-8] However, phosphorescent materials usually contain rare metals inducing efficient intersystem crossing (ISC), which significantly increased the cost of OLEDs. In the late 2000s, pure organic light-emitting materials based on TTA and TADF have been developed.[9-11] In particular, TADF materials have attracted much more interest because almost 100% internal quantum efficiencies (IQEs) can be achieved. Thereafter, a large number of efficient TADF molecules have been developed, and highly efficient TADF-based OLEDs have been achieved. Consequently, TADF materials have been considered as the third-generation organic light-emitting materials to achieve high performance OLEDs.

1-2-2. Structure of OLEDs

As mentioned above, in 1987, the first practical OLEDs based on small molecules contained only two organic layers, TAPC as the hole transport layer and Alq_3 as the light-emitting and electron transport layer were reported.[1] After fast development of OLED techniques in the past several decades, the structure of advanced OLEDs has become more and more complicated because advanced device structures provide better optical and electrical performances. To attain high EL efficiencies, it is necessary to achieve efficient charge injection from both the anode and the cathode into the adjacent organic layers at low driving voltage, good charge balance, and confinement of the injected charge carriers within the emitting layer to increase the probability of the desired emissive recombination. For instance, an OLED can be composed of a substrate, an anode, a hole injection layer (HIL), a hole transport layer (HTL), an electron blocking layer (EBL), an emitting layer (EML), a hole blocking layer (HBL), an electron transport layer (ETL), an electron injection layer (EIL) and a cathode. A

schematic structure of a multilayer OLED consisting of these layers is shown in Fig. 1-1. The HIL and EIL are introduced to reduce the hole and electron injection barrier and facilitate charge injection, respectively. The insertion of HTLs and ETLs can transport charge carriers and further reduce the energy barriers by a stepwise process, resulting in efficient charge injection and charge balance. The EBL and HBL can confine the electrons and holes within the emitting layer and prevent them from escaping to the adjacent carrier transport layers. The performance of OLEDs, therefore, depends upon various materials functioning in specialized roles. Generally, materials using in OLEDs should meet the following requirements: (a) Suitable ionization potentials and electron affinities to well-match energy levels for the injection of charge carriers. (b) Be able to form smooth and uniform films. (c) Thermally stable. (d) Materials should meet further special requirements according to the roles in the device structures such as hole transport, electron transport, charge blocking and light emission.

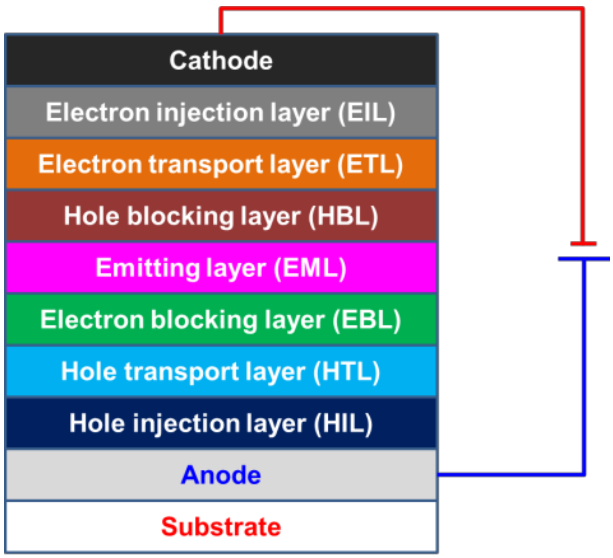

Figure 1-1. Schematic structure of a multilayer OLED.

1-2-3. Operating principle of OLEDs

OLEDs are current-driven devices that utilize emissions from the electronically excited states of molecules. The operation of OLEDs involves charge injection from the anode and the cathode into the adjacent organic layers, transport of injected charge carriers through the organic layers, recombination of holes and electrons to generate electronically excited states of molecules that are usually called excitons, followed by their radiative decay by the emission of either fluorescence or phosphorescence.

The process of carrier injection from electrodes to organic layers plays an important role in the optimization of the carrier balance in OLEDs. Hole injection takes place from the Fermi level of the anode into the highest occupied molecular orbital (HOMO) level of the adjacent organic layer, while electron injection takes place from the Fermi level of the cathode into the lowest occupied molecular orbital (LUMO) level of the adjacent organic layer. Therefore, to realize low driving voltages, it is important to reduce the barrier heights for carrier injections. Injected charge carriers are transported towards the emitting layer under an applied electric field. The carrier transport mechanism in organic layers is different from that of inorganic semiconductor materials. Inorganic semiconductor materials have energy band structures composed of valence band and conduction band, while organic semiconductor materials are comprised of molecules bounding by weak intermolecular interactions, especially Van der Waals forces. Thus, the dominant carrier transport mechanism in organic semiconductor materials is associated with charge hopping from one molecule to another, and holes and electrons correspond to the radical cations and radical anions, respectively. Under electrical excitation, holes (electrons) sequentially transport from the radical cations (anions) to the neutral molecules through HOMO (LUMO) levels for hole (electron)

transport. Subsequently, excitons formed by the recombination of holes and electrons can be at the singlet or triplet excited state, depending on how the spins of two particles combine. Statistically, 25% singlet excitons and 75% triplet excitons are formed.[17] Radiative decay of excitons results in spontaneous light emission. For fluorescent emitters, they can only harvest 25% singlet excitons, leading to low EL efficiencies. While for phosphorescent emitters, both singlet and triplet excitons can be utilized due to strong spin-orbit coupling and efficient intersystem crossing (ISC) induced by heavy atoms, leading to high EL performance.

External quantum efficiency (EQE) is the most important factor to describe the OLED performance. EQE is defined as the fraction of the number of photons escaping from the OLED to the number of injected hole-electron pairs. It is determined by several factors and can be calculated by following formula, $EQE = \gamma \cdot \eta_r \cdot \eta_{PL} \cdot \eta_{out}$, where γ is the electron/hole recombination ratio, η_r is the exciton formation ratio for radiative transitions ($\eta_r = 0.25$ for conventional fluorescent emitters), η_{PL} is fluorescence quantum efficiency of the emitting layer, and η_{out} is the light out-coupling efficiency. According to this formula, the theoretical maximum EQE should be limited to 5–7.5% for fluorescence-based OLEDs when $\gamma = 1.0$, $\eta_r = 0.25$, $\eta_{PL} = 1$ and $\eta_{out} = 0.2–0.3$, while for phosphorescence-based OLEDs, the theoretical maximum EQE can reach 20-30% because $\eta_r = 1$.

1-3. Organic light-emitting materials

Organic light-emitting materials have naturally attracted much more interest in OLEDs because they ultimately generate the light output. In many cases, an EML in OLEDs is actually a mixture of two or more materials wherein there is at least one electroluminescent emissive material in conjunction with a charge transporting host material. Such guest–host molecular systems are common in small-molecule based OLEDs whereas in polymer-based OLEDs the EML is usually composed of a single polymer thin film.

1-3-1. Fluorescent materials

The first practical organic EL was first demonstrated using a small-molecule fluorescent emitter in a vacuum thermal deposited OLED device. The octahedral complex tris(8-hydroxyquinoline)aluminum (Alq_3) was firstly used as a green fluorescent emitter.[1] After that, a large number of fluorescent emitters are developed. Green fluorescent emitters based on the Coumarin derivatives have been widely investigated, such as 10-(2-benzothiazolyl)-1,1,7,7-tetramethyl-2,3,6,7-tetrahydro-1H,5H,11H-[l]benzo-pyrano[6,7,8-ij]quinolizin-11-one) (C-545T), its methyl group substituted C-545MT and the bulky *tert*-butyl group substituted derivative C-545TB.[18] The chemical structures of C-545T, C-545MT and C-545TB are shown in Fig. 1-2. Red fluorescent emitters based on the dicyanomethylene (DCM) derivatives have been also developed such as 4-(Dicyanomethylene)-2-methyl-6-[p-(dimethylamino)styryl]-4H-pyran (DCM) and 4-(dicyanomethylene)-2-methyl-6-(julolidyl-9-enyl)-4H-pyran (DCJ) (Fig. 1-3).[5,19-20] DCM as a red light-emitting material was firstly introduced into OLEDs in 1989. The device showed high EQE of

2.3%. Interestingly, the wavelength of emission peak can change in the range of 570–620 nm at various doping concentrations. This is because high doping concentration results in more saturated red emission and low EL efficiency due to concentration quenching. Moreover, tremendous efforts have been made to investigate various kinds of blue fluorescent emitters such as di(styryl)arylene[22] and spirobifluorene derivatives (Fig. 1-4).[23-24] However, OLEDs based on fluorescent emitters usually show low EL efficiencies due to the dissipation of 75% triplet excitons under electrical excitation. Therefore, it is necessary to develop other mechanisms to enhance the utilization of triplet excitons and then increase the EL efficiencies.

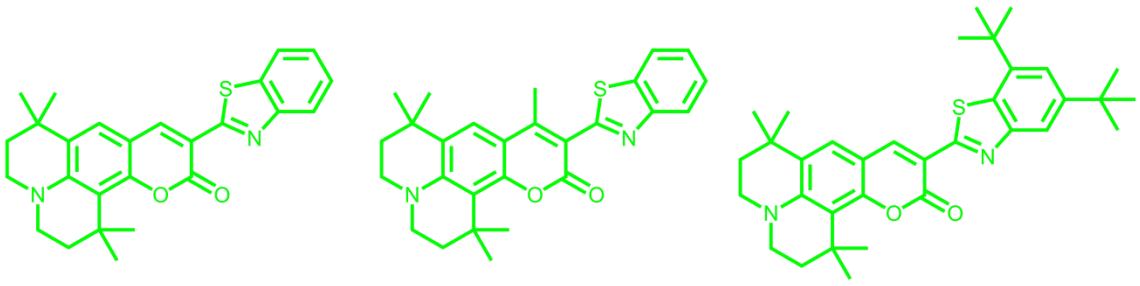

Figure 1-2. Chemical structures of C-545T, C-545MT and C-545TB as green emitters.

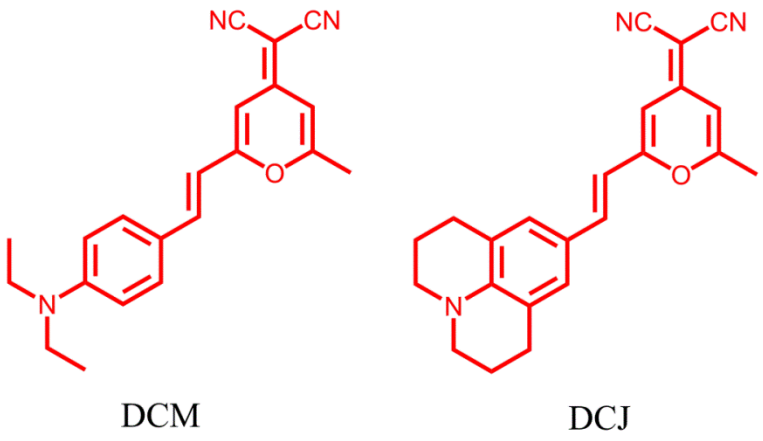

Figure 1-3. Chemical structures of DCM and DCJ as red emitters.

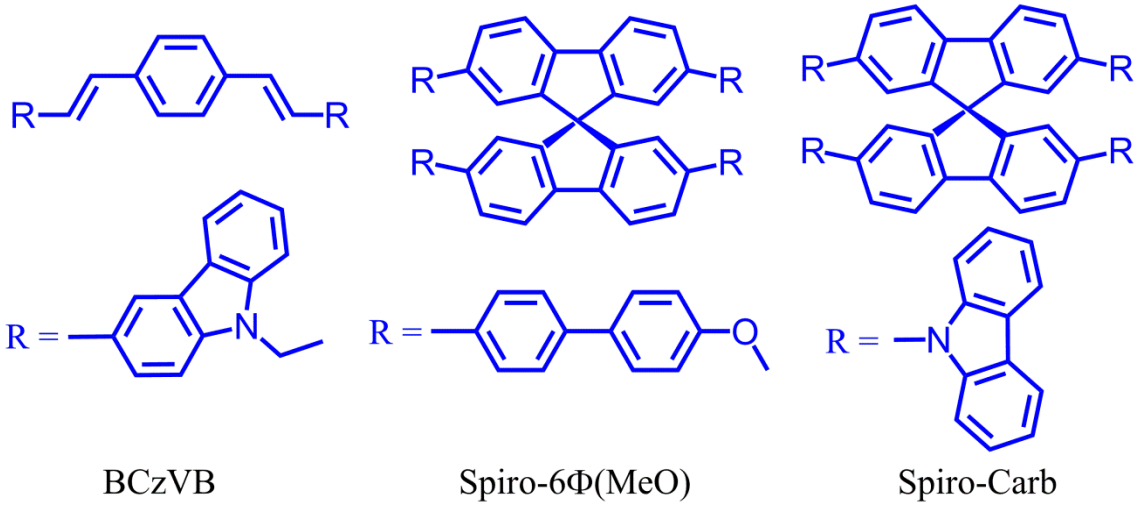

Figure 1-4. Molecular structures of several blue fluorescent emitters based on di(styryl)arylene and spirobifluorene derivatives, 1-((*E*)-2-(9-ethyl-9*H*-carbazol-3-yl)vinyl)-4-((*Z*)-2-(9-ethyl-9*H*-carbazol-3-yl)vinyl)benzene (BCzVB), 2,2',7,7'-tetrakis (4'-methoxy-[1,1'-biphenyl]-4-yl)-9,9'-spirobi[fluorene] (Spiro-6Φ(MeO)), 2,2',7,7'-tetra (9H-carbazol-9-yl)-9,9'-spirobi[fluorene] (Spiro-Carb).

1-3-2. Phosphorescent materials

As compared to fluorescent materials, the introduction of phosphorescent materials into OLEDs is a significant breakthrough in improving the EL efficiencies.[3-4,7-8,25] Since the ratio of singlet and triplet excitons formed under electrical excitation is approximately 1:3,[17] OLEDs based on phosphorescent materials can, in theory, approach 100% IQEs by harvesting both singlet and triplet excitons simultaneously through intersystem crossing (ISC), which significantly overcomes the limitation of 25% IQE of conventional fluorescent OLEDs.

Since 1998, a large number of phosphorescent emitters of transition metal complexes such as Ir(III), Pt(II), Os(II), Ru(II) and Re(I) complexes have been developed.[26-30] In particular, interest has been mainly focused on phosphorescent Ir(III) complexes

because of their rather high EL efficiencies.[31] It is worth noting that the triplet lifetime of this class of materials is very short, normally around 1–100 μs. In addition, OLEDs based on Ir(III) complexes can exhibit slow roll-off characteristics in EL efficiencies at high current densities, which should be ascribed to the reduced TTA resulting from the short triplet lifetime. Among them, the best well-known and widely investigated triplet emitters are blue iridium(III) bis(4′,6′-difluorophenylpyridinato)tetrakis(1-pyrazolyl) borate (Fir6),[32] bis[(4′,6′-difluoro phenyl)pyridinato-N,$C^{2'}$]iridium(III) picolinate (FIrpic),[33-34] green fac-tri(2-phenylpyridinato-N,$C^{2'}$)iridium(III) [$Ir(ppy)_3$],[35-36] bis(2-phenylpyridinato-N,$C^{2'}$)iridium(III) acetylacetonate [$(ppy)_2Ir(acac)$],[37] and red bis(1-phenylisoquinolinato)(acetylacetonate)iridium [$(piq)_2Ir(acac)$][38]. Their chemical structures are shown in Fig. 1-5.

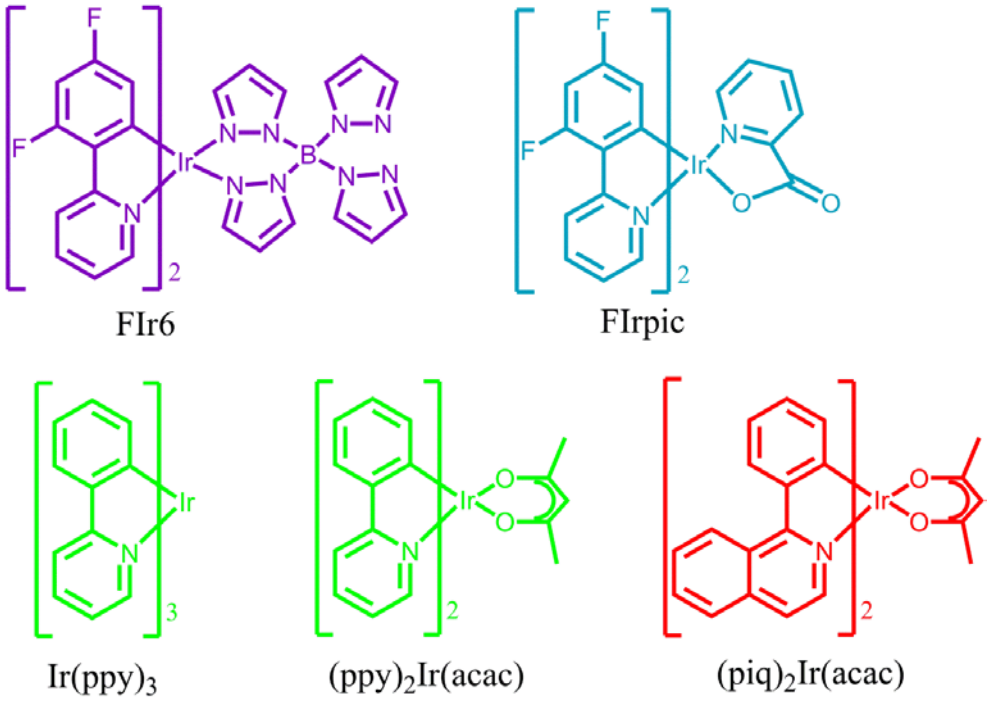

Figure 1-5. Chemical structures of Fir6, FIrpic, $Ir(ppy)_3$, $(ppy)_2Ir(acac)$ and $(piq)_2Ir(acac)$.

1-3-3. Triple-triplet annihilation (TTA) materials

Unfortunately, although OLEDs based on phosphorescent emitters have achieved high EL efficiencies, they still have some obvious disadvantages such as high cost and unsustainable due to the use of rare metals. Therefore, a novel way to develop organic light-emitting materials with both high efficiencies and low cost is significantly required. As the exciton formation ratio for radiative transitions (η_r) of conventional fluorescence-based OLEDs is limited to 0.25 since the singlet and triplet excitons are generated at a ratio of 1:3 under electrical excitation, the key strategy to improve the efficiencies of fluorescent OLEDs is to increase the utilization of triplet excitons. One possible mechanism is TTA, i.e., P-type delayed fluorescence. Schematic diagram for TTA is described in Fig. 1-6. In the TTA process, two molecules both in the triplet excited states often interact (usually upon collision) to produce one molecule in the singlet excited state and another in the ground state. Generally, the energy gap between S_0 and T_1 is larger than the energy gap between T_1 and S_1. Hence, if two triplet excitons encounter, the process might have enough energy to excite one of them to the higher singlet excited state, which can make delayed fluorescence happen in this system. In another aspect, TTA has been considered as a significant energy loss mechanism and the main reason of efficiency roll-off in OLEDs.[39] However, the additional singlet exciton production can increase the EL efficiency by 15-37.5% depending on the up-conversion mechanism.[9,40] Therefore, the maximum η_r can be increased to be 40% or 62.5%. Recently, there have been several reports on efficient TTA-based fluorescent OLEDs using anthracene derivatives.[41-46] Molecular structures of several anthracene derivatives participating in the TTA process are shown in Fig. 1-7. It has been found that delayed fluorescence induced by TTA contributes to the high EL efficiencies and anthracene

units play an important role in the TTA process.[9,40,47-49]

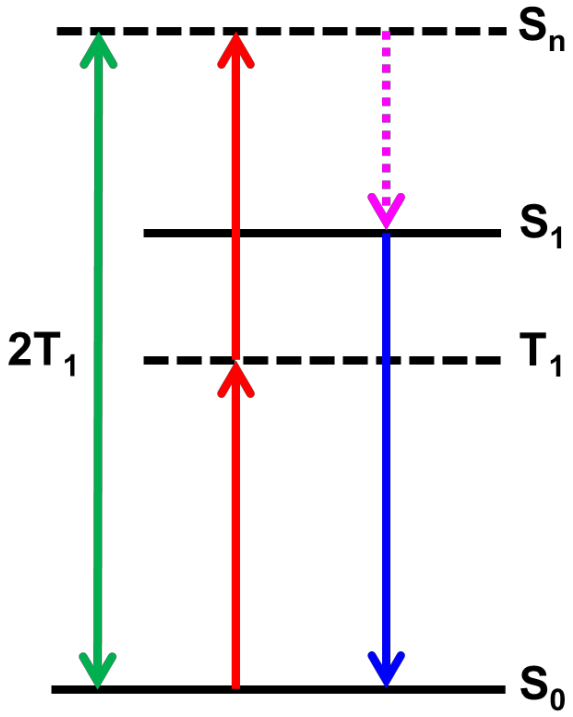

Figure 1-6. Schematic diagram for triplet-triplet annihilation.

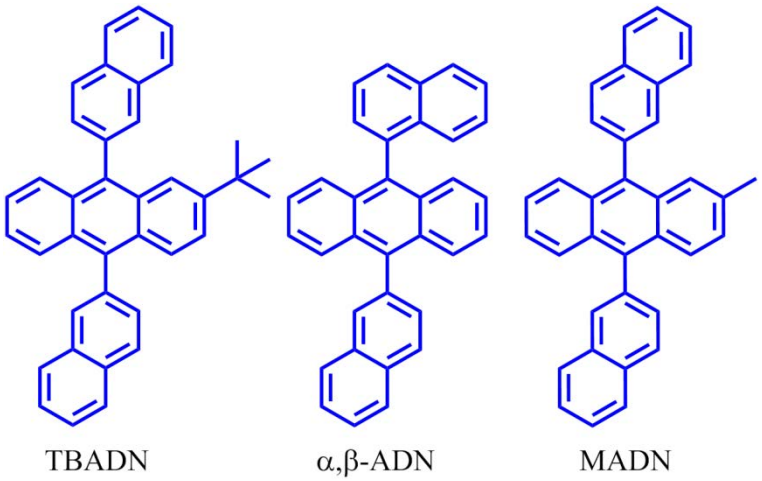

Figure 1-7. Molecular structures of several anthracene derivatives, 2-(*tert*-butyl)-9,10-di(naphthalen-2-yl)anthracene (TBADN), 9-(naphthalen-1-yl)-10-(naphthalene-2-yl)anthracene (α,β-ADN), 2-methyl-9,10-di(naphthalen-2-yl)anthracene (MADN).

1-3-4. Thermally activated delayed fluorescence (TADF) materials

Another possible mechanism to harvest triplet excitons is TADF, i.e., E-type delayed fluorescence. Schematic diagram for TADF is described in Fig. 1-8. In the TADF process, it is fairly important to design molecules with small energy differences (ΔE_{ST}) between the lowest singlet (S_1) and triplet (T_1) excited states in order to realize efficient reverse intersystem crossing (RISC) by up-converting triplet excitons from T_1 to S_1, which results in delayed fluorescence and high EL efficiencies. The ΔE_{ST} is given by $\Delta E_{ST} = E(S_1) - E(T_1) = 2J$, indicating that ΔE_{ST} is proportional to the exchange integral (J) between the spatial wave functions of the highest occupied molecular orbital (HOMO) and the lowest unoccupied molecular orbital (LUMO).[50] The first TADF molecule applied to OLEDs is based on a metal complex, tin(IV) fluoride-octaethylporphine (SnF_2-OEP),[10] which showed a very low EQE and low TADF efficiency. In 2011, the first pure organic TADF compound, 2-biphenyl-4,6-bis(12-phenylindolo(2,3-a)carbazole-11-yl)-1,3,5-triazine (PIC-TRZ), was developed.[11] PIC-TRZ showed a very small ΔE_{ST} of 0.11 eV, and the OLED incorporating this compound as an emitter exhibited a rather high EQE of 5.3%, approaching the theoretical limitation. After that, a large number of efficient TADF emitters are developed.[51-57] Molecular structures of some TADF emitters are shown in Fig. 1-9. Especially, OLEDs containing 4CzIPN showed a very high EQE of more than 19%, indicating that OLEDs based on pure organic TADF emitters are comparable to phosphorescence-based OLEDs.

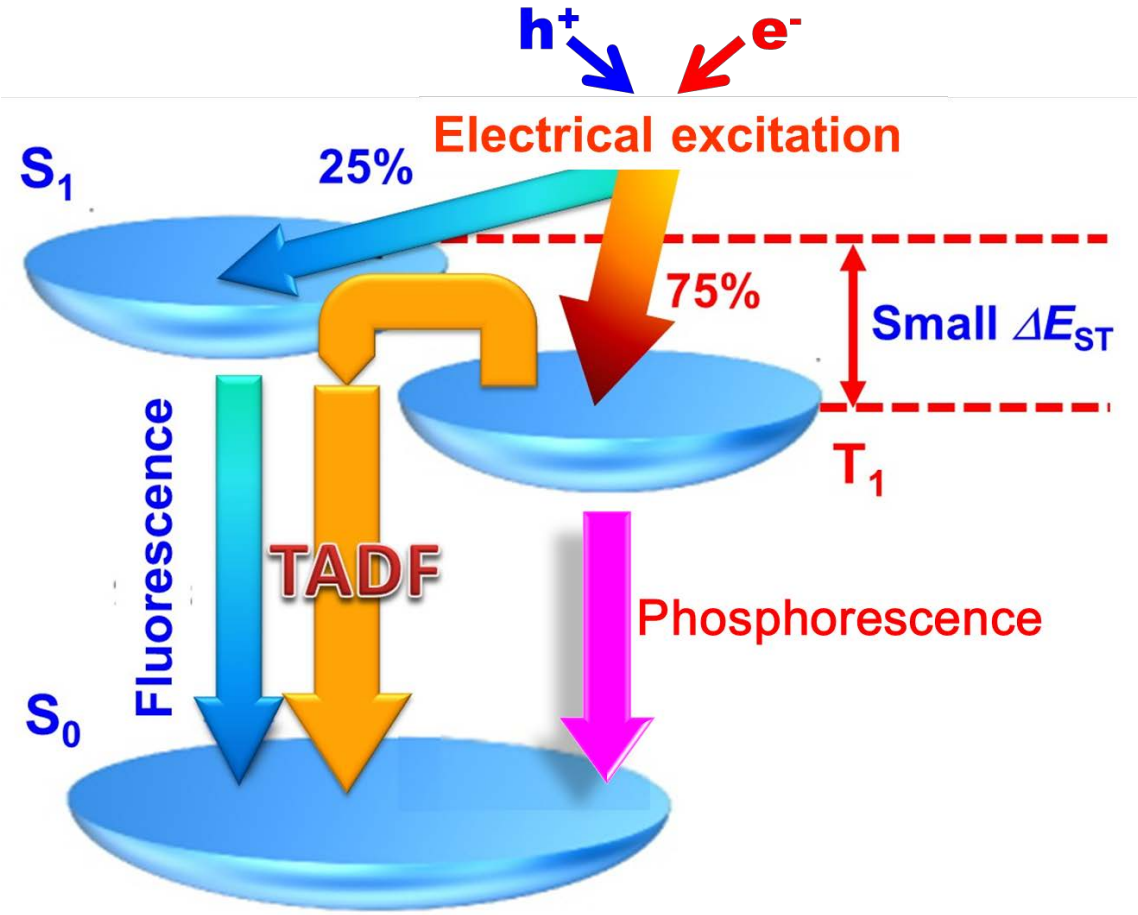

Figure 1-8. Schematic diagram for thermally activated delayed fluorescence.

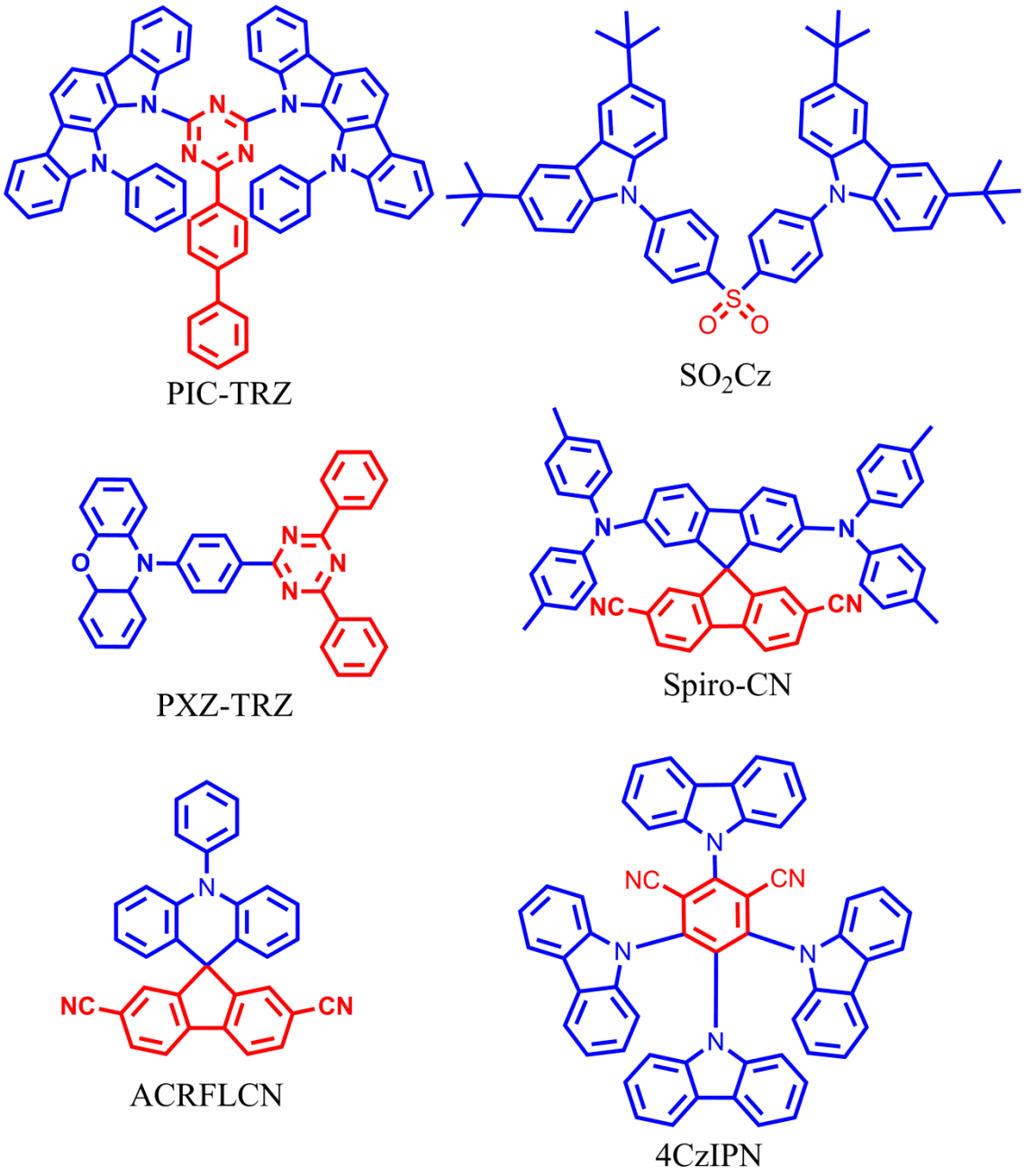

Figure 1-9. Molecular structures of some TADF emitters, 12,12'-(6-([1,1'-biphenyl]-4-yl)-1,3,5-triazine-2,4-diyl)bis(11-phenyl-11,12-dihydroindolo[2,3-*a*]carbazole) (PIC-TRZ), 9,9'-(sulfonylbis(4,1-phenylene))bis(3,6-di-*tert*-butyl-9*H*-carbazole) (SO_2Cz), 10-(4-(4,6-diphenyl-1,3,5-triazin-2-yl)phenyl)-10,10a-dihydro-4a*H*-phenoxazine (PXZ-TRZ), 2',7'-bis(di-*p*-tolylamino)-9,9'-spirobi[fluorene]-2,7-dicarbonitrile (Spiro-CN), 10-phenyl-10*H*-spiro[acridine-9,9'-fluorene]-2',7'-dicarbonitrile (ACRFLCN), 2,4,5,6-tetra(9*H*-carbazol-9-yl)isophthalonitrile (4CzIPN).

1-4. Outline

This thesis mainly focuses on the realization of thermally activated delayed fluorescence (TADF) based on the design and synthesis of new heptazine derivatives, aiming to obtain highly efficient pure organic TADF emitters and subsequently high-performance organic light-emitting diodes (OLEDs).

In Chapters 2, a dendritic heptazine derivative, 4,4',4''-(1,3,3a^1,4,6,7,9-heptaazaphenalene-2,5,8-triyl)tris(*N*,*N*-bis(4-(*tert*-butyl)phenyl)aniline) (HAP-3TPA) containing a heptazine core (HAP) as an acceptor and three 4-(*tert*-butyl)-*N*-(4-(*tert*-butyl)phenyl)-*N*- phenylaniline (TPA) units as donor units, is designed and synthesized. Photophysical properties of HAP-3TPA are carefully characterized, and TADF and relatively high photoluminescence quantum efficiencies (PLQEs) are observed in both solution and a doped fim. Subsequently, the EL performance of an OLED incorporating HAP-3TPA as an emitter is conducted. In addition, transient EL of the device is performed and EL decay mechanism is discussed.

In Chapter 3, an electron-accepting heptazine derivative, 2,5,8-tris(4-fluoro-3-methylphenyl)-1,3,4,6,7,9,9b-heptaazaphenalene (HAP-3MF) is designed and synthesized in order to realized highly efficient exciplex molecular systems. By choosing 1,3-di(9H-carbazol-9-yl)benzene (mCP) as an electron donor, exciplex systems of HAP-3MF:mCP with various weight ratios are investigated and optimized. Photophysical properties at 300 and 50 K are systematically characterized and discussed. Finally, using the exciplex-based TADF characteristics, OLEDs containing HAP-3MF:mCP with various weight ratios as emitting layers are fabricated and analyzed.

In Chapter 4, based on the theory that n-π* transitions are overlap-forbidden and tend to have a small singlet-triplet splitting, TADF from n-π* transitions based on a

heptazine derivative (HAP-3MF) is carefully characterized and analyzed by photophysical experiments and time-dependent density functional theory (TD-DFT) calculations. Finally, EL and transient EL properties of an OLED incorporating HAP-3MF as an emitter are characterized and discussed.

Finally, the contents of the thesis are summarized in Chapter 5.

1-5. References

1. C. W. Tang and S. A. Vanslyke, *Appl. Phys. Lett.* **51**, 913 (1987).
2. J. H. Burroughes, D. D. C. Bradley, A. R. Brown, R. N. Marks, K. Mackay, R. H. Friend, P. L. Burns, and A. B. Holmes, *Nature* **347**, 539 (1990).
3. M. A. Baldo, D. F. O'Brien, Y. You, A. Shoustikov, S. Sibley, M. E. Thompson, and S. R. Forrest, *Nature* **395**, 151 (1998).
4. S. Reineke, F. Lindner, G. Schwartz, N. Seidler, K. Walzer, B. Lussem, and K. Leo, *Nature* **459**, 234 (2009).
5. C. W. Tang, S. A. Vanslyke, and C. H. Chen, *J. Appl. Phys.* **65**, 3610 (1989).
6. W. C. Wu, H. C. Yeh, L. H. Chan, and C. T. Chen, *Adv. Mater.* **14**, 1072 (2002).
7. C. Adachi, M. A. Baldo, M. E. Thompson, and S. R. Forrest, *J. Appl. Phys.* **90**, 5048 (2001).
8. H. Yersin, *Highly Efficient OLEDs with Phosphorescent Materials*. (WILEY-VCH, Weinheim, 2008).
9. D. Y. Kondakov, T. D. Pawlik, T. K. Hatwar, and J. P. Spindler, *J. Appl. Phys.* **106**, 124510 (2009).
10. A. Endo, M. Ogasawara, A. Takahashi, D. Yokoyama, Y. Kato, and C. Adachi, *Adv. Mater.* **21**, 4802 (2009).
11. A. Endo, K. Sato, K. Yoshimura, T. Kai, A. Kawada, H. Miyazaki, and C. Adachi, *Appl. Phys. Lett.* **98**, 083302 (2011).
12. H. Kallmann and M. Pope, *J. Chem. Phys.* **32**, 300 (1960).
13. H. Kallmann and M. Pope, *Nature* **186**, 4718 (1960).
14. P. S. Vincett, W. A. Barlow, R. A. Hann, and G. G. Roberts, *Thin Solid Films* **94**, 171 (1982).

15. P. Mark and W. Helfrich, *J. Appl. Phys.* **33**, 205 (1962).
16. M. Pope, H. P. kallmann, and P. Magnante, *J. Chem. Phys.* **38**, 2042 (1963).
17. M. A. Baldo, D. F. O′Brien, M. E. Thompson, and S. R. Forrest, *Phys. Rev. B: Condens. Matter Mater. Phys.* **60**, 14422 (1999).
18. C. H. Chen and C. W. Tang, *Appl. Phys. Lett.* **79**, 3711 (2001).
19. C. H. Chen, K. P. Klubek, and J. Shi, *U.S. Patent* 5,908,581 (1999).
20. C. H. Chen, C. W. Tang, and J. Shi, *U.S. Patent* 5,935,720 (1999).
21. G. Schwartz, S. Reineke, T. C. Rosenow, K. Walzer, and K. Leo, *Adv. Funct. Mater.* **19**, 1319 (2009).
22. C. Hosokawa, H. Higashi, H. Nakamura, and T. Kusumoto, *Appl. Phys. Lett.* **67**, 3853 (1995).
23. J. Salbeck, N. Yu, J. Bauer, F. Weissortel, and H. Bestgen, *Synth. Met.* **91**, 209 (1997).
24. T. Spehr, R. Pudzich, T. Fuhrmann, and J. Salbeck, *Org. Electron.* **4**, 61 (2003).
25. Y. Sun, N. C. Giebink, H. Kanno, B. Ma, M. E. Thompson, and S. R. Forrest, *Nature* **440**, 908 (2006).
26. Y. Chi and P.-T. Chou, *Chem. Soc. Rev.* **39**, 638 (2010).
27. W. Y. Wong and C. L. Ho, *Coord. Chem. Rev.* **253**, 1709 (2009).
28. C. Ulbricht, B. Beyer, C. Friebe, A. Winter and U. S. Schubert, *Adv. Mater.* **21**, 4418 (2009).
29. E. Holder, B. M. W. Langeveld and U. S. Schubert, *Adv. Mater.* **17**, 1109 (2005).
30. L. Xiao, Z. Chen, B. Qu, J. Luo, S. Kong, Q. Gong, and J. Kido. *Adv. Mater.* **23**, 926 (2011).
31. F. Liang, L. Wang, D. Ma, X. Jing, and F. Wang, *Appl. Phys. Lett.* **81**, 4 (2002).

32. R. J. Holmes, B. W. D'Andrade, S. R. Forrest, X. Ren, J. Li, and M. E. Thompson, *Appl. Phys. Lett.* **83**, 3818 (2003).

33. S. J. Yeh, M. F. Wu, C. T. Chen, Y. H. Song, Y. Chi, M. H. Ho, S. F. Hsu, and C. H. Chen, *Adv. Mater.* **17**, 285 (2005).

34. M. H. Tsai, H. W. Lin, H. C. Su, T. H. Ke, C. Wu, F. C. Fang, Y. L. Liao, K. T. Wong, and C. I. Wu, *Adv. Mater.* **18**, 1216 (2006).

35. C. Adachi, M. A. Baldo, S. R. Forrest, and M. E. Thompson, *Appl. Phys. Lett.* **77**, 904 (2000).

36. M. A. Baldo, S. Lamansky, P. E. Burrows, M. E. Thompson, and S. R. Forrest, *Appl. Phys. Lett.* **75**, 4 (1999).

37. S. Lamansky, P. Djurovich, D. Murphy, F. Abdel-Razzaq, H. E. Lee, C. Adachi, P. E. Burrows, S. R. Forrest, and M. E. Thompson, *J. Am. Chem. Soc.* **123**, 4304 (2001).

38. C. L. Li, Y. J. Su, Y. T. Tao, P. T. Chou, C. H. Chien, C. C. Cheng, and R. S. Liu, *Adv. Funct. Mater.* **15**, 387 (2005).

39. M. A. Baldo, C. Adachi, and S. R. Forrest, *Phys. Rev. B* **62**, 10967 (2000).

40. D. Y. Kondakov, *J. Appl. Phys.* **102,** 114504 **(**2007**)**.

41. J. Shi and C. W. Tang, *Appl. Phys. Lett.* **80**, 3201 (2002).

42. M. T. Lee, H. H. Chen, C. H. Liao, C. H. Tsai, and C. H. Chen, *Appl. Phys. Lett.* **85**, 3301 (2004).

43. M. T. Lee, C. H. Liao, C. H. Tsai, and C. H. Chen, *Adv. Mater.* **17**, 2493 (2005).

44. Z. Q. Gao, B. X. Mi, C. H. Chen, K. W. Cheah, Y. K. Cheng, and W. S. Wen, *Appl. Phys. Lett.* **90**, 123506 (2007).

45. S. K. Kim, B. Yang, Y. Ma, J. H. Lee, and J. W. Park, *J. Mater. Chem.* **18**, 3376 (2008).
46. S. K. Kim, B. Yang, Y. I. Park, Y. Ma, J. Y. Lee, H. J. Kim, and J. Park, *Org. Electron.* **10**, 822 (2009).
47. Z. D. Popovic and H. Aziz, *J. Appl. Phys.* **98**, 013510 (2005).
48. Y. Luo and H. Aziz, *Adv. Funct. Mater.* **20**, 1285 (2010).
49. H. Fukagawa, T. Shimizu, N. ohbe, S. Tokito, K. Tokumaru, and H. Fujikake, *Org. Electron.* **13**, 1197 (2012).
50. N. J. Turro, *Modern Molecular Photochemistry*. (University Science Books, 1991).
51. K. Goushi, K. Yoshida, K. Sato, and C. Adachi, *Nat. Photon.* **6**, 253 (2012).
52. T. Nakagawa, S. Y. Ku, K. T. Wong, and C. Adachi, *Chem. Commun.* **48**, 9580 (2012).
53. G. Méhes, H. Nomura, Q. Zhang, T. Nakagawa, and C. Adachi, *Angew. Chem. Int. Ed.* **51**, 11311 (2012).
54. Q. Zhang, J. Li, K. Shizu, S. P. Huang, S. Hirata, H. Miyazaki, and C. Adachi, *J. Am. Chem. Soc.* **134**, 14706 (2012).
55. H. Uoyama, K. Goushi, K. Shizu, H. Nomura, and C. Adachi, *Nature* **492**, 234 (2012).
56. J. Li, T. Nakagawa, J. MacDonald, Q. Zhang, H. Nomura, H. Miyazaki, and C. Adachi, *Adv. Mater.* **25**, 3319 (2013).
57. Q. Zhang, B. Li, S. P. Huang, H. Nomura, H. Tanaka, and C. Adachi, *Nat. Photon.* **8**, 326 (2014).

Chapter 2

Highly Efficient Organic Light-Emitting Diode Based on a Hidden Thermally Activated Delayed Fluorescence Channel in a Heptazine Derivative

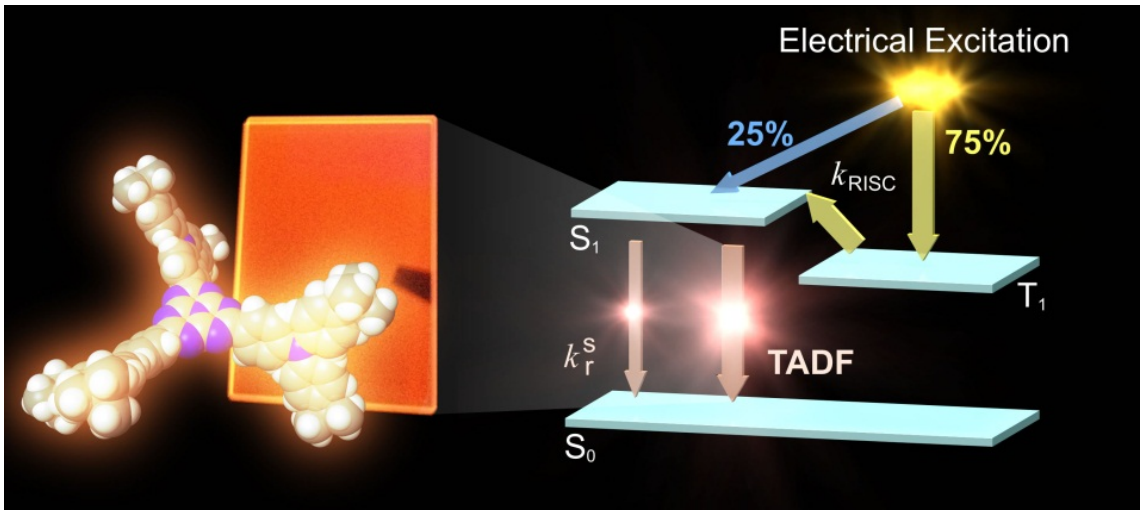

J. Li, T. Nakagawa, J. MacDonald, Q. Zhang, H. Nomura, H. Miyazaki, and C. Adachi. *Adv. Mater.* 2013, **25**, 3319.

2-1. Introduction

Considerable progress in organic light-emitting diodes (OLEDs) has triggered intensive effort to develop efficient solid-state EL materials over the past two decades. Among the many classes of materials being investigated, transition metal complexes are highly attractive because phosphorescent OLEDs containing Ir (III), Pt (II) and Os (II) complexes exhibit very high external quantum efficiencies (EQEs).[1-3] This is because such complexes effectively harvest triplet excitons, so their efficiencies are four times higher than that of conventional fluorescent OLEDs. However, phosphorescent OLEDs containing transition metal-based compounds are rather expensive and unsustainable because they contain rare metals. While OLEDs containing Cu (I) complexes that exhibit high EQEs comparable to those with transition metal complexes have been examined as an alternative, the relatively low reliability and high driving voltage of such OLEDs are fundamental problems.[4] Therefore, a novel way to realize high EL efficiency is required. Although fluorescent OLEDs have been assumed to show limited efficiency because of the branching ratio of singlet and triplet excitons of 1:3, the most recent fluorescence-based OLEDs have overcome this limitation using TTA and TADF.[5-7] In particular, we have developed promising blue, green and yellow TADF materials.[8-13] However, the design of efficient orange or red emitters is inherently difficult because the PLQEs tend to decrease as the emission wavelength increases according to the energy gap law.[14]

In this study, we designed and synthesized an efficient orange-red TADF emitter, 4,4',4''-(1,3,4,6,7,9,9b-heptaazaphenalene-2,5,8-triyl)tris(*N*,*N*-bis(4-(*tert*-butyl)phenyl)aniline) (**HAP-3TPA**). An orange-red OLED incorporating **HAP-3TPA** exhibits high EL performance with a maximum EQE of 17.5%, a maximum power efficiency

of 22.1 lm W^{-1}, a maximum current efficiency of 25.9 cd A^{-1}, a turn-on voltage of 4.4 V at a luminance of 100 cd m^{-2}, and a peak luminance of 17000 cd m^{-2} without any light out-coupling enhancement. Furthermore, even though **HAP-3TPA** showed weak TADF in both solution and a doped film, a significant delayed fluorescence was demonstrated in transient EL.

2-2. Molecular design, synthesis and characterization

2-2-1. Molecular design

An effective separation of electron densities of the highest occupied molecular orbital (HOMO) and the lowest unoccupied molecular orbital (LUMO) in a single molecule is essential for realization of a small energy gap (ΔE_{ST}) between the lowest singlet state (S_1) and lowest triplet state (T_1) and induces charge transfer transition. To realize the effective separation, a heptazine (**HAP**) core, which has a planar and rigid heterocyclic system of six C=N bonds surrounding a central sp^2-hybridised N-atom, was selected to be a strong electron acceptor. Three 4-(*tert*-butyl)-*N*-(4-(*tert*-butyl)phenyl)-*N*-phenylaniline (**TPA**) units were chosen to be strong electron donors. Especially, *tert*-butyl groups in the **TPA** units were introduced to increase the electron donating ability, and meanwhile maintain a certain distance between adjacent molecules in order to suppress the excimer formation. The molecular structure of **HAP-3TPA** with the HOMO and LUMO are depicted in Fig. 2-1. The HOMO of **HAP-3TPA** is mainly distributed on the **TPA** units, whereas the LUMO is mostly localized over the **HAP** core. The small overlap between the HOMO and LUMO leads to a small ΔE_{ST} of 0.27 eV calculated at the B3LYP/6-31G(d) level using time-dependent density functional theory (TD-DFT).[15]

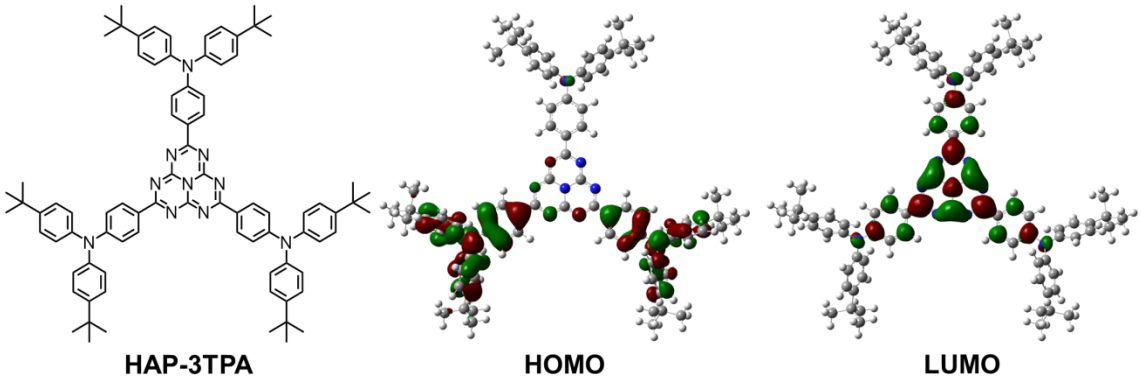

Figure 2-1. Molecular structure of **HAP-3TPA** and the distribution of electron density in its HOMO and LUMO calculated at the B3LYP/6-31G(d) level.

Details of the quantum chemical calculations by TD-DFT are as follows,

Excitation energies and oscillator strengths for **HAP-3TPA**:

Excited State 1: Triplet-A 2.1443 eV 578.21 nm f=0.0000 <S**2>=2.000

330 -> 334 -0.11900

331 -> 333 0.13959

331 -> 334 0.10828

332 -> 333 0.63868

332 -> 335 0.10688

Excited State 2: Triplet-A 2.1461 eV 577.73 nm f=0.0000 <S**2>=2.000

330 -> 335 -0.12191

331 -> 333 0.63854

332 -> 333 -0.13972

332 -> 334 0.10802

Excited State 3: Triplet-A 2.1966 eV 564.43 nm f=0.0000 <S**2>=2.000

330 -> 333 0.63633

331 -> 334 -0.14479

331 -> 335 -0.12370

332 -> 334 -0.11721

332 -> 335 0.14089

Excited State 4: Singlet-A 2.4226 eV 511.78 nm f=0.8267 <S**2>=0.000

332 -> 333 0.70303

Excited State 5: Singlet-A 2.4253 eV 511.22 nm f=0.8272 <S**2>=0.000

331 -> 333 0.70299

Excited State 6: Singlet-A 2.6476 eV 468.29 nm f=0.0001 <S**2>=0.000

330 -> 333 0.69766

Excited State 7: Triplet-A 2.6826 eV 462.18 nm f=0.0000 <S**2>=2.000

329 -> 333 0.69874

Excited State 8: Singlet-A 2.8316 eV 437.86 nm f=0.0000 <S**2>=0.000

329 -> 333 0.69144

Excited State 9: Triplet-A 2.8692 eV 432.13 nm f=0.0000 <S**2>=2.000

330 -> 333 -0.29633

331 -> 334 -0.31856

331 -> 335 -0.26805

332 -> 334 -0.27903

332 -> 335 0.32987

Excited State 10: Triplet-A 2.9249 eV 423.90 nm f=0.0000 <S**2>=2.000

330 -> 334 -0.21495

330 -> 335 0.23001

331 -> 334 0.36026

331 -> 335	-0.10926
332 -> 333	-0.25009
332 -> 334	0.10824
332 -> 335	0.35339

2-2-2. Molecular synthesis and characterization

All reactions were carried out under N_2 atmosphere. ^{1}H NMR and ^{13}C NMR spectra were recorded in $CDCl_3$ using an Avance III 500 spectrometer (Bruker Biospin, Germany) operating at 500 MHz for ^{1}H NMR and 125 MHz for ^{13}C NMR experiments. Matrix-assisted laser desorption/ionization time-of-flight (MALDI-TOF) mass spectra were obtained on an Autoflex III spectrometer (Bruker Daltonics, Germany) in reflection/positive mode with dithranol as a matrix. Elemental analysis was performed on an MT-5 CHN analyzer (Yanaco, Japan). Spectral grade solvents and starting materials were purchased from commercial sources, and used without further purification. 26mCPy was synthesized following a procedure described previously,[16] and was further purified by sublimation after recrystallization from dichloromethane/methanol.

The synthetic pathway of **HAP-3TPA** is shown in Scheme 2-1.

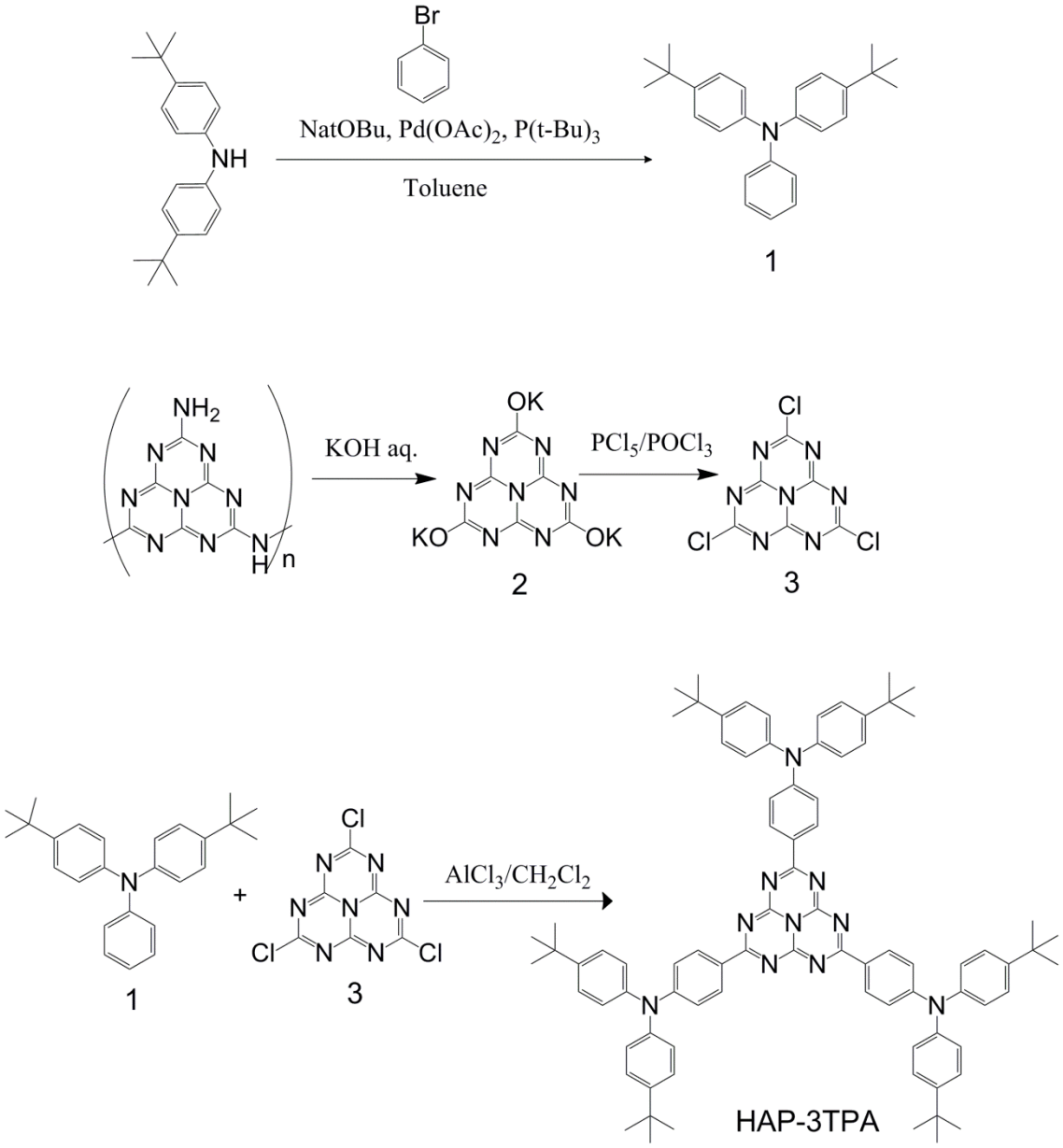

Scheme 2-1. Synthetic route of **HAP-3TPA**.

Synthesis of 4-(*tert*-butyl)-*N*-(4-(*tert*-butyl)phenyl)-*N*-phenylaniline (1): Bromobenzene (6.44 g, 41mmol) and sodium *tert*-butoxide (4.73 g, 49.2 mmol) were added to a solution of bis(4-(*tert*-butyl)phenyl)amine (11.54 g, 41 mmol) in dry toluene (60 mL). After the solution was stirred at room temperature for 30 min, palladium(II) acetate (230 mg, 1.0 mmol) and a solution of tri-*tert*-butylphosphine (829.5 mg, 4.1

mmol) in dry toluene (4.1 mL) were added. The mixture was stirred under reflux at 110 °C for 10 h. The cooled mixture was extracted with toluene, and then washed with water. The organic layer was dried over $MgSO_4$, filtered and then evaporated. The residue was purified by column chromatography (eluent: hexane) to give 4-(*tert*-butyl)-*N*-(4-(*tert*-butyl)phenyl)-*N*-phenylaniline (9.36 g, yield: 64%). ^{1}H NMR (500 MHz, $CDCl_3$) δ[ppm] = 1.31 (s, 18H), 6.94 (t, *J* = 7.5 Hz, 1H), 7.00 (d, *J* = 8.5 Hz, 4H), 7.06 (dd, *J* = 8.5 Hz, 1.0 Hz, 2H), 7.19-7.25 (m, 6H). ^{13}C NMR (125 MHz, $CDCl_3$) δ[ppm] = 31.45, 34.26, 121.88, 123.40, 123.77, 125.96, 129.01, 145.20, 145.45, 148.20. MALDI-TOF MS (*m/z*): calcd for $C_{26}H_{31}N$, 357.25; found: 357.11. Anal. calcd for $C_{26}H_{31}N$: C, 87.34; H, 8.74; N, 3.92; found: C, 87.09; H, 8.68; N, 3.87.

Synthesis of potassium 1,3,4,6,7,9,9b-heptaazaphenalene-2,5,8-tris(olate) (2): Melon powder (5.0 g) was added to an aqueous KOH solution (50 mL of a 3 mol/L solution, 0.15 mol) and then the mixture was heated at 100 °C for 6 h under reflux. The remaining solid materials were recovered by filtering the mixture rapidly through a Buchner funnel. The filtrate was cooled at 0 °C for 6 h. The resulting crystals were collected and washed three times with cold ethanol. Colorless prisms were obtained (7.0 g, yield: 90%).

Synthesis of 2,5,8-trichloro-1,3,4,6,7,9,9b-heptaazaphenalene (3): A mixture of potassium 1,3,4,6,7,9,9b-heptaazaphenalene-2,5,8-tris(olate) (3.87 g, 11.5 mmol) and PCl_5 (8.64 g, 41.5 mmol) in $POCl_3$ (70 mL) was heated at 110 °C under reflux for 6 h. The mixture was cooled to room temperature and then concentrated. Cold H_2O (50 mL) was added to the residue and the resulting suspension was stirred for few minutes and then quickly filtered under reduced pressure. The yellow residue was washed with cold H_2O and dried briefly under reduced pressure. The yellow residue was further dried by

pressing the solid between filter papers and then placed in a desiccator under reduced pressure for 24 h. Potassium 1,3,4,6,7,9,9b-heptaazaphenalene-2,5,8-tris(olate) was obtained as a yellow solid which was used without further purification (2.50 g, yield: 78%).

Synthesis of HAP-3TPA: $AlCl_3$ (3.86 g, 28.9 mmol) was added to a solution of 4-(*tert*-butyl)-*N*-(4-(*tert*-butyl)phenyl)-*N*-phenylaniline (10.35 g, 28.9 mmol) in CH_2Cl_2 (240 mL) at 0 °C for 30 min. Subsequently, 2,5,8-trichloro-1,3,4,6,7,9,9b-heptaazaphenalene (2.0 g, 7.23 mmol) was added and the reaction mixture was allowed to warm to room temperature and then stirred for 48 h. The reaction mixture was quenched with H_2O (50 mL), NaOH (3.2 g, 80 mmol) was added and then the reaction mixture was stirred for 6 h. The reaction mixture was extracted with $H_2O/CHCl_3$. The organic layer was separated, washed with saturated brine, dried over $MgSO_4$, filtered and concentrated *in vacuo*. The residue was further purified by column chromatography (eluent: toluene/hexane = 1:1, then 2:1) and sublimated to give **HAP-3TPA** (1.0 g, yield: 12%) as an orange solid. ^{1}H NMR (500 MHz, $CDCl_3$) δ [ppm] = 1.34 (s, 9H), 6.94 (d, J = 10.0 Hz, 1H), 7.11 (d, J = 5.0 Hz, 2H), 7.34 (d, J = 5.0 Hz, 2H), 8.36 (d, J = 5.0 Hz, 1H) (Fig. 2-2). ^{13}C NMR (125 MHz, $CDCl_3$) δ [ppm] = 31.41, 34.50, 118.21, 125.36, 125.94, 126.47, 132.11, 143.36, 148.05, 153.61, 157.22, 173.26 (Fig. 2-3). MALDI-TOF MS (*m/z*): calcd for $C_{84}H_{90}N_{10}$, 1238.73; found: 1239.85 (Fig. 2-4). Anal. calcd for $C_{84}H_{90}N_{10}$: C, 81.38; H, 7.32; N, 11.30; found: C, 81.31; H, 7.22; N, 11.42.

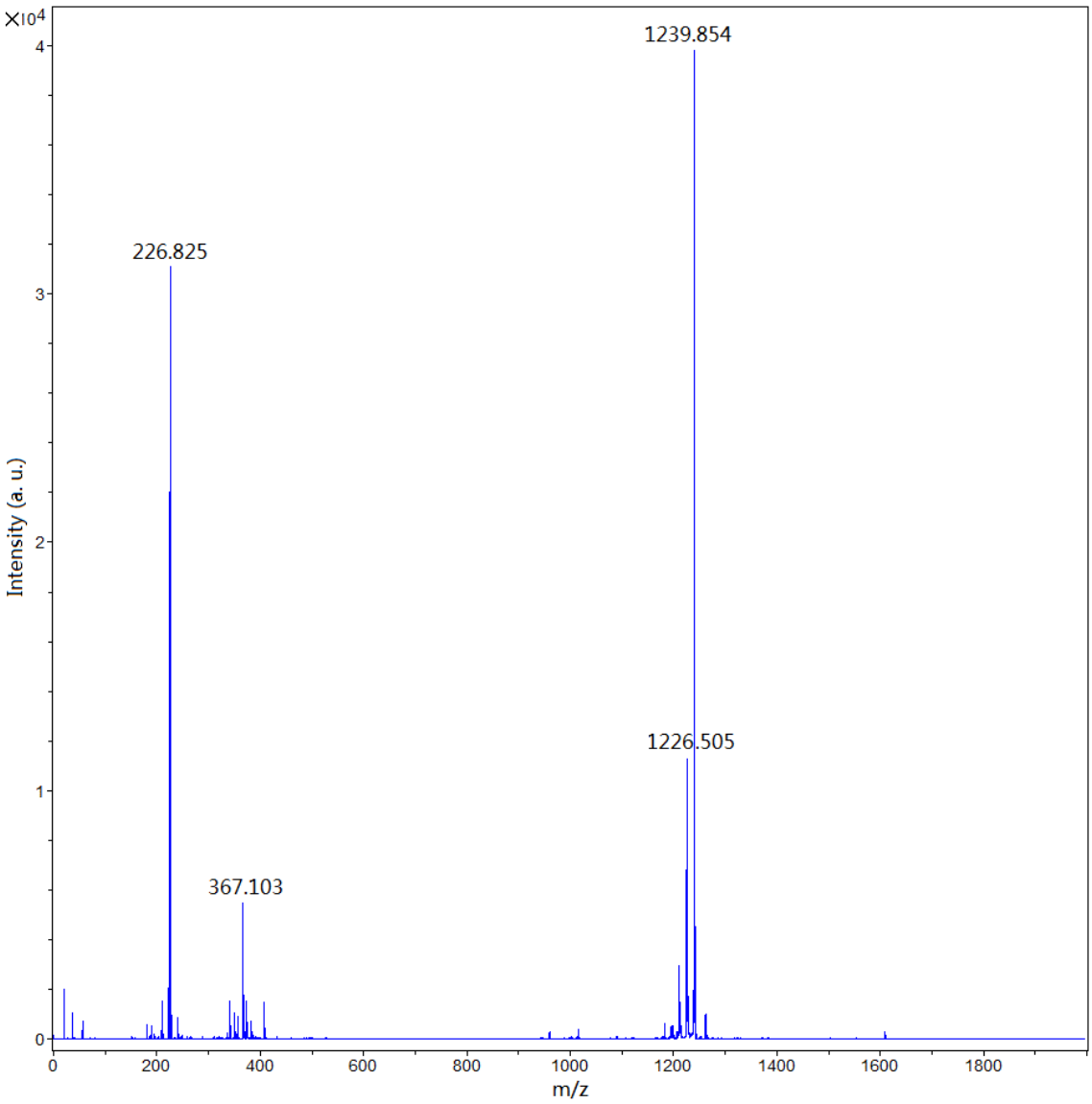

Figure 2-2. MALDI-TOF mass spectrum of **HAP-3TPA**.

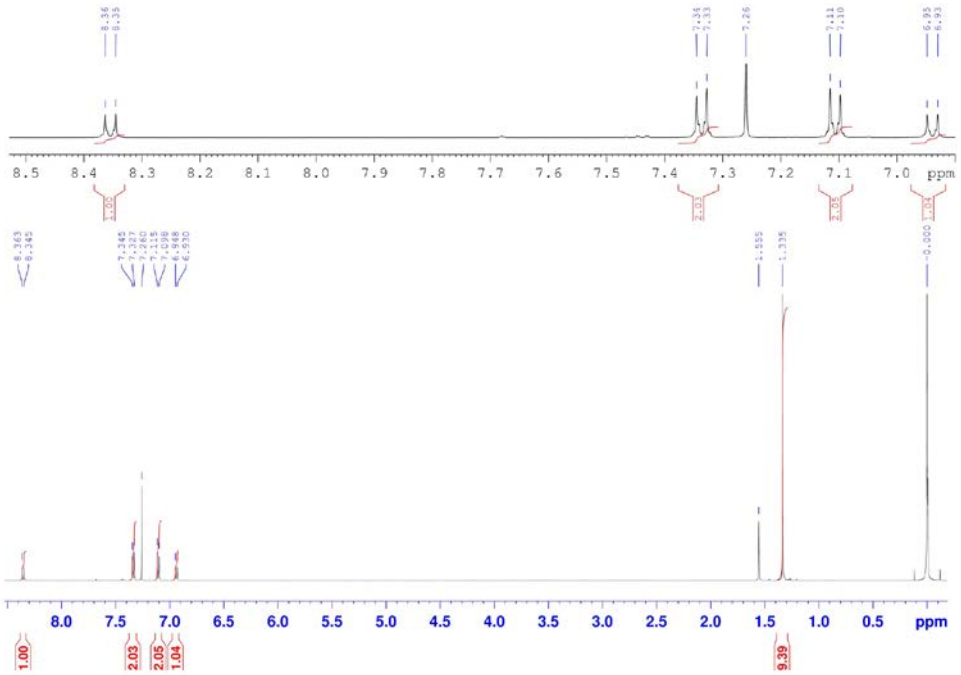

Figure 2-3. ^{1}H NMR spectrum of **HAP-3TPA**.

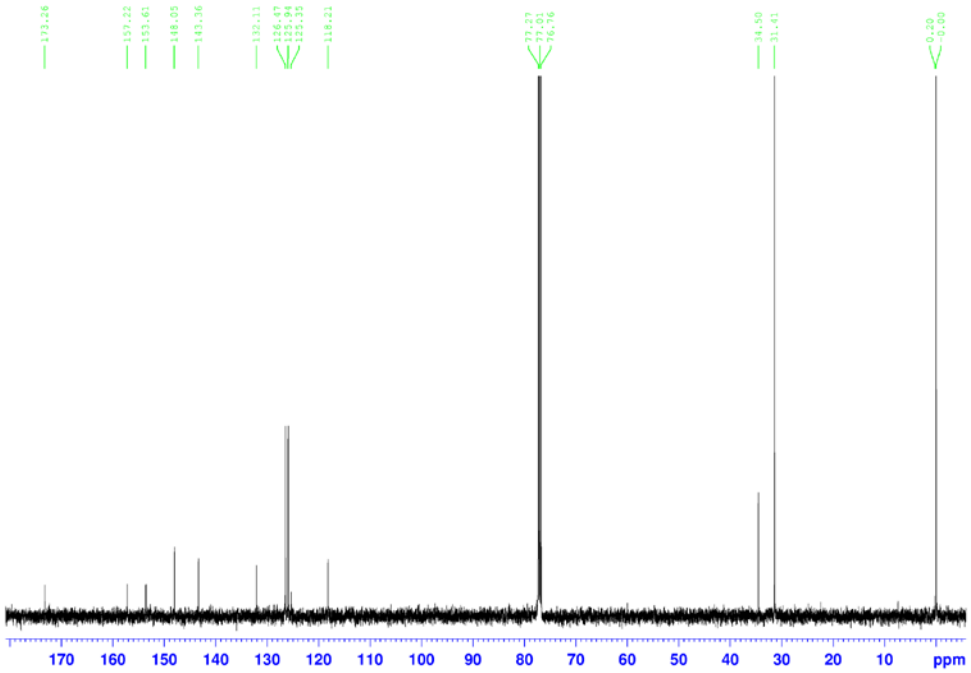

Figure 2-4. ^{13}C NMR spectrum of **HAP-3TPA**.

2-3. Experimental

2-3-1. Optical characterization

Sample solutions (1×10^{-4} mol l^{-1}) were degassed with N_2 for 15 min prior to use unless otherwise indicated. Pure and doped films (100 nm) were deposited on quartz and silicon substrates by vacuum thermal evaporation at a pressure lower than 4×10^{-4} Pa. Absorption spectra were measured with a UV-visible spectrophotometer (UV-2550, Shimadzu, Japan) in the range of 200–800 nm. PL spectra were recorded using a JASCO FP-6500 spectrofluorometer containing a liquid N_2 attachment. The transient PL decay characteristics of solution and film samples were measured with a Quantaurus-Tau fluorescence lifetime measurement system (C11367-03, Hamamatsu Photonics Co., Japan). The short lifetime range (from 50 ns to 50 μs) was measured using the TCC900 mode in conjunction with an LED excitation source, while the long lifetime range (from 400 μs to 10 ms) was measured using the M9003-01 mode in conjunction with a flash lamp source. Transient PL decay characteristics of film samples were measured under vacuum conditions on a streak camera (C4334, Hamamatsu Photonics Co., Japan) equipped with a cryostat using a Nd:YAG laser with an excitation wavelength of 355 nm. PLQE was measured using an integrating sphere (C9920-02, Hamamatsu Photonics Co., Japan) with a Xe lamp as the excitation source and a multichannel spectrometer (Hamamatsu PMA-11) as the optical detector. The highest occupied molecular orbital (HOMO) energy level of **HAP-3TPA** was determined by atmospheric ultraviolet photoelectron spectroscopy (AC-3E, Riken Keiki, Japan). The lowest unoccupied molecular orbital (LUMO) level was calculated by subtracting the energy gap from the HOMO level.

2-3-2. OLED fabrication and measurements

OLEDs were fabricated by vacuum thermal evaporation under a pressure lower than 4 $\times 10^{-4}$ Pa. OLEDs were prepared on a glass substrate precoated with a 150 nm-thick ITO layer. Prior to the deposition of the organic layers, the substrate was cleaned with ultra-purified water and organic solvents, and then treated with UV-ozone for 15 min. A 60 nm-thick α-NPD layer was then deposited on the substrates as a hole transport layer. Subsequently, a 6 wt% **HAP-3TPA**:26mCPy doped film was evaporated to form a 20 nm-thick emitting layer, and then a 40 nm-thick Bphen layer was deposited as an electron transport layer. Finally, the cathode was fabricated by thermal co-evaporation of a 100 nm-thick Mg:Ag layer with a ratio of 10:1, followed by a 20 nm-thick Ag layer. The intersection of ITO and the metal electrodes gave an active device area of 4 mm^2. For the measurement of EL characteristics, the devices were measured in air condition without any encapsulation and light out-coupling enhancement. The current density-voltage-luminance characteristics of the OLEDs were measured using a semiconductor parameter analyzer (E5270, Agilent, FL USA) with an optical power meter (model 1930, Newport, CA, USA). EL spectra were obtained using a spectrometer (USB2000, Ocean Optics, FL, USA). For the transient EL characteristics, the devices were encapsulated under nitrogen atmosphere using UV-epoxy resin and a glass cover, and measured under an electrical pulse excitation in combination with a streak camera (C4334, Hamamatsu Photonics Co., Japan).

2-3-3. Quantum chemical calculation

All calculations were performed using the Gaussian 09 program package. The HOMO and LUMO of **HAP-3TPA** were calculated using the nonlocal density functional of Becke's 3-parameters employing Lee-Yang-Parr functional (B3LYP) with 6-31G(d) basis sets. The S_1 and T_1 of **HAP-3TPA** were calculated by the time-dependent density functional theory (TD-DFT) method at the optimized ground-state geometries using the B3LYP mode with a 6-31G (d) basis set.

2-4. Optical properties

2-4-1. Neat film

The HOMO and LUMO levels of **HAP-3TPA** were estimated to be 5.6 and 3.4 eV, respectively, according to ultraviolet photoelectron spectroscopy and UV-vis absorption spectrum (Fig. 2-5).

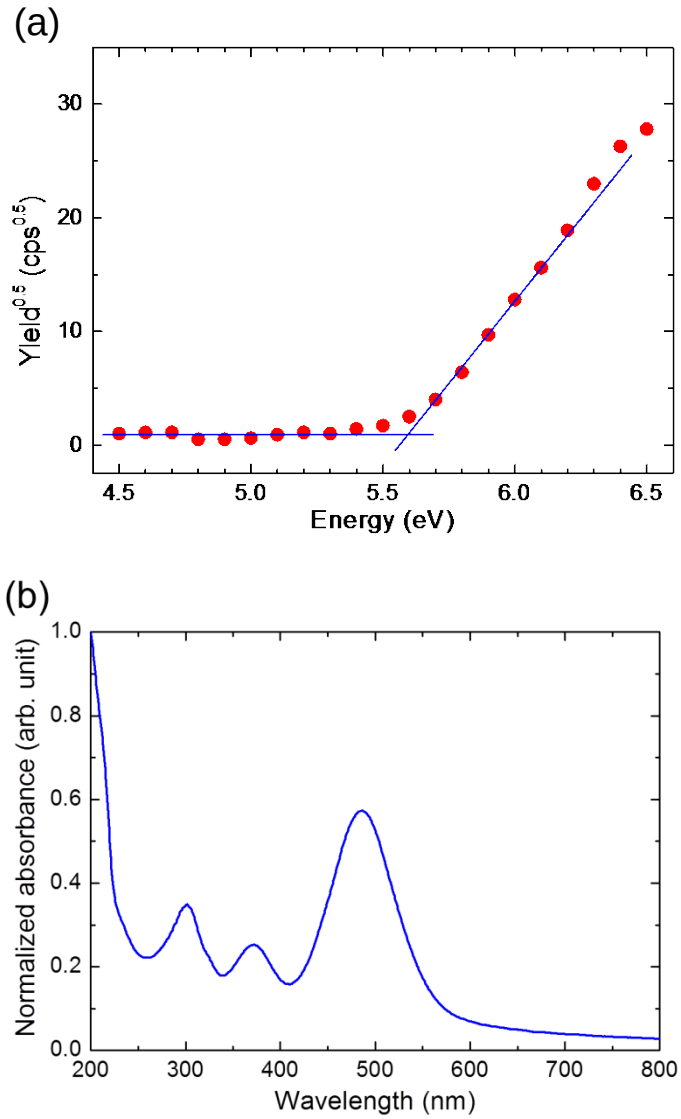

Figure 2-5. (a) Ultraviolet photoelectron spectroscopy and (b) UV-vis absorption spectrum of **HAP-3TPA** in a neat film.

The thermal stability of **HAP-3TPA** was examined by thermogravimetric-differential thermal analysis (TG-DTA). **HAP-3TPA** showed relatively high thermal stability with an initial decomposition temperature of 519.9 °C (Fig. 2-6).

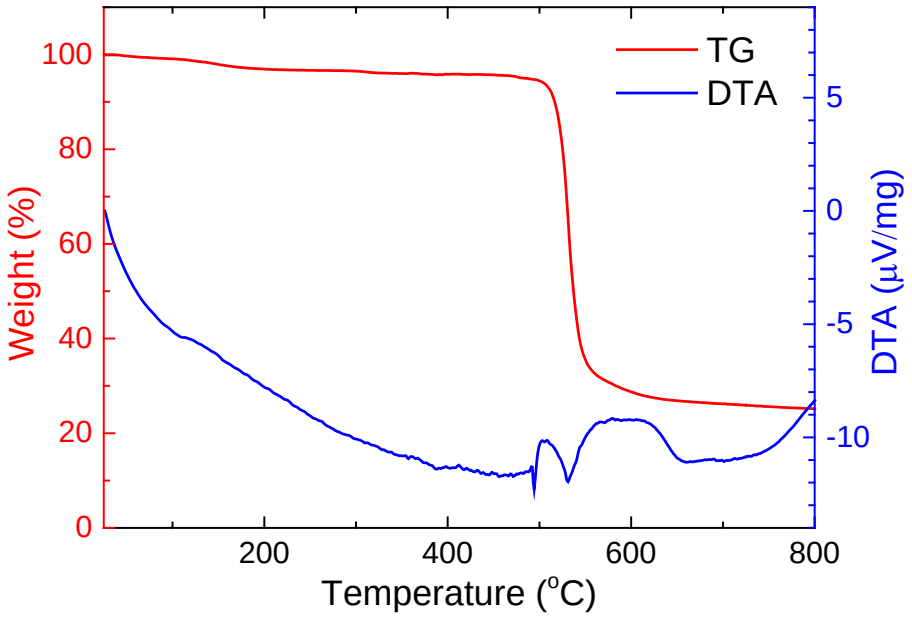

Figure 2-6. TG-DTA curves of **HAP-3TPA** under nitrogen flow.

2-4-2. Solution

The absorption and emission spectra of **HAP-3TPA** in oxygen-free toluene are shown in Fig. 2-7. **HAP-3TPA** in toluene exhibits yellow emission with a peak emission wavelength (λ_{max}) of 560 nm at room temperature. At 77 K, the fluorescent emission spectrum showed a large blue shift compared with that at 300 K, with λ_{max} = 538 nm (green emission). In addition, a delayed component was clearly observed at 77 K after 100 ms, with λ_{max} = 579 nm, which can be ascribed to phosphorescence. In this case, ΔE_{st} can be calculated from the onsets of fluorescence and phosphorescence emission spectra, giving a small ΔE_{ST} of 0.17 eV. Transient PL decay characteristics of

HAP-3TPA in oxygen-free toluene are shown in Fig. 2-8. The lifetime (τ) of prompt emission was estimated as 3.3 ns in the time range of 100 ns. Moreover, a delayed component with τ = 48.0 μs was observed in the time range of 350 μs, which can be assigned to TADF. Moreover, **HAP-3TPA** in oxygen-free toluene showed very high PLQE of 95.0%. From PLQE and τ, the PLQEs of prompt (Φ_p) and delayed (Φ_d) components are calculated to be 89.0% and 6.0%, respectively. Based on the experimental results, the radiative decay rate constants of the singlet state (k_r^S) and the quantum efficiency for intersystem crossing (Φ_{ISC}) were estimated to be 2.70 × 10^8 s^{-1}, and 11.0%, respectively.

The methods used to calculate these values are described by following equations,[7]

$$\Phi_p = \frac{k_r^S}{k_r^S + k_{nr}^S + k_{ISC}} \quad (2\text{-}1)$$

$$\Phi_d = \sum_{k=1}^{\infty} (\Phi_{ISC}\Phi_{RISC})^k \Phi_p \quad (2\text{-}2)$$

$$\Phi_{ISC} = \frac{k_{ISC}}{k_r^S + k_{nr}^S + k_{ISC}} \quad (2\text{-}3)$$

where k_{nr}^S is the non-radiative decay rate constant of the singlet state, k_{ISC} is the rate constant of intersystem crossing from singlet to triplet states, and Φ_{RISC} is the quantum efficiency for reverse intersystem crossing.

These values indicate that emission from the S_1 state to the ground state (S_0) is very efficient (Φ_p = 89%) and only a small amount of singlet excitons convert into the triplet excited state (Φ_{ISC} = 11%) and then up-convert into the singlet state again under optical excitation *via* TADF. Moreover, **HAP-3TPA** displays a significant solvatochromic effect in solvents with various dielectric constants (Fig. 2-9), exhibiting green emission in hexane and red emission in chloroform.

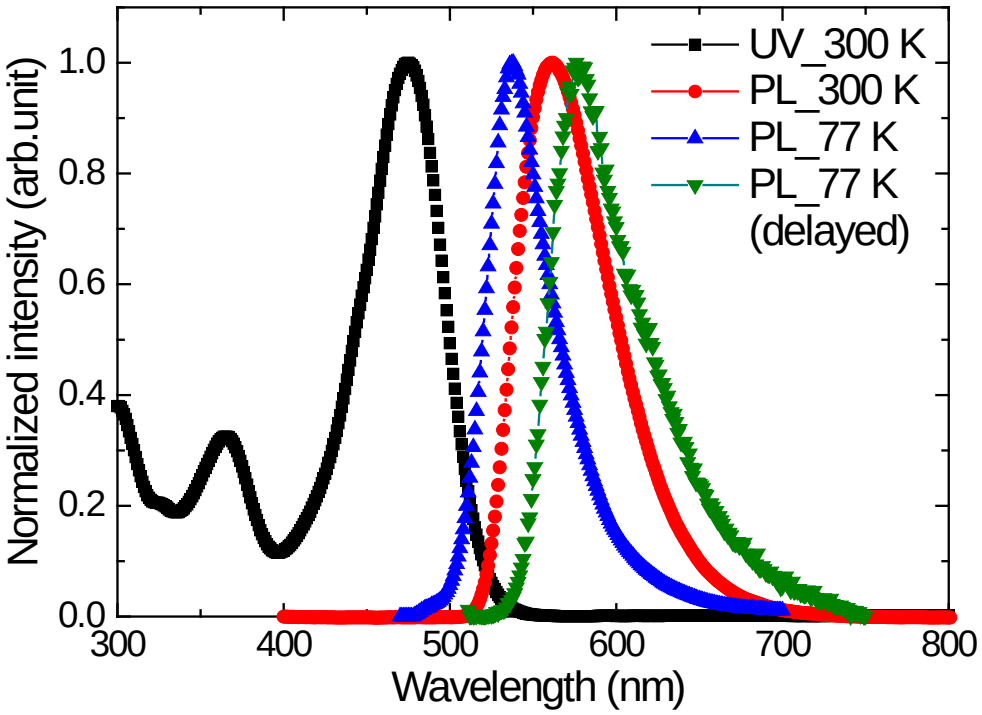

Figure 2-7. Absorption and emission spectra of **HAP-3TPA** at 300 and 77 K, and at 77 K with a 100 ms delay in oxygen-free toluene.

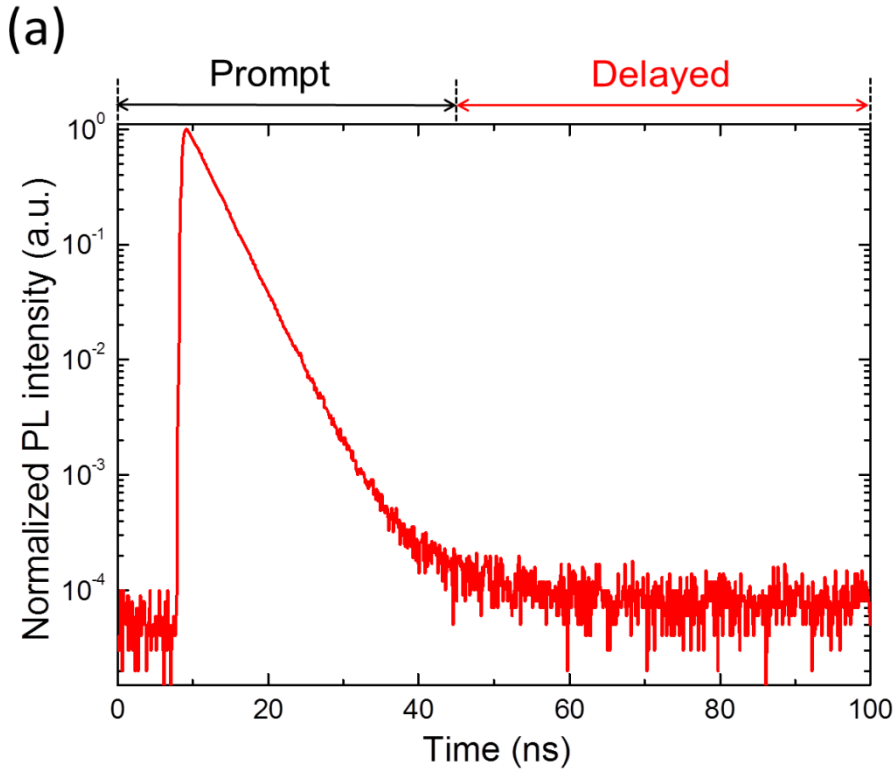

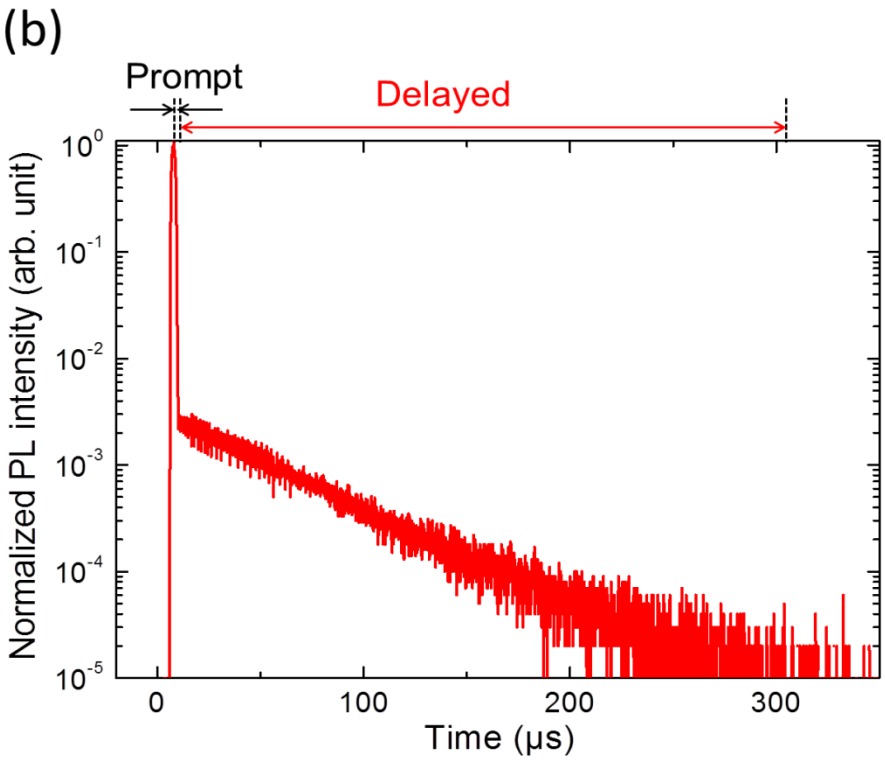

Figure 2-8. Transient PL decay of **HAP-3TPA** in oxygen-free toluene at 300 K with a lifetime range of (a) 100 ns and (b) 350 μs.

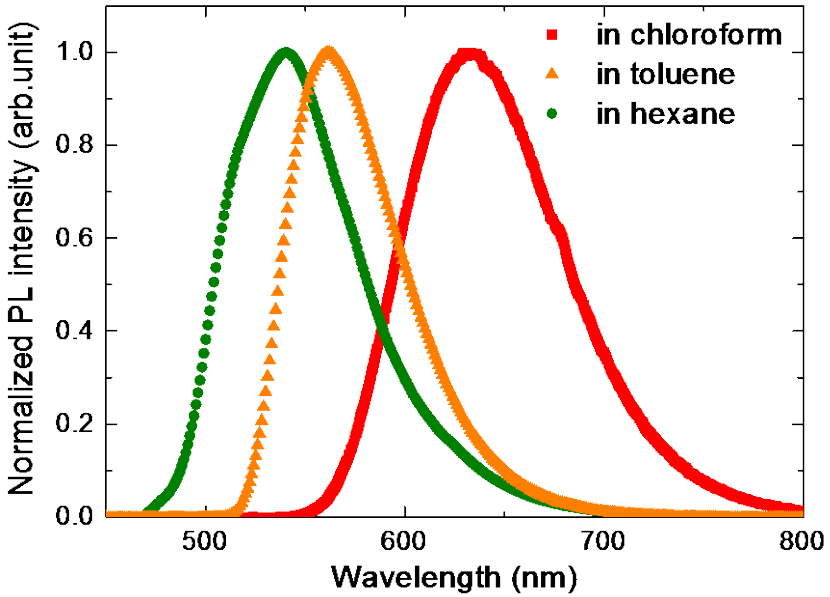

Figure 2-9. Emission spectra of **HAP-3TPA** in various solvents at 300 K.

2-4-3. Doped film

To confirm that TADF occurs in **HAP-3TPA** in the solid state, a 6 wt% **HAP-3TPA**:2,6-dicarbazolo-1,5-pyridine (26mCPy) doped film was fabricated, and its transient PL decay and temperature dependence characteristics were measured using a streak camera (Fig. 2-10). The peak emission wavelength was significantly red-shifted compared with that in toluene, with λ_{max} = 610 nm. Despite the large red-shift, a high PL efficiency of PLQE = 91.0% was maintained in the solid film. At 300 K, the transient PL decay showed a very weak delayed component with τ = 100 μs. According to the integrated photon counts, Φ_p and Φ_d were calculated to be 85.0% and 6.0%, respectively, which is consistent with the results of **HAP-3TPA** in toluene. Interestingly, unusual temperature dependence of the TADF component was observed. The delayed component significantly decreased as the temperature increased from 77 to 300 K, which is the opposite behavior to that found for other TADF molecules.[8-11] To clarify this phenomenon, the PL quantum efficiencies of total (η_{PL}), prompt (Φ_p), delayed (Φ_d), TADF (Φ_{TADF}) and phosphorescence (Φ_{phos}) components were calculated (Fig. 2-10d). The TADF component gradually increased with temperature increasing from 77 to 200 K, which is consistent with other TADF molecules. However, it then gradually decreased from Φ_{TADF} = 23.2% at 200 K to Φ_{TADF} = 6.0% at 300 K. Moreover, we found that Φ_p increased dramatically from 19.3% to 85.0% and Φ_{ISC} decreased rapidly from 78.7% to 15.0% as the temperature increased from 77 to 300 K (Table 2-1), which is also unlike the behavior of other TADF molecules. Based on these results, we interpret the unusual temperature dependence of TADF as follows: As the temperature increases from 77 to 300 K, the number of singlet excitons decaying to the triplet state through intersystem crossing decreases because of the monotonic

enhancement of radiative decay rate of fluorescence. k_r^S increases from 2.9×10^7 s^{-1} at 77 K to 1.4×10^8 s^{-1} at 300 K. Because the phosphorescence predominantly appeared below 200 K, as indicated by Φ_{phos}, the TADF component gradually decreases from 200 to 77 K. The prompt and delayed emission spectra at 77 K are shown in the inset of Fig. 2-10c. The well-overlapped emission spectra indicates that HAP-3TPA possesses a small ΔE_{ST} in the doped film although the intensity of delayed emission seems weak due to long phosphorescence lifetime and short integrating time range.

Table 2-1. Temperature dependence of PL characteristics for a 6 wt% **HAP-3TPA**:26mCPy doped film.

Temperature (K)	η_{PL} (%)	Φ_p (%)	Φ_d (%)	Φ_{TADF} (%)	Φ_{phos} (%)	Φ_{ISC} (%)
300	91.0	85.0	6.0	6.0	-	15.0
250	85.1	72.3	12.8	12.7	-	27.7
200	81.2	57.8	23.4	23.2	-	42.2
150	74.3	34.3	40.0	10.4	29.3	65.7
100	75.5	28.5	47.0	3.5	43.5	68.8
77	76.1	19.3	56.8	1.5	55.3	78.7

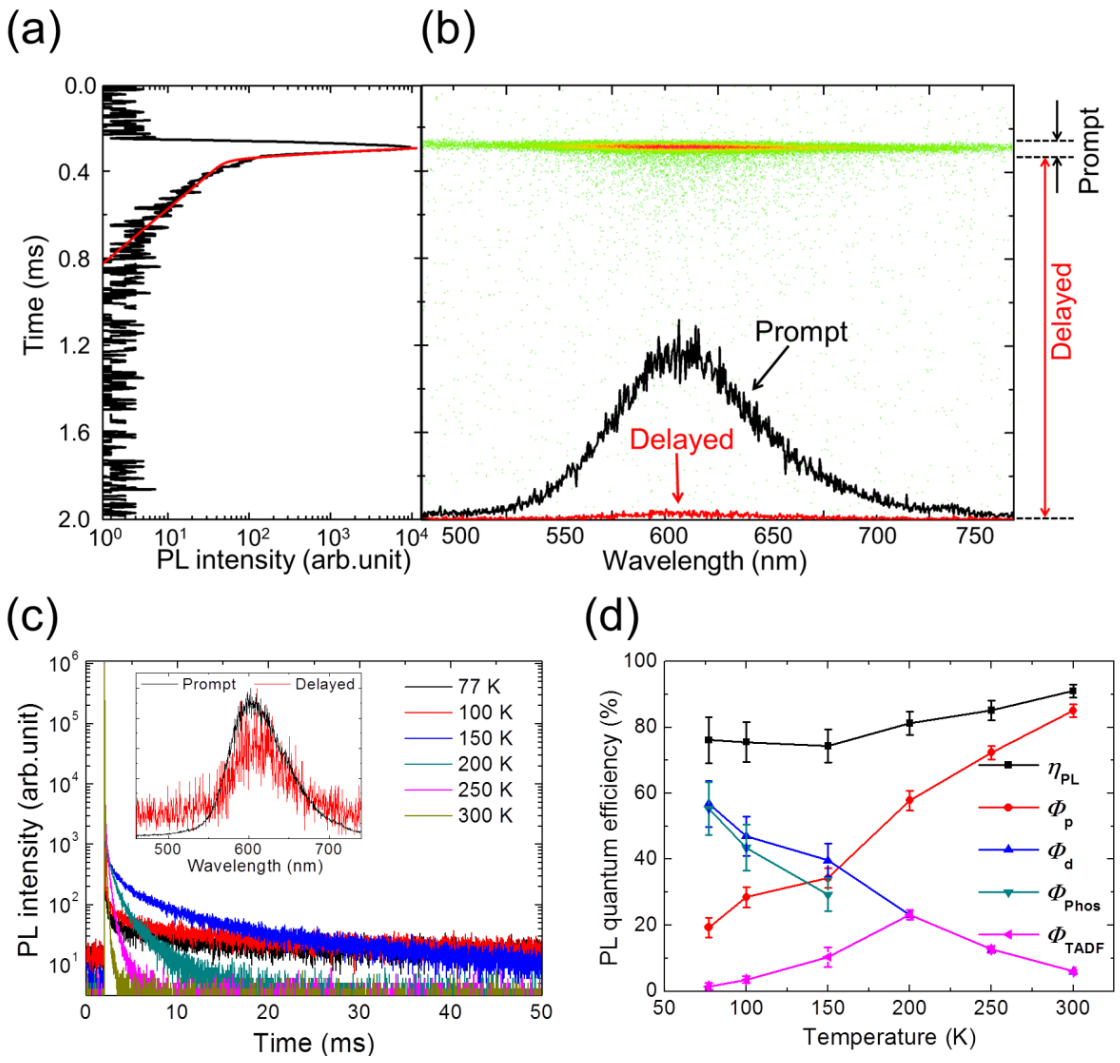

Figure 2-10. Transient PL characteristics of a 6 wt% **HAP-3TPA**:26mCPy doped film. (a) Transient PL decay (black) and second-order fitting (red) at 300 K. (b) Streak image and PL spectra were resolved into prompt (black) and delayed components (red). Each dot corresponds to the photon intensity of PL. (c) Temperature dependence of transient PL decay. Inset: Prompt and delayed emission spectra at 77 K. (d) Temperature dependence of PL quantum efficiencies of total (η_{PL}), prompt (Φ_p), delayed (Φ_d), TADF (Φ_{TADF}) and phosphorescence (Φ_{phos}) components for the doped film.

2-5. OLED characteristics

2-5-1. OLED performance

Based on the unique characteristics of **HAP-3TPA**, an OLED containing an emitting layer of 6 wt% **HAP-3TPA**:26mCPy was fabricated. The structure was ITO/α-NPD (60 nm)/6 wt% **HAP-3TPA**:26mCPy (20 nm)/Bphen (40 nm)/Mg:Ag (10:1, 100 nm)/Ag (20 nm), where ITO is indium tin oxide, α-NPD is *N*,*N'*-di(naphthalen-1-yl)-*N*,*N'*-diphenylbenzidine as a hole transport layer. Bphen is 4,7-Diphenyl-1,10-phenanthroline as an electron transport layer. The energy diagram and chemical structures of materials used in this device are shown in Fig. 2-11. The EL characteristics of this device are shown in Fig. 2-12 and 2-13. The OLED showed EQE = 17.5% with CIE coordinates of (0.60, 0.40), a turn-on voltage of 4.4 V at a luminance of 100 cd m^{-2}, a current efficiency of 25.9 cd A^{-1}, a power efficiency of 22.1 lm W^{-1}, and a peak luminance of 17000 cd m^{-2} without any light out-coupling enhancement. The EL spectrum recorded at 10 mA cm^{-2} is almost identical to the PL spectrum of the 6 wt% **HAP-3TPA**:26mCPy doped film (Figure 2-13c). This is one of the best performances achieved by fluorescence and phosphorescence-based OLEDs to date.[17-24] The excellent performance of this OLED is partly attributed to the well-balanced electron and hole fluxes into the emitting zone. It is also ascribed to efficient up-conversion of triplet excitons from T_1 to S_1 through TADF, because the actual EQE exceeds the theoretical maximum of conventional fluorescent OLEDs. For traditional fluorescent emitters, the theoretical value of EQE can be calculated from following equation, EQE = $\eta_{int} \times \eta_{out} = \gamma \times \eta_r \times$ PLQE $\times \eta_{out}$, where η_{int} is the internal quantum efficiency, η_{out} is the light out-coupling efficiency, γ is the electron/hole recombination ratio, and η_r is the ratio of exciton formation for radiative

transition (η_r = 0.25 for conventional fluorescent emitters). Therefore, if we assume that **HAP-3TPA** is a conventional fluorescent emitter, the theoretical maximum of EQE should be limited to 4.6–6.8% with γ = 1.0 and η_{out} = 0.2–0.3. It is noteworthy that the value of EQE gradually decreased with increasing current densities above 0.1 mA cm^{-2}. This efficiency roll-off effect should be ascribed to TTA process in which two molecules in the triplet excited states can interact to produce one molecule in the singlet excited state and another one in the ground state. Although TTA has been considered as a possible mechanism to increase the use of triplet excitons in order to achieve high-performance OLEDs, it plays an important role in the energy loss mechanism and induces efficiency roll-off for TADF-based OLEDs.

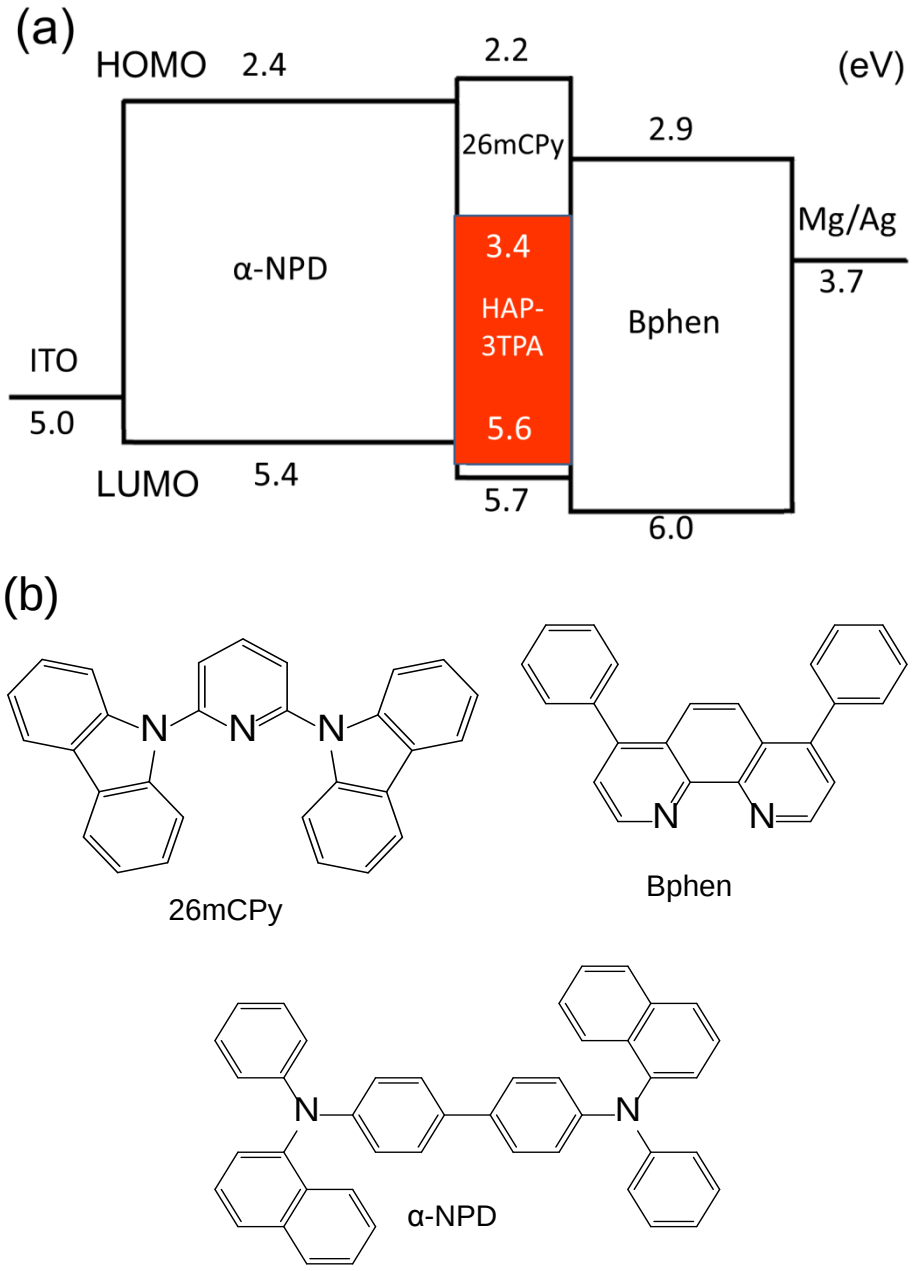

Figure 2-11. (a) Energy diagram and (b) molecular structures of compounds used in a device with the structure ITO/α-NPD (60 nm)/6 wt% **HAP-3TPA**:26mCPy (20 nm)/Bphen (40 nm)/Mg:Ag (10:1, 100 nm)/Ag (20 nm).

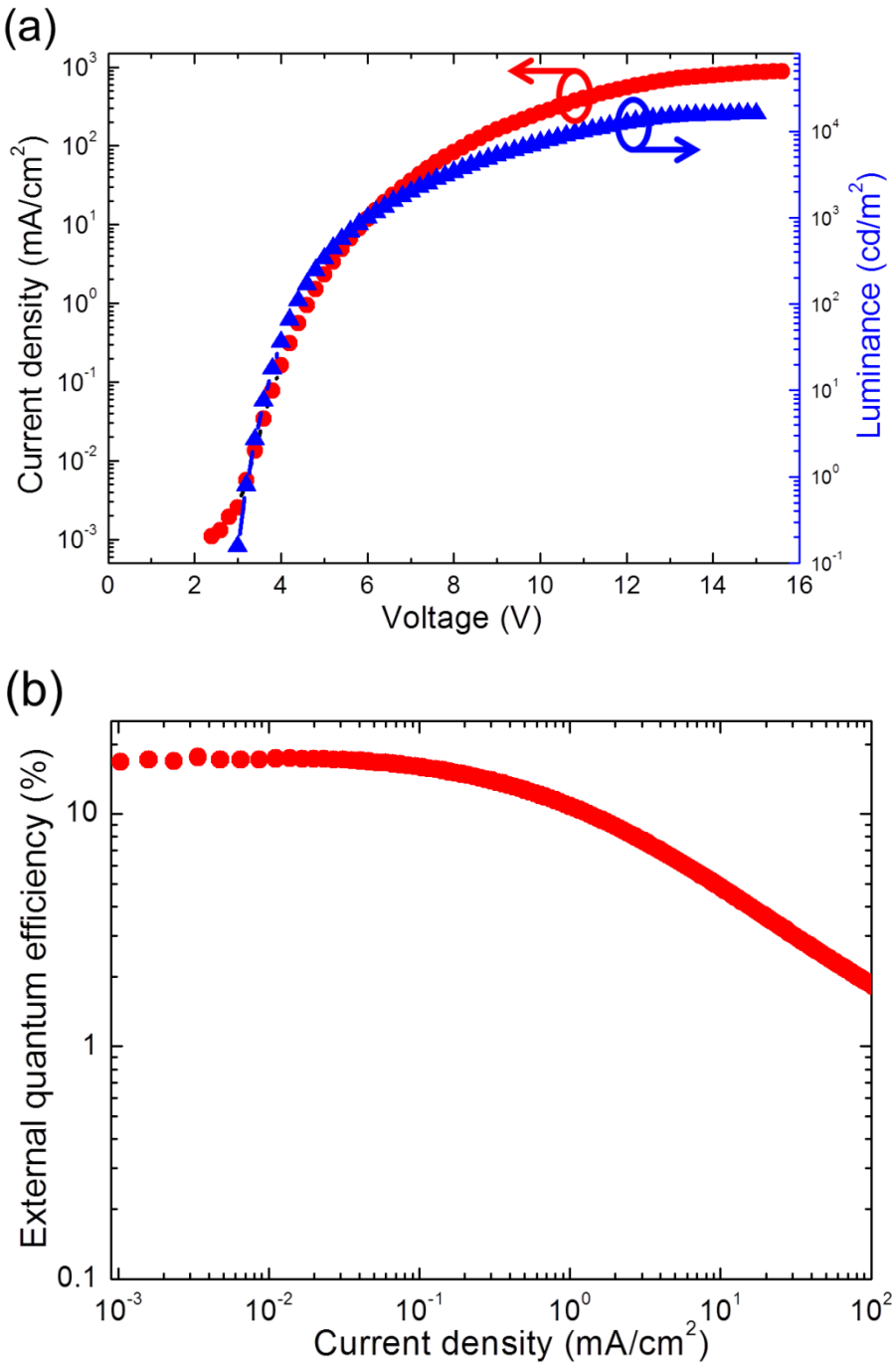

Figure 2-12. EL characteristics of an OLED device containing **HAP-3TPA**. (a) Current density-voltage-luminance characteristics. (b) External quantum efficiency-current density characteristics.

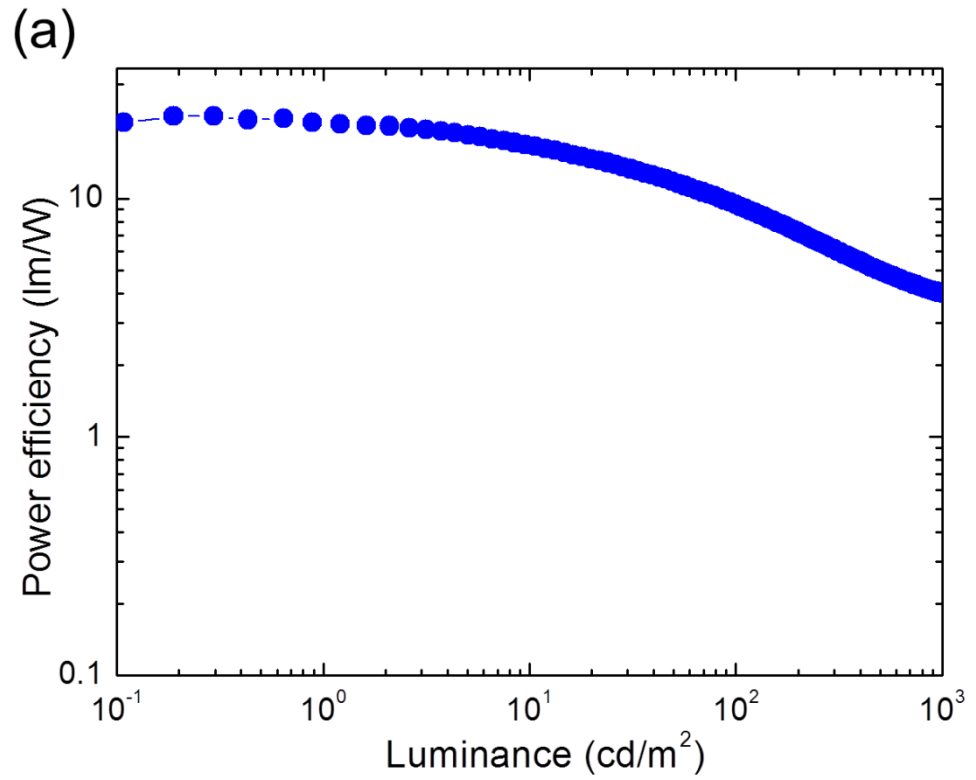
(a)
Power efficiency (lm/W)
10
1
0.1
10^{-1}
10^{0}
10^{1}
10^{2}
10^{3}
Luminance (cd/m^2)

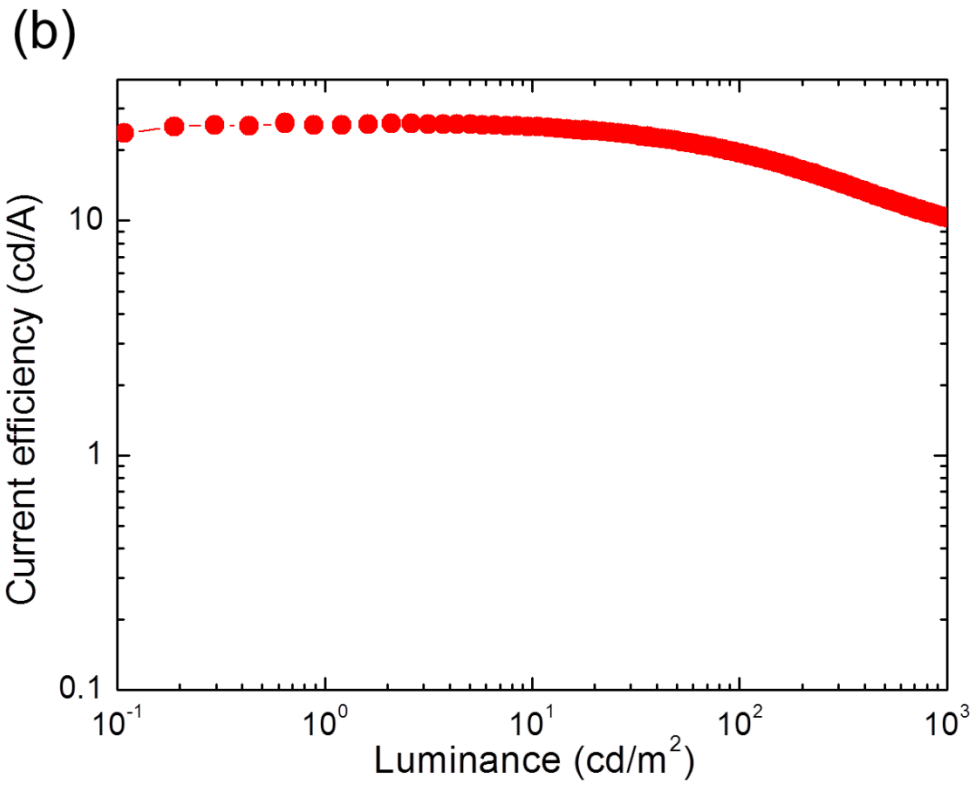
(b)
Current efficiency (cd/A)
10
1
0.1
10^{-1}
10^{0}
10^{1}
10^{2}
10^{3}
Luminance (cd/m^2)

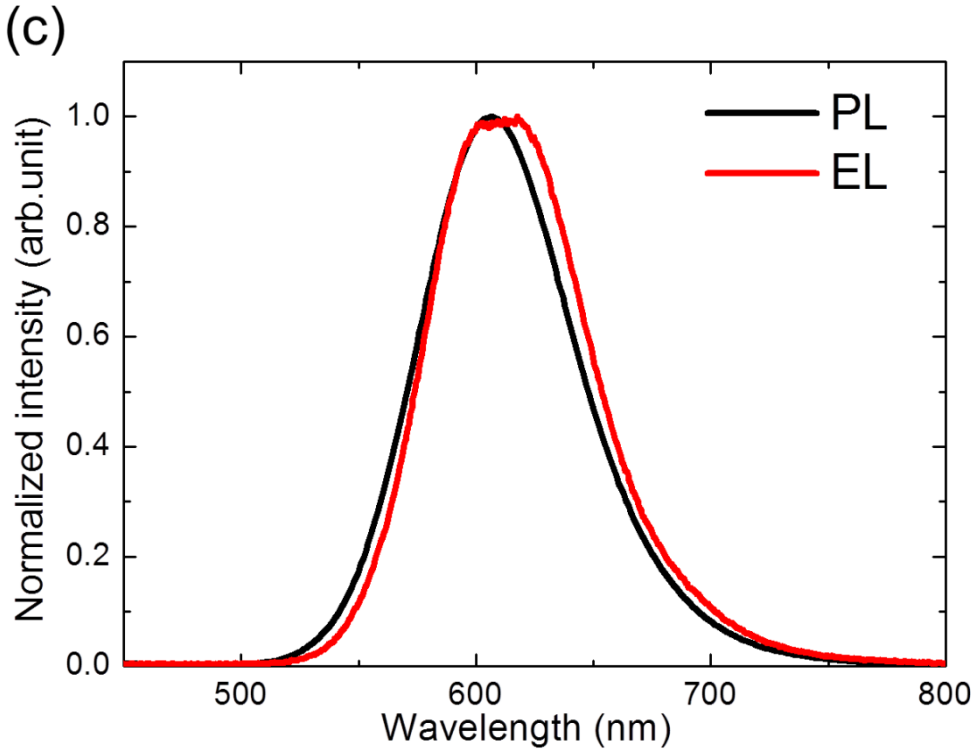

Figure 2-13. (a) Power efficiency-luminance and (b) current efficiency-luminance characteristics of the OLED based on **HAP-3TPA**. (c) Normalized EL spectrum recorded at a current density of 10 mA cm^{-2} and normalized PL spectrum of 6 wt% **HAP-3TPA**:26mCPy.

2-5-2 Transient electroluminescence

To obtain definitive evidence of the contribution of singlet exciton generation *via* reverse intersystem crossing (RISC) in the OLED, transient EL measurements were obtained with an electrical excitation pulse of 500 ns at 300 K (Fig. 2-14). A second-order transient decay was obviously observed, and the delayed component with a lifetime of τ = 0.11 ms can be attributed to TADF caused by RISC. Therefore, the delayed fluorescence induced by EL is significantly enhanced compared with that from PL. From the integrals of prompt and delayed components, the ratio of the delayed component is 61.3%, indicating that the EL efficiency mostly depends on delayed

fluorescence. These results show that efficient RISC from T_1 to S_1 leads to intense delayed fluorescence under electrical excitation, which contributes to the high EL efficiency of this OLED.

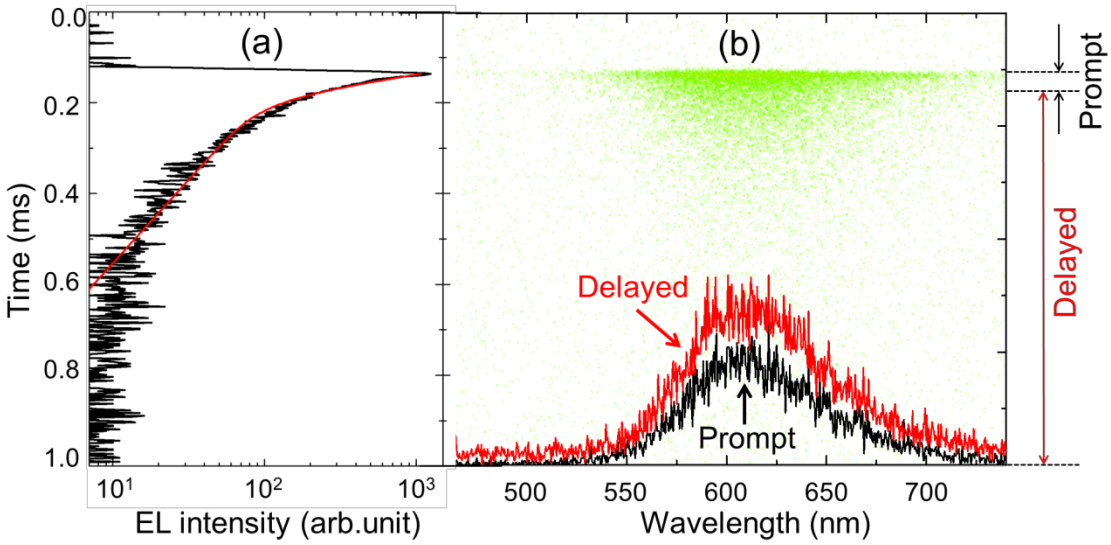

Figure 2-14. (a) Transient EL decay (black) of an OLED device containing **HAP-3TPA** under electrical excitation with a pulse of 500 ns at 300 K and second-order fitting (red). (b) Streak image and EL spectra were resolved into a prompt component (black) and delayed component (red). The dots correspond to the EL intensity.

The decay processes of PL and EL in **HAP-3TPA** are illustrated in Fig. 2-15. In the PL process, Φ_d/Φ_p was 0.07 in both toluene and the doped film, indicating that the radiative decay of singlet excitons from S_1 to S_0 is dominant and ISC between singlet and triplet states is very weak. Consequently, strong prompt fluorescence and weak TADF were obtained in the PL process. In contrast, the dominant process is TADF and Φ_d/Φ_p = 1.58 in the EL process, which results in strong delayed fluorescence and high EL efficiency.

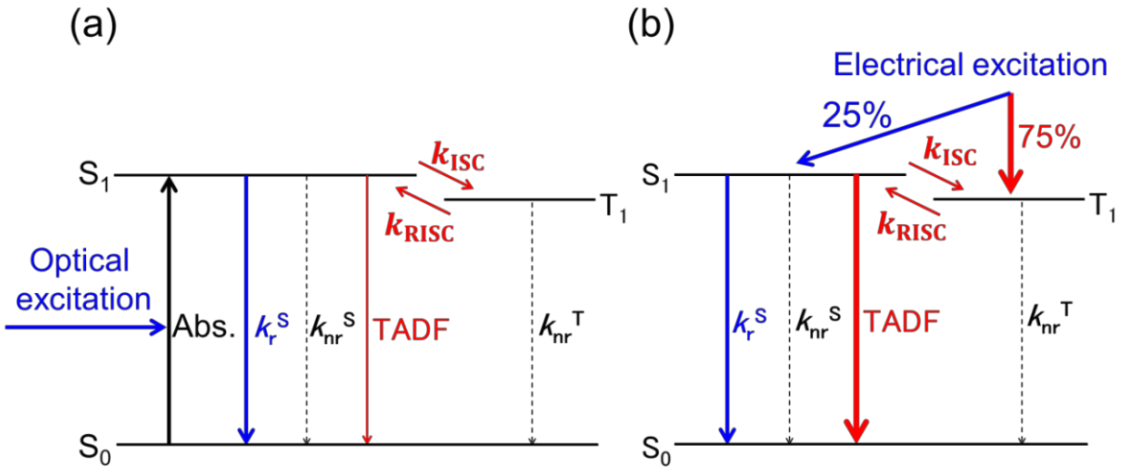

Figure 2-15. Schematic representation of (a) PL and (b) EL decay processes in **HAP-3TPA**. k_{nr}^T is the rate constant of non-radiative decay of the triplet state.

2-6. Conclusion

We designed and synthesized an orange-red TADF emitter, **HAP-3TPA**, which has a **HAP** core as an electron-accepting unit and three electron-donating units of **TPA**. An OLED containing **HAP-3TPA** showed high performance with EQE = 17.5%, maximum luminance of 17000 cd m^{-2}, maximum current and power efficiencies of 25.9 cd A^{-1} and 22.1 lm W^{-1}, respectively, and a turn-on voltage of 4.4 V at a luminance of 100 cd m^{-2} without any light out-coupling enhancement. Although **HAP-3TPA** demonstrated very weak TADF in the PL process, up-conversion from T_1 to S_1 was quite efficient under electrical excitation, resulting in high EL efficiency. Thus, in principle, even though molecules show only fluorescence and very faint TADF in PL, they may have an efficient pathway for TADF in EL. This study shows that the TADF of molecules should be carefully ascertained.

2-7. References

1. Y. C. Chiu, J. Y. Hung, Y. Chi, C. C. Chen, C. H. Chang, C. C. Wu, Y. M. Cheng, Y. C. Yu, G. H. Lee, and P. T. Chou, *Adv. Mater.* 2009, ***21***, 2221.
2. M. Cocchi, D. Virgili, V. Fattori, D. L. Rochester, and J. A. G. Williams, *Adv. Func. Mater*. 2007, ***17***, 285.
3. T. H. Liu, S. F. Hsu, M. H. Ho, C. H. Liao, Y. S. Wu, C. H. Chen, Y. L. Tung, P. C. Wu, and Y. Chi, *Appl. Phys. Lett.* 2006, ***88***, 063508.
4. Q. Zhang, T. Komino, S. Huang, S. Matsunami, K. Goushi, and C. Adachi, *Adv. Funct. Mater.* 2012, ***22***, 2327.
5. D. Y. Kondakov, T. D. Pawlik, T. K. Hatwar, and J. P. Spindler, *J. Appl. Phys.* 2009, ***106***, 124510.
6. A. Endo, K. Sato, K. Yoshimura, T. Kai, A. Kawada, H. Miyazaki, and C. Adachi, *Appl. Phys. Lett*. 2011, ***98***, 083302.
7. K. Goushi, K. Yoshida, K. Sato, and C. Adachi, *Nat. phtonics.* 2012, ***6***, 253
8. S. Y. Lee, T. Yasuda, H. Nomura, and C. Adachi, *Appl. Phys. Lett.* 2012, ***101***, 093306.
9. T. Nakagawa, S.-Y. Ku, K.-T. Wong, and C. Adachi, *Chem. Commun.* 2012, ***48***, 9580.
10. G. Méhes, H. Nomura, Q. Zhang, T. Nakagawa, and C. Adachi, *Angew. Chem. Int. Ed.* 2012, ***51***, 11311.
11. H. Tanaka, K. Shizu, H. Miyazaki, and C. Adachi, *Chem. Commun.* 2012, ***48***, 11392.
12. Q. Zhang, J. Li, K. Shizu, S. Huang, S. Hirata, H. Miyazaki, and C. Adachi, *J. Am. Chem. Soc.* 2012, ***134***, 14706.

13. H. Uoyama, K. Goushi, K. Shizu, H. Nomura, and C. Adachi, *Nature* 2012, ***492***, 234.
14. S. D. Cummings and R. Eisenberg, *J. Am. Chem. Soc.* 1996, ***118***, 1949.
15. M. J. Frisch, G. W. Trucks, H. B. Schlegel, G. E. Scuseria, M. A. Robb, J. R. Cheeseman, J. A. Montgomery, T. Vreven Jr., K. N. Kudin, J. C. Burant, J. M. Millam, S. S. Iyengar, J. Tomasi, V. Barone, B. Mennucci, M. Cossi, G. Scalmani, N. Rega, G. A. Petersson, H. Nakatsuji, M. Hada, M. Ehara, K. Toyota, R. Fukuda, J. Hasegawa, M. Ishida, T. Nakajima, Y. Honda, O. Kitao, H. Nakai, M. Klene, X. Li, J. E. Knox, H. P. Hratchian, J. B. Cross, C. Adamo, J. Jaramillo, R. Gomperts, R. E. Stratmann, O. Yazyev, A. J. Austin, R. Cammi, C. Pomelli, J. W. Ochterski, P. Y. Ayala, K. Morokuma, G. A. Voth, P. Salvador, J. J. Dannenberg, V. G. Zakrzewski, S. Dapprich, A. D. Daniels, M. C. Strain, O. Farkas, D. K. Malick, A. D. Rabuck, K. Raghavachari, J. B. Foresman, J. V. Ortiz, Q. Cui, A. G. Baboul, S. Clifford, J. Cioslowski, B. B. Stefanov, G. Liu, A. Liashenko, P. Piskorz, I. Komaromi, R. L. Martin, D. J. Fox, T. Keith, M. A. Al-Laham, C. Y. Peng, A. Nanayakkara, M. Challacombe, P. M. W. Gill, B. Johnson, W. Chen, M. W. Wong, C. Gonzalez, and J. A. Pople, *Gaussian 03, revision B05*, Gaussian, Inc., Pittsburgh, PA 2003.
16. K. S. Son, M. Yahiro, T. Imai, H. Yoshizaki, J. Nishide, H. Sasabe, and C. Adachi, *Jpn. J. Appl. Phys.* 2008, ***47***, 7363.
17. E. Orselli, J. Maunoury, D. Bascour, and J. P. Catinat, *Org. Electron.* 2012, ***3***, 1506.
18. W. C. Wu, H. C. Yeh, L. H. Chan, and C. T. Chen, *Adv. Mater*. 2002, ***14***, 1072.
19. X. Yang, D. C. Müller, D. Neher, and K. Meerholz, *Adv. Mater.* 2006, ***18***, 948.

20. F. I. Wu, H. J. Su, C. F. Shu, L. Luo, W. G. Diau, C. H. Cheng, J. P. Duan, G. H. Lee, *J. Mater. Chem.* 2005, ***15***, 1035.

21. Y. J. Su, H. L. Huang, C. L. Li, C. H. Chien, Y. T. Tao, P. T. Chou, S. Datta, and R. S. Liu, *Adv. Mater.* 2003, ***15***, 884.

22. G. Zhou, W. Y. Wong, B. Yao, Z. Xie, and L. Wang, *Angew. Chem. Int. Ed.* 2007, ***46***, 1149.

23. Q. Zhang, J. Ding, Y. Cheng, L. Wang, Z. Xie, X. Jing, and F. Wang, *Adv. Funct. Mater*. 2007, ***17***, 2983.

24. B. S. Du, J. L. Liao, M. H. Huang, C. H. Lin, H. W. Lin, Y. Chi, H. A. Pan, G. L. Fan, K. T. Wong, G. H. Lee, and P. T. Chou, *Adv. Funct. Mater.* 2012, ***22***, 3491.

Chapter 3

Highly Efficient Exciplex Organic Light-Emitting Diodes Incorporating a Heptazine Derivative as an Electron Acceptor

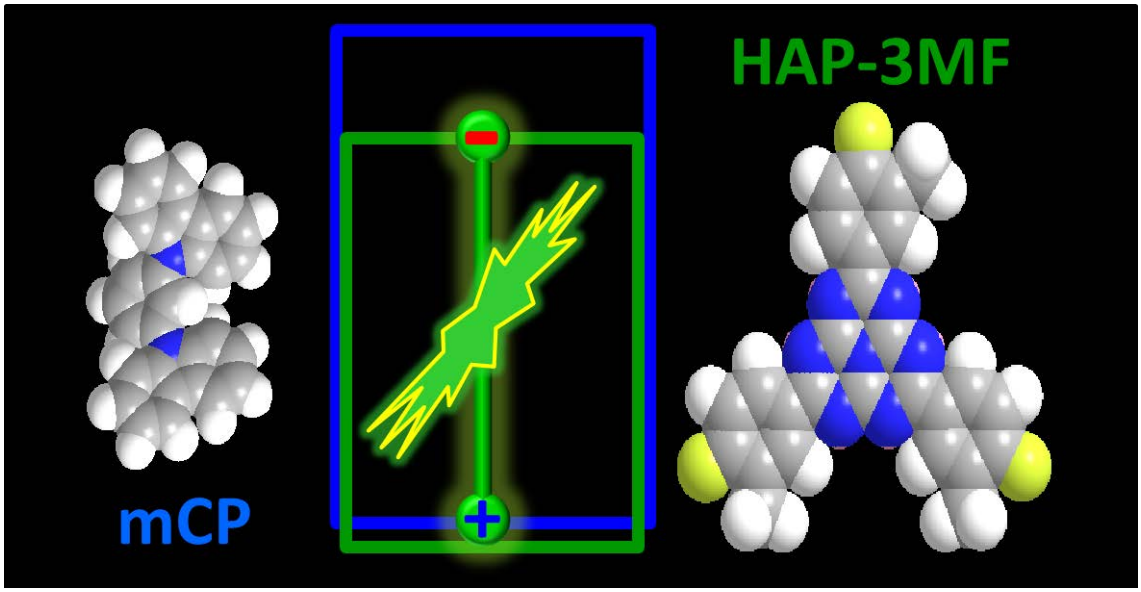

J. Li, H. Nomura, H. Miyazaki, C. Adachi. *Chem. Comm.* 2014, **50**, 6174.

3-1. Introduction

OLEDs have attracted tremendous interest because of their promise in optoelectronic devices, especially flat-panel displays and general lighting.[1] Phosphorescent OLEDs containing transition metal complexes can exhibit very high EQEs as a result of effective use of both singlet and triplet excitons.[2] Although OLEDs based on conventional fluorescent materials typically show a limited EQE of 5% because only singlet excitons can be harvested under electrical excitation,[3] two new tactics to harvest triplet excitons through TTA[4] and TADF[5] have been exploited to markedly enhance the EQE of fluorescent OLEDs. In particular, TADF molecules have attracted much more interest because almost 100% internal quantum efficiencies can be achieved. The crucial design strategy of TADF molecules is to possess a small energy gap (ΔE_{ST}) between S_1 and T_1 to allow efficient ISC. Elaborate molecular design is necessary to obtain a small ΔE_{ST} because it is proportional to the exchange energy between the highest occupied molecular orbital (HOMO) and the lowest unoccupied molecular orbital (LUMO) of electron donating and accepting moieties, respectively. Alternatively, small ΔE_{ST} can be readily realized by exciplex formation *via* intermolecular charge transfer between electron donors and acceptors.[6] Over the past two decades, interest in exciplexes formed at solid interfaces and in physically blended structures has expanded.[7] With judicious molecule selection, exciplex-based organic light-emitting diodes (ExOLEDs) with EQEs as high as 10.0% have been obtained.[8] However, it is still challenging to explore highly efficient exciplex systems because exciplex formation is usually accompanied with a large red-shift of emission spectra, which tends to decrease PLQE as well as EL performance.

In this study, we developed a highly efficient exciplex system with a blended structure containing 1,3-di(9H-carbazol-9-yl)benzene (**mCP**) as an electron donor, 2,5,8-tris(4-fluoro-3-methylphenyl)-1,3,4,6,7,9,9b-heptaazaphenalene (**HAP- 3MF**) as an electron acceptor.

3-2. Molecular design, synthesis and characterization

3-2-1. Molecular design

The molecular structures of **mCP** and **HAP-3MF** are depicted in Fig. 3-1. **mCP** is a widely used host molecule possessing two electron-donating carbazole moieties.[9] **HAP-3MF**, which is composed of a heptazine core and three 2-fluorotoluene groups, was designed and synthesized as an electron acceptor. 2-Fluorotoluene groups were introduced to increase the solubility and maintain the electron-withdrawing ability of **HAP-3MF**. We chose a heptazine derivative as an electron acceptor in the exciplex system because it exhibits a number of intriguing thermal,[10] optical,[11,5g] and electronic[12] properties. Although heptazine derivatives are promising candidates for OLEDs, no exciplex system containing a heptazine derivative has been reported. Herein, we examine the photophysical characteristics and EL performance of an **HAP-3MF**:**mCP** exciplex system.

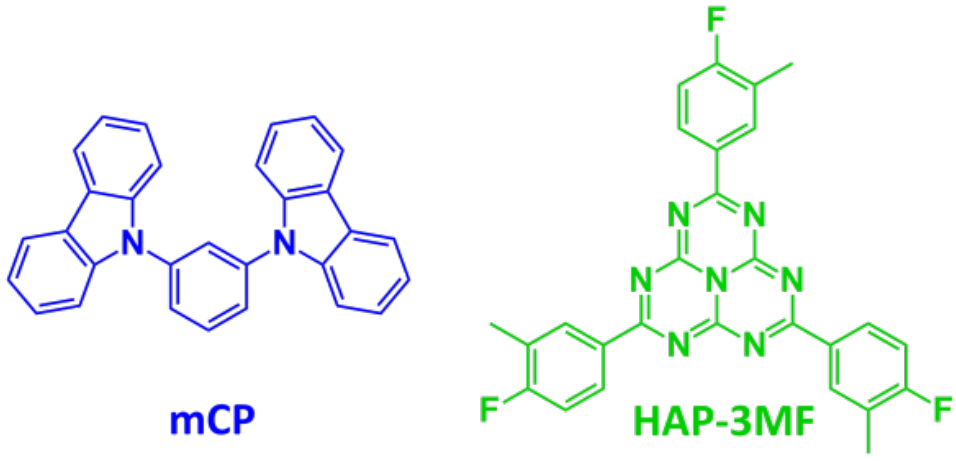

Figure 3-1. Molecular structures of **mCP** and **HAP-3MF**.

3-2-2. Molecular synthesis and characterization

All spectrophotometric-grade solvents and starting materials were purchased and used as received unless otherwise noted. All reactions were carried out under N_2 atmosphere. High-resolution mass spectrometry (HRMS) by fast atom bombardment was conducted using a JEOL JMS-700 spectrometer. Elemental analysis was performed with a Yanaco MT-5 elemental analyzer. ^{1}H NMR spectrum was obtained with a Bruker Biospin Avance-III 500 NMR spectrometer at ambient temperature. Because **HAP-3MF** was not sufficiently soluble in common deuterated solvents, its ^{13}C NMR spectrum was not obtained.

Scheme 3-1 shows the synthetic pathway of **HAP-3MF**.

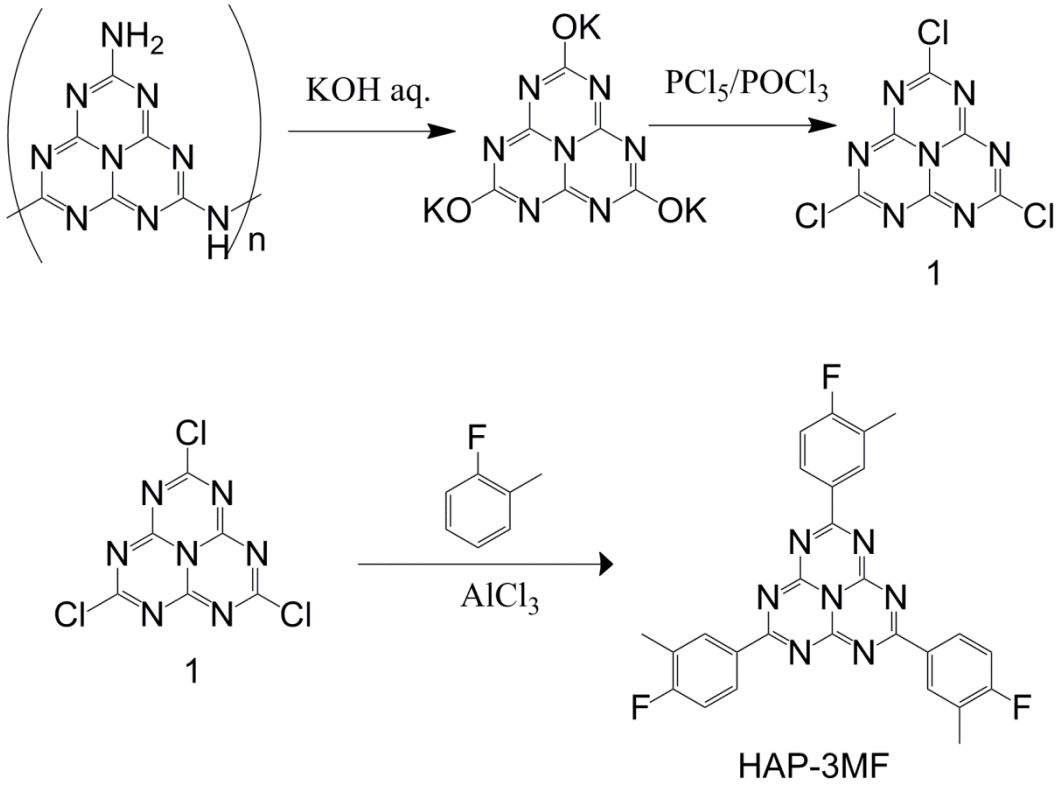

Scheme 3-1. Synthetic route of **HAP-3MF**.

Synthesis of 2,5,8-Trichloro-1,3,4,6,7,9,9b-heptaazaphenalene (1): Compound 1 was synthesized according to the method reported previously.[19]

Synthesis of 2,5,8-tris(4-fluoro-3-methylphenyl)-1,3,4,6,7,9,9b-heptaazaphena- lene **(HAP-3MF):** Compound 1 (1.0 g, 3.6 mmol) was added to a solution of $AlCl_3$ (2.41 g, 18 mmol) in 2-fluorotoluene (10 mL) at 0 °C. The mixture was stirred at 0 °C for 30 min and then at 80 °C for 6 h. The reaction mixture was cooled to room temperature, ice was added, and the mixture was stirred for vigorously for 1 h. Subsequently, the mixture was heated at 100 °C for 30 min, allowed to cool to room temperature, filtered, washed with H_2O, and then taken up in toluene and pre-adsorbed onto silica. The pre-adsorbed materials were subjected to flash chromatography (EtOAc/toluene, 0:100 *v/v* and then 10:90 *v/v*) to give **HAP-3MF** (1.07 g, yield: 60%) as a yellow-green solid. **HAP-3MF** was further purified by sublimation. ^{1}H NMR (500 MHz, C_6D_6): δ 8.63 (dd, *J* =7.5, 1.5 Hz, 1H), 8.58–8.55 (m, 1H), 6.79 (t, *J* = 8.8 Hz, 1H), 2.05 (s, 3H) (Fig. 3-2). mp: 375–385 ^{o}C. HRMS (*m/z*): $[M]^-$ calcd for $C_{27}H_{18}N_7F_3$: 497.1576; found: 497.1558. Elemental anal. calcd for $C_{27}H_{18}N_7F_3$ (%): C 65.19, H 3.65, N 19.71; found: C 65.05, H 3.63, N 19.81.

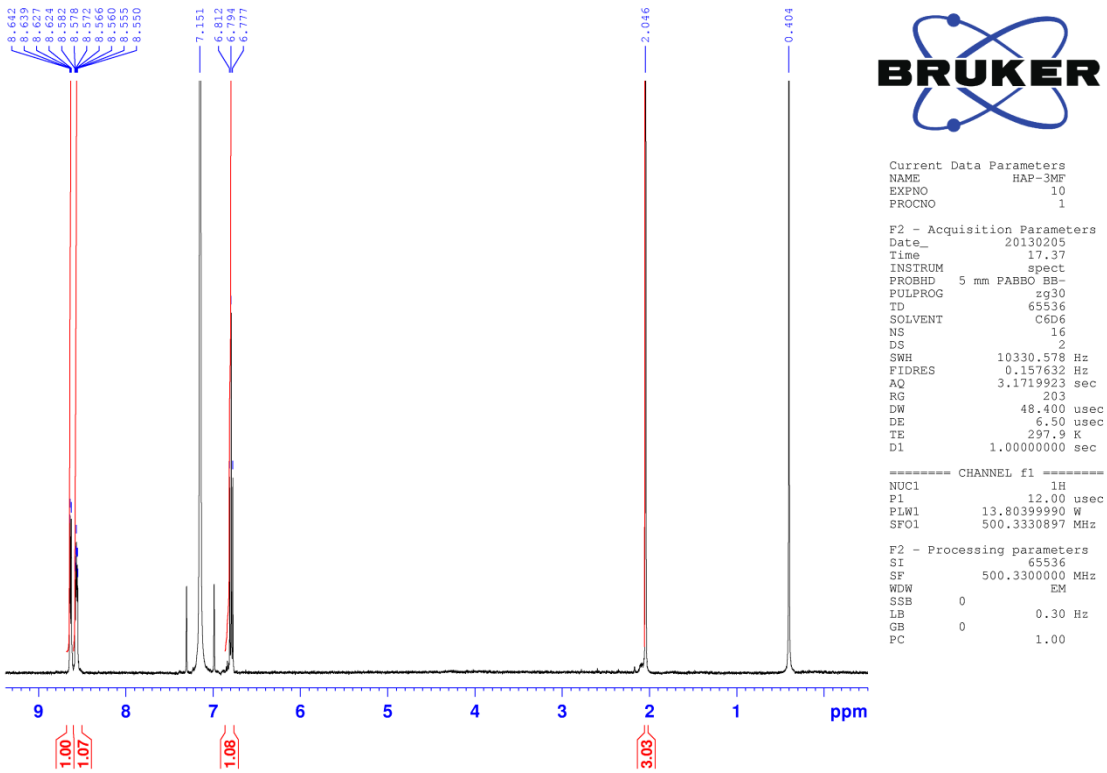

Figure 3-2. ^{1}H NMR spectrum of **HAP-3MF** in C_6D_6.

3-3. Optical properties

The HOMO and LUMO levels of **HAP-3MF** are 6.0 and 3.4 eV, which were estimated by ultraviolet photoelectron spectroscopy and subtracting the energy gap from the HOMO level, respectively (Fig. 3-3).

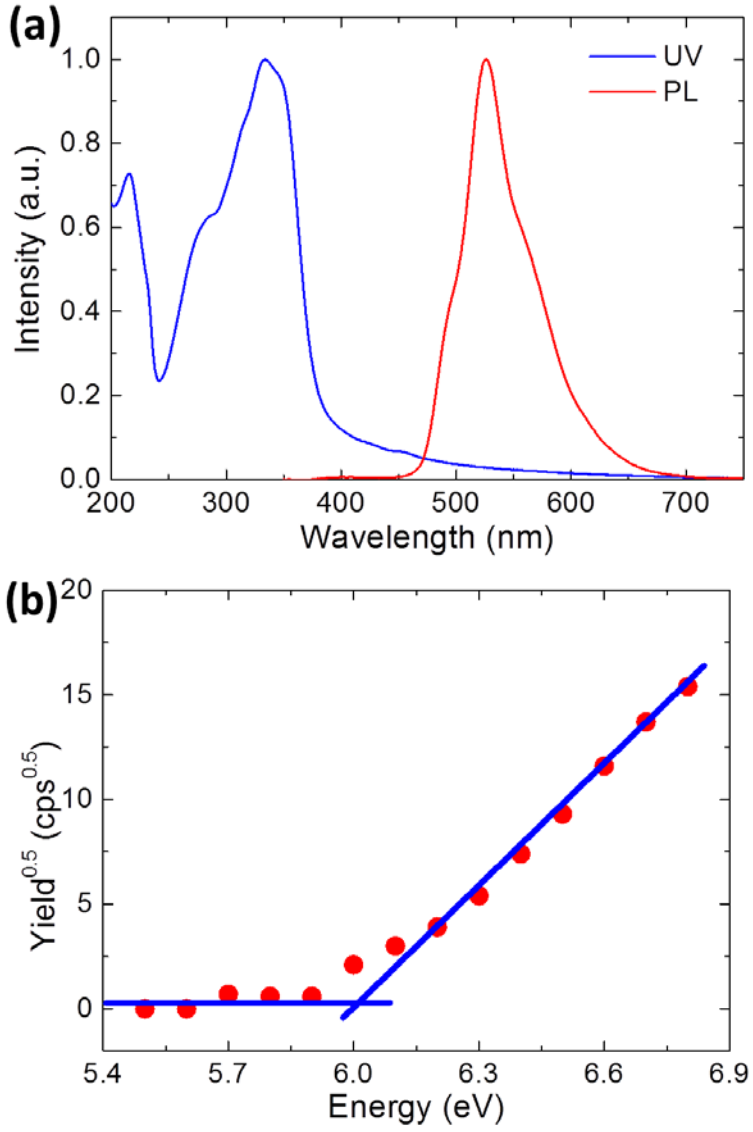

Figure 3-3. (a) UV-vis absorption and PL spectra and (b) UPS of **HAP-3MF** in a solid film. The predominant absorption peak is centered at 334 nm, and the band gap was calculated to be 2.6 eV.

The thermal stability of **HAP-3MF** was measured by thermogravimetric-differential thermal analysis; it exhibited fairly high thermal stability with an initial decomposition temperature of 413.5 °C (Fig. 3-4).

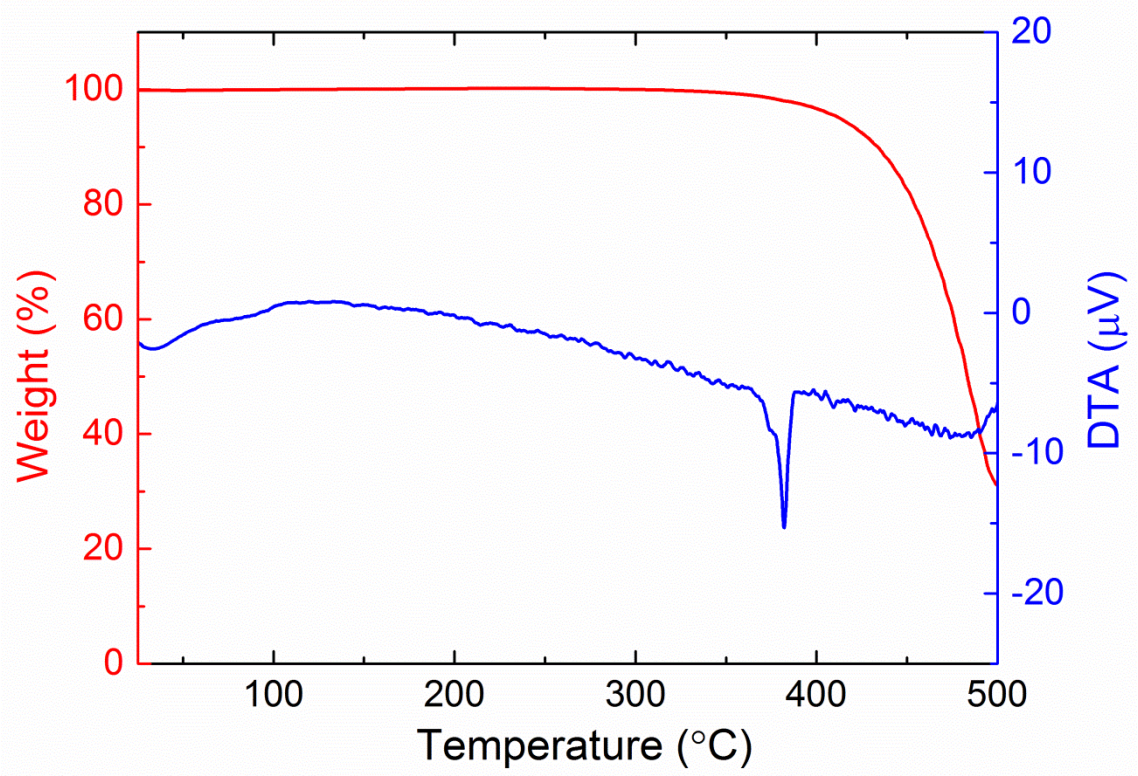

Figure 3-4. TG-DTA of **HAP-3MF** under nitrogen flow. **HAP-3MF** is thermally stable up to around 370 °C.

The ultraviolet-visible (UV-vis) absorption and PL spectra of **mCP**, **HAP-3MF**, and 25 wt% **HAP-3MF**:**mCP** films are presented in Fig. 3-5. Absorption peaks at 329 and 342 nm originate from **mCP**, and the dominant absorption peak of **HAP-3MF** is centered at 334 nm. The UV-vis absorption spectrum of a 25 wt% **HAP-3MF**:**mCP** blend film is similar to that of an **mCP** one. No new absorption band appeared at longer wavelength, indicating the absence of charge transfer

between **mCP** and **HAP-3MF**. Both **mCP** and **HAP-3MF** solid films show well-resolved PL spectra resulting from π-π* or n-π* emissions.[13] In contrast, the PL of the blend film exhibits typical exciplex characteristics with a peak at around 550 nm, which is red-shifted compared with those of **mCP** and **HAP-3MF** films. Interestingly, the exciplex system shows a rather high PLQE of 55.7%, which is much higher than that of a **HAP-3MF** film with a PLQE of 12.7%. This is unusual behavior compared with conventional exciplex systems, which usually possess PLQEs lower than that of each single layer. Furthermore, the red-shift between the PL peaks of **HAP-3MF** (526 nm) and 25 wt% **HAP-3MF**:**mCP** blend film (550 nm) is just 24 nm. The photon energy of the exciplex is therefore only slightly lower than that of **HAP-3MF**. The similar HOMO levels of **mCP** and **HAP-3MF** suppress the red-shift of exciplex emission. Moreover, the full width at half maximum (FWHM) of the exciplex emission is narrow compared with that observed for other conventional exciplex systems.[6-8] The FWHM of 83 nm of the blend film is only slightly larger than that of **HAP-3MF** alone (66 nm). These unique PL characteristics could be ascribed to the rigid and relatively planar geometries of **HAP-3MF** and **mCP** molecules, which tend to result in tight molecular packing of π-conjugated moieties and very strong intermolecular interactions.[7]

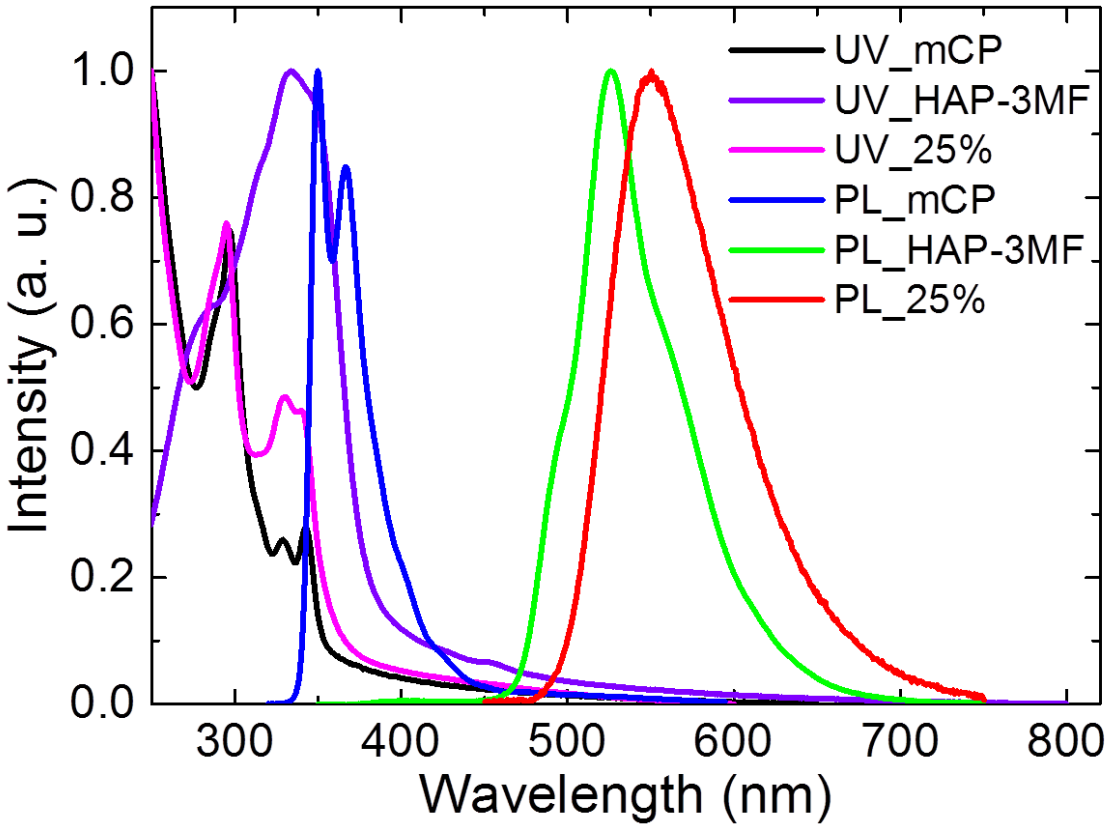

Figure 3-5. UV-vis absorption and PL spectra of **mCP**, **HAP-3MF**, and 25 wt% **HAP-3MF**:**mCP** in solid films at 300 K.

To obtain an optimized exciplex system, **HAP-3MF**:**mCP** blend films with various weight ratios were fabricated and characterized. The UV-vis absorption and PL spectra of these films are depicted in Fig. 3-6, and the PLQEs of **HAP-3MF**:**mCP** exciplex systems with various weight ratios in air and nitrogen are summarized in Table 3-1. We found that the 8 wt% **HAP-3MF**:**mCP** exciplex system exhibits a remarkably high PLQE of 66.1% and rather small PL spectral red-shift of 12 nm compared with that of an **HAP-3MF** film. Considering the exciplex mechanism, the transient PL decay properties of an 8 wt% **HAP-3MF**:**mCP** exciplex system were characterized (Fig. 3-7). The well-overlapped prompt and delayed emission spectra at

300 K confirm that all photons are generated from the same excited state (Fig. 3-7a). Considerable overlap was also observed between the prompt and delayed spectra at 50 K (Fig. 3-7b), indicating the exciplex system possesses a fairly small ΔE_{ST}. Figure 3-7c shows the transient PL decay of an 8 wt% **HAP-3MF**:**mCP** film in air and under vacuum conditions at 300 K. The transient PL decay can be divided into prompt and delayed components. The prompt component with a transient lifetime of 184 ns can be ascribed to conventional fluorescence-based exciplex emission, while the delayed ones with transient lifetimes of 1.7 and 5.7 μs are generated from the delayed exciplex emission after up-conversion of triplet exciplex excitons into the singlet excited state as discussed in a previous report.[6] While we cannot fully characterize the origin of the multiple decay components, it should be caused by the inhomogeneous distribution of **HAP-3MF** molecules in the **mCP** host matrix. Here, we note that the transient PL decay curves in air and under vacuum conditions overlap well, suggesting that oxygen has almost no influence on the PL characteristics, probably because of the rigid and tightly packed environment of an **mCP** host layer. As a consequence, the PLQE of an 8 wt% **HAP-3MF**:**mCP** exciplex system in air is 65.8%, which is nearly equal to that in nitrogen (66.1%). We can approximately estimate the PLQE of the prompt component, Φ_{prompt} = 18.6%, while that of the delayed component is $\Phi_{delayed}$ = 47.5% in nitrogen. The transient PL properties of 25 wt% and 50 wt% **HAP-3MF**:**mCP** exciplex systems are analogous to that of 8 wt% **HAP-3MF**:**mCP** (Figs. 3-8 and 3-9).

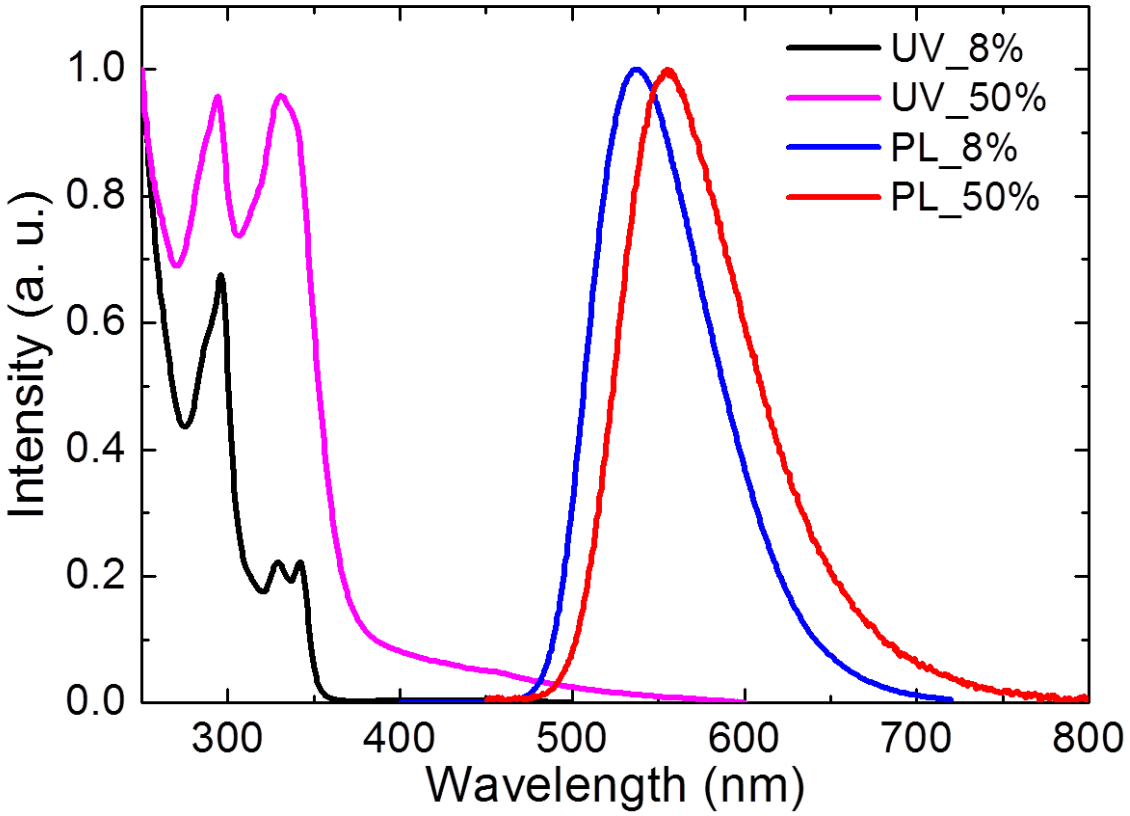

Figure 3-6. UV-vis absorption and PL spectra of 8 wt% and 50 wt% **HAP-3MF**:**mCP** blend films with various weight ratios at 300 K.

Table 3-1 PLQEs of **HAP-3MF**:**mCP** exciplex systems with various weight ratios in air and nitrogen.

	PLQE in air	PLQE in nitrogen
8 wt% **HAP-3MF**:**mCP**	0.658	0.661
25 wt% **HAP-3MF**:**mCP**	0.543	0.557
50 wt% **HAP-3MF**:**mCP**	0.440	0.470
100 wt% **HAP-3MF**:**mCP**	0.127	0.127

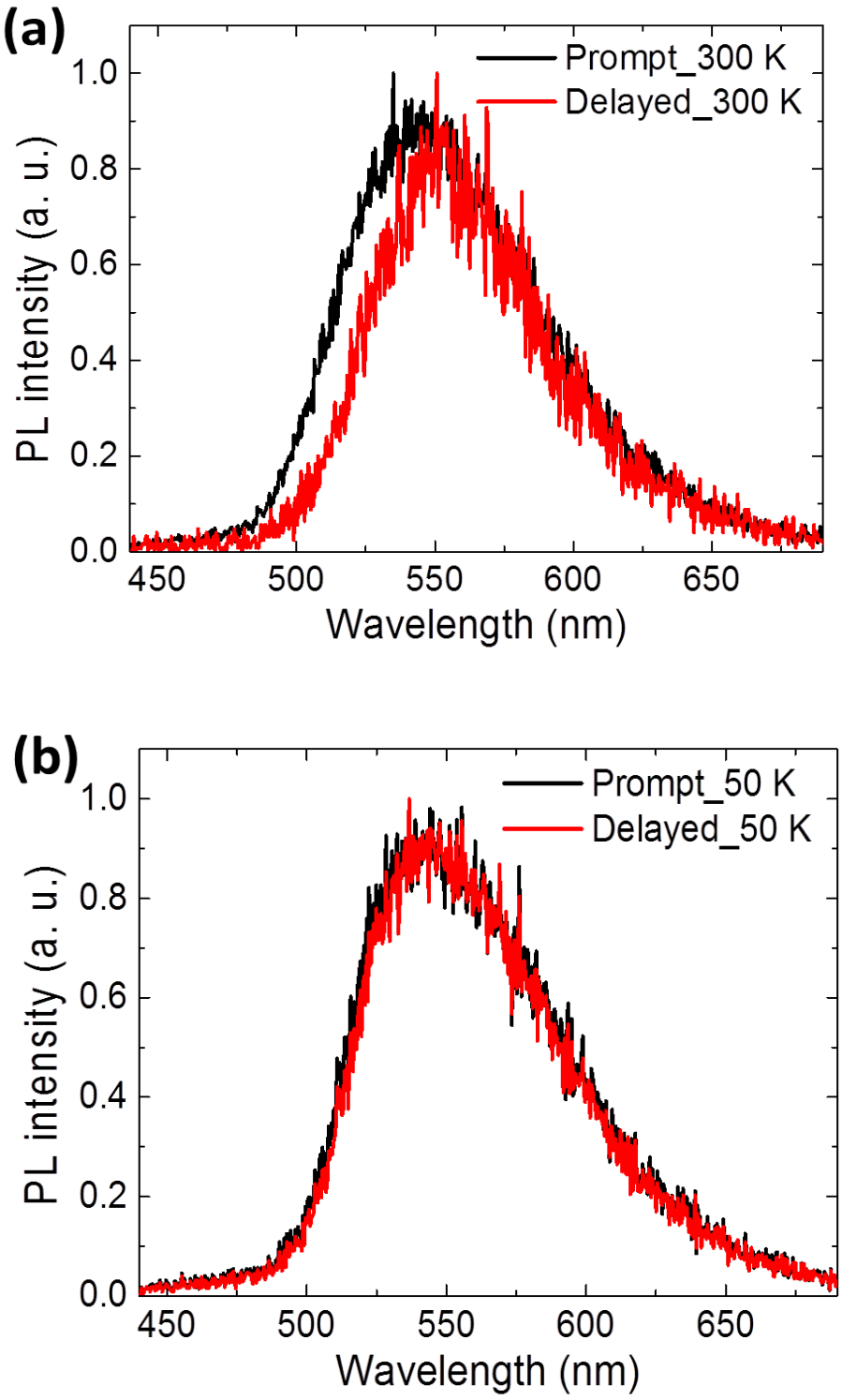
(a)
Prompt_300 K
Delayed_300 K
PL intensity (a. u.)
0.0
0.2
0.4
0.6
0.8
1.0
450
500
550
600
650
Wavelength (nm)
(b)
Prompt_50 K
Delayed_50 K
PL intensity (a. u.)
0.0
0.2
0.4
0.6
0.8
1.0
450
500
550
600
650
Wavelength (nm)

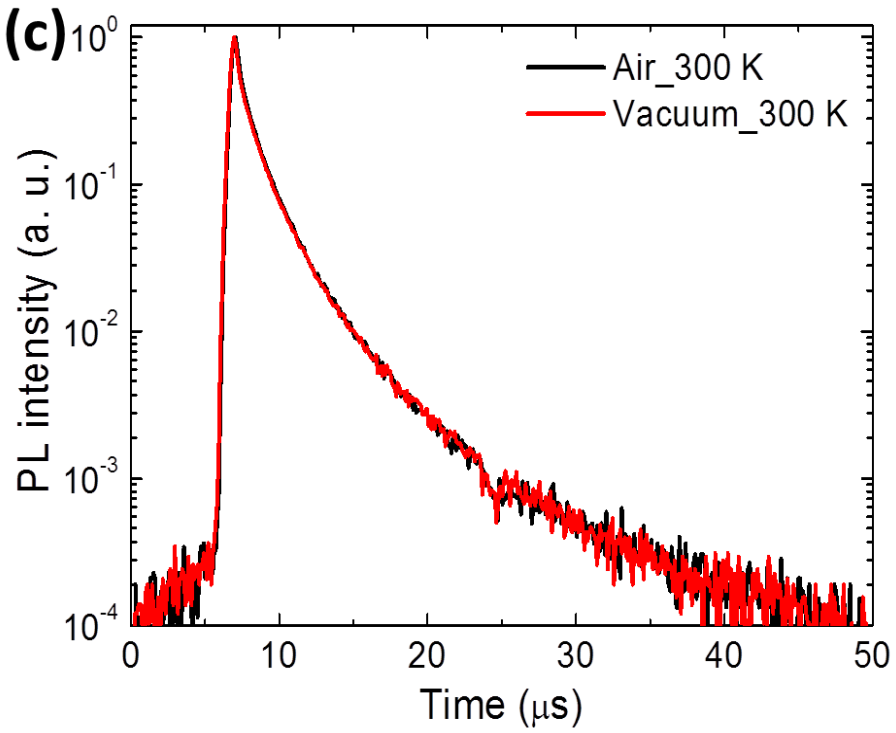

Figure 3-7. Transient PL decay properties of an 8 wt% **HAP-3MF**:**mCP** exciplex system. (a) Prompt and delayed PL spectra under vacuum condition at 300 K. (b) Prompt and delayed PL spectra under vacuum condition at 50 K. (c) Transient PL decay in air and under vacuum conditions at 300 K.

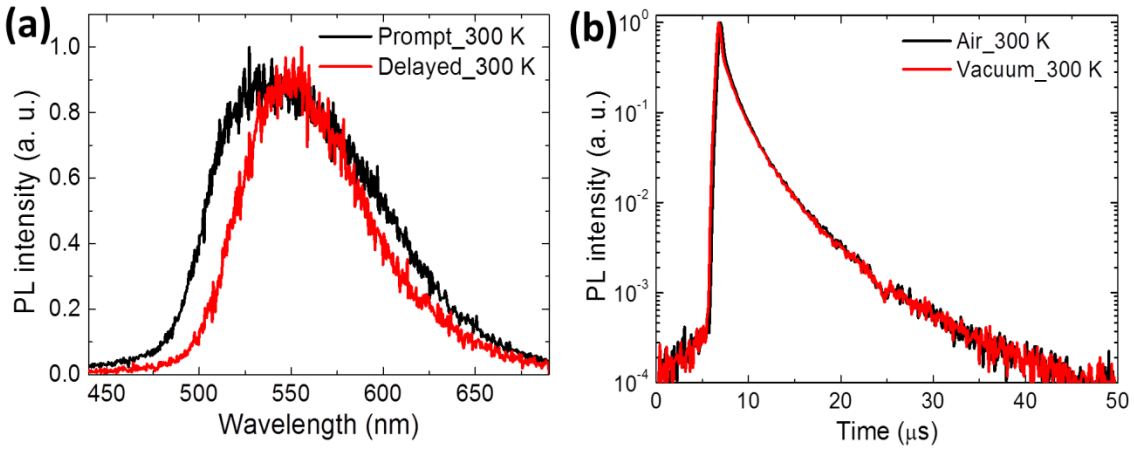

Figure 3-8. Transient PL decay properties of a 25 wt% **HAP-3MF**:**mCP** exciplex system. (a) Prompt and delayed PL spectra under vacuum condition at 300 K. (b) Transient PL decay in air and under vacuum conditions at 300 K.

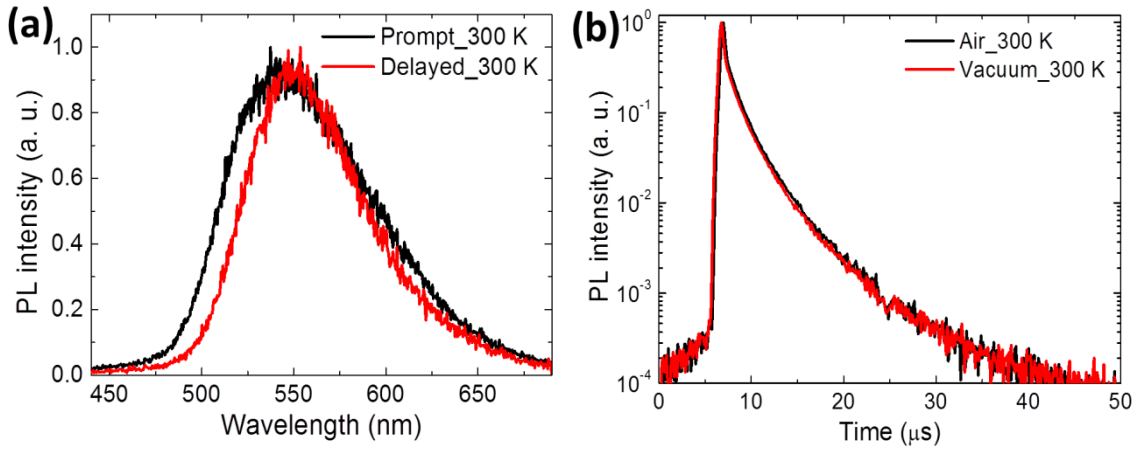

Figure 3-9. Transient PL decay properties of a 50 wt% **HAP-3MF**:**mCP** exciplex system. (a) Prompt and delayed PL spectra under vacuum condition at 300 K. (b) Transient PL decay in air and under vacuum conditions at 300 K.

3-4. OLED characteristics

Using the exciplex-based TADF characteristics, ExOLEDs containing **HAP-3MF**:**mCP** with various weight ratios were fabricated. The device structure was ITO/α-NPD (30 nm)/TCTA (10 nm)/**HAP-3MF**:**mCP** (20 nm)/DPEPO (10 nm)/TPBI (40 nm)/LiF (0.8 nm)/Al (100 nm), where ITO is anode, α-NPD acts as a hole transport layer, TPBI is 1,3,5-tris(*N*-phenylbenzimidazole-2-yl)benzene as an electron transport layer, and LiF and Al act as the cathode. Thin tris(4-(9H-carbazol-9-yl)phenyl)amine (TCTA) and bis(2-(diphenylphosphino) phenyl)ether oxide (DPEPO) layers were inserted to block electrons coming from the cathode and holes from the anode, respectively, and simultaneously confine the excitons in the emitting layer. The device structure and energy diagram are presented in Fig. 3-10. In accordance with PLQE trends, the ExOLED containing 8 wt% **HAP-3MF**:**mCP** exhibited best EL performance. Its EL spectra measured at 1, 10, and 100 mA cm^{-2} are shown in Fig. 3-11. The photon energy of the exciplex obtained from the onset of the EL spectra (490 nm) is determined to be 2.5 eV, which is consistent with the difference between the LUMO of **HAP-3MF** (3.4 eV) and HOMO of **mCP** (5.9 eV). Current density-voltage- luminance (*J*-*V*-*L*) characteristics of the ExOLED are depicted in Fig. 3-12. A low turn-on voltage of 4.0 V and quite high peak luminance of 22000 cd m^{-2} at 12.2 V were observed. More importantly, the ExOLED incorporating 8 wt% **HAP-3MF**:**mCP** as an emitting layer showed a rather high maximum EQE of 11.3% along with rather low roll-off characteristics, which is higher than those of 25 wt% (9.6%), 50 wt% (8.5%) and 100 wt% (0.53%) **HAP-3MF**:**mCP** systems (Fig. 3-13 and Fig. 3-14). Consequently, the EQE decreased as the weight ratio of **HAP-3MF** was increased. We believe that it should

be due to concentration quenching in consideration of relatively planar molecular geometry of **HAP-3MF.** The EQE substantially exceeds the theoretical maximum if the emitter is assumed to be a conventional fluorescent molecule. The theoretical maximum EQE can be calculated from the following equation, EQE = $\gamma \times \eta_r \times$ PLQE $\times \eta_{out}$, where γ is the electron/hole recombination ratio, η_r is the exciton formation ratio for radiative transitions (η_r = 0.25 for conventional fluorescent emitters), and η_{out} is the light out-coupling efficiency. Therefore, the theoretical maximum EQE should be limited to 3.3–5.0% when γ = 1.0, η_r = 0.25, PLQE = 66.1% and η_{out} = 0.2–0.3. However, based on the exciton formation mechanism of TADF, we estimate the theoretical maximum EQE is 12.1–18.1% based on Φ_{prompt} and $\Phi_{delayed}$ values, which results from efficient harvest of triplet exciplex excitons through reverse ISC from T_1 to S_1.[5d] Because our device structure was not fully optimized, higher EQE would be expected through careful device structure design. Thus, the extraordinarily high EQE of this ExOLED should be ascribed to efficient up-conversion of triplet exciplex excitons under electrical excitation.

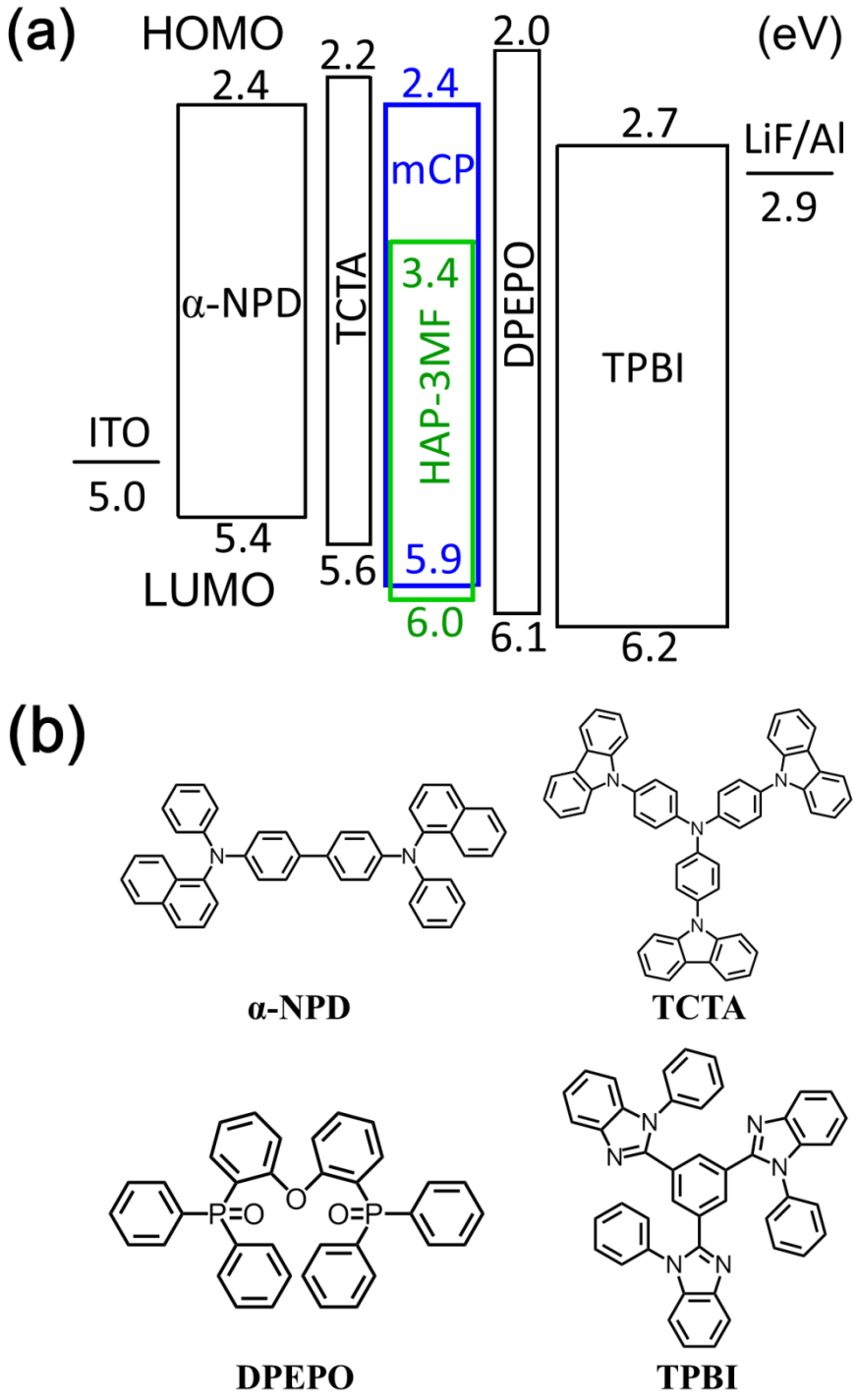

Figure 3-10. An ExOLED containing an 8 wt% **HAP-3MF**:**mCP** blend film as an emitting layer. (a) Device structure and energy level diagram. (b) Molecular structures of compounds used in the device.

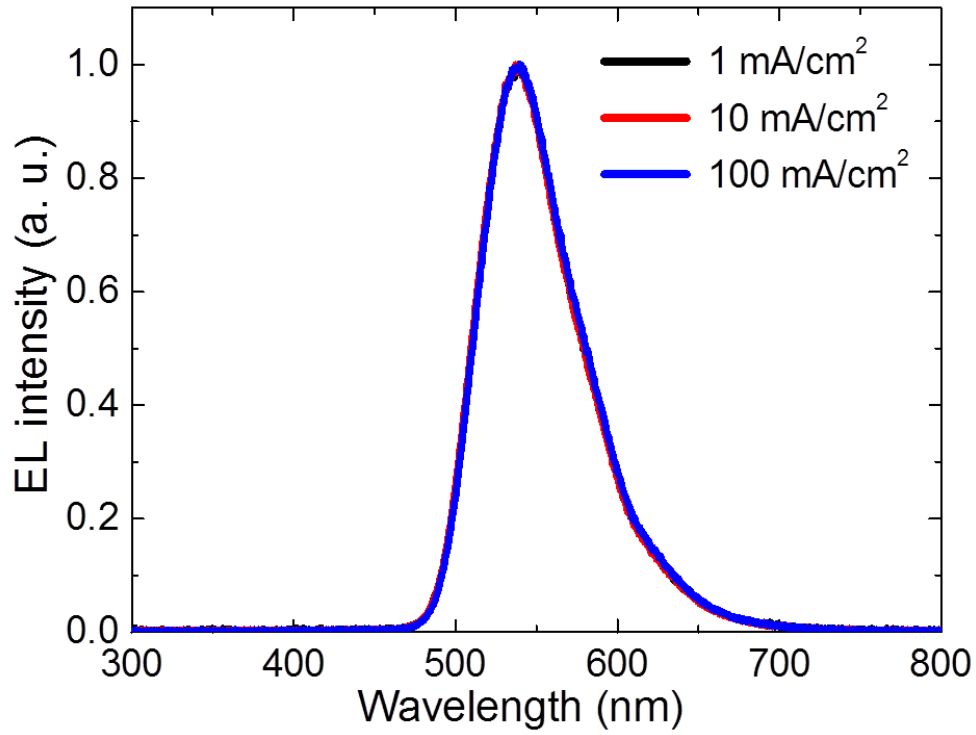

Figure 3-11. EL spectra recorded at various current densities.

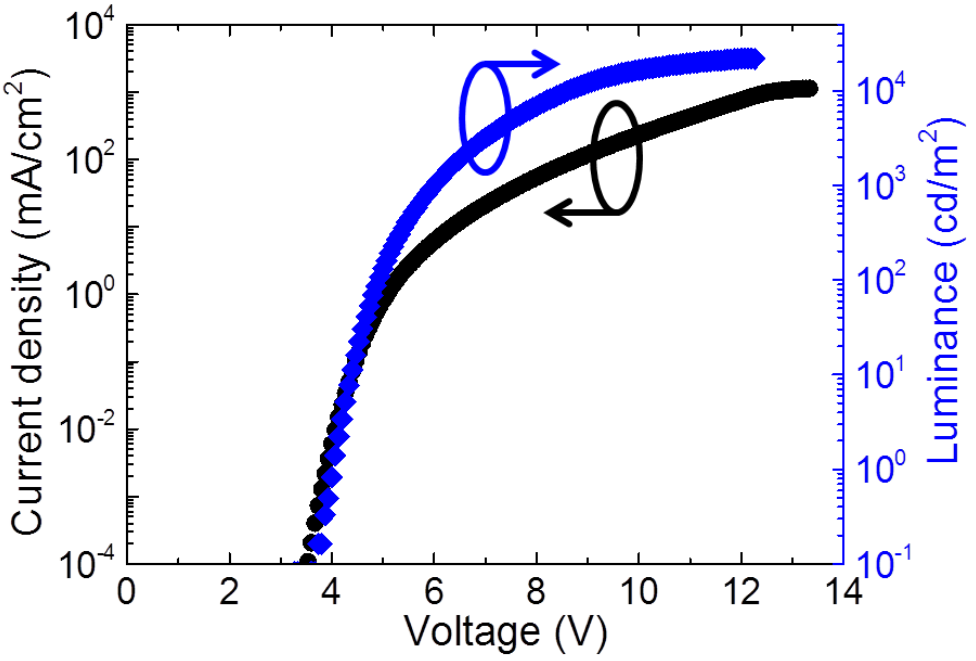

Figure 3-12. Current density-voltage-luminance (*J-V-L*) characteristics.

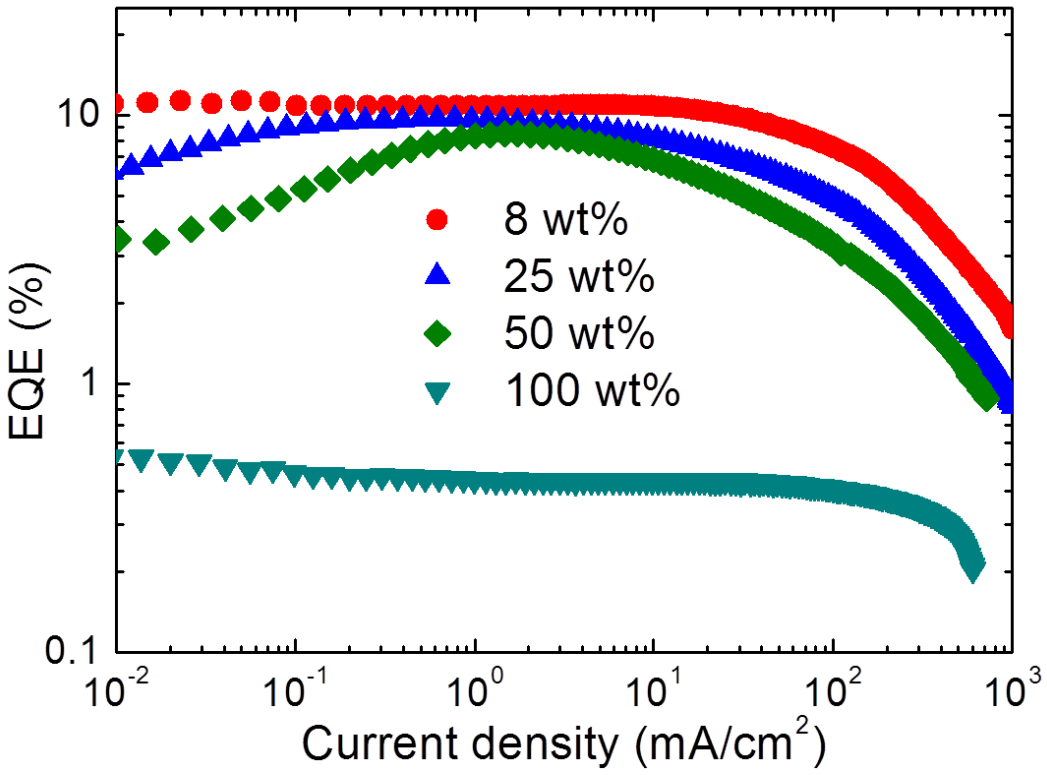

Figure 3-13. EQE as a function of current density for ExOLEDs containing 8 wt%, 25 wt%, 50 wt% and 100 wt% **HAP-3MF**:**mCP** blend films as emitting layers.

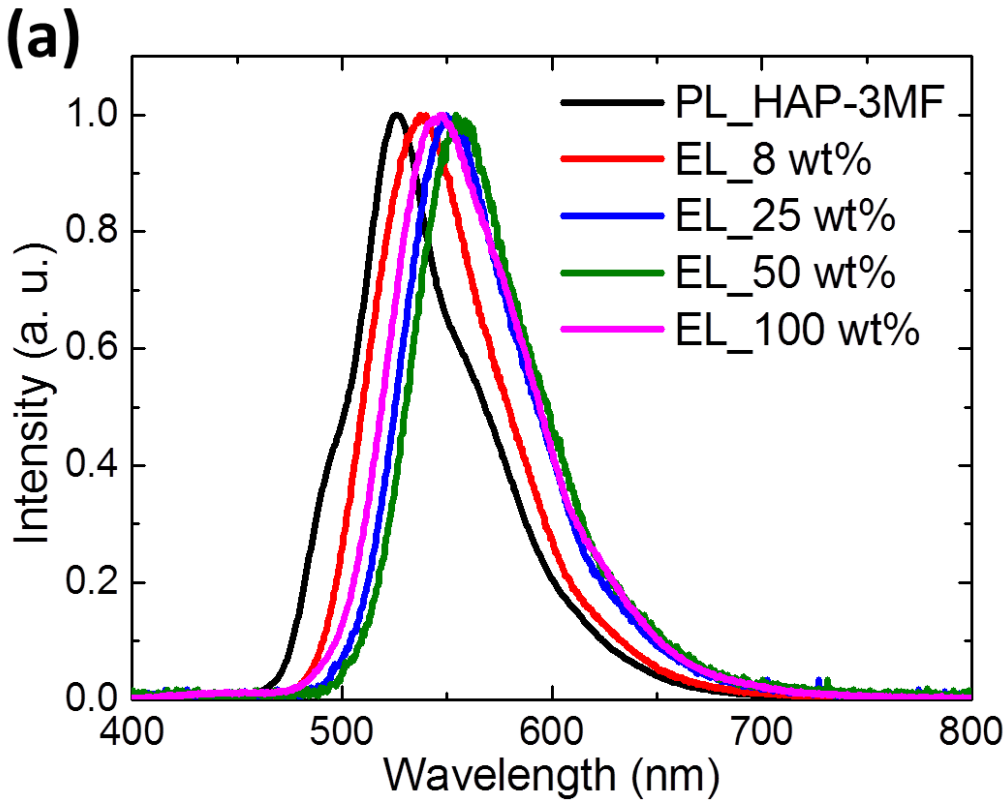

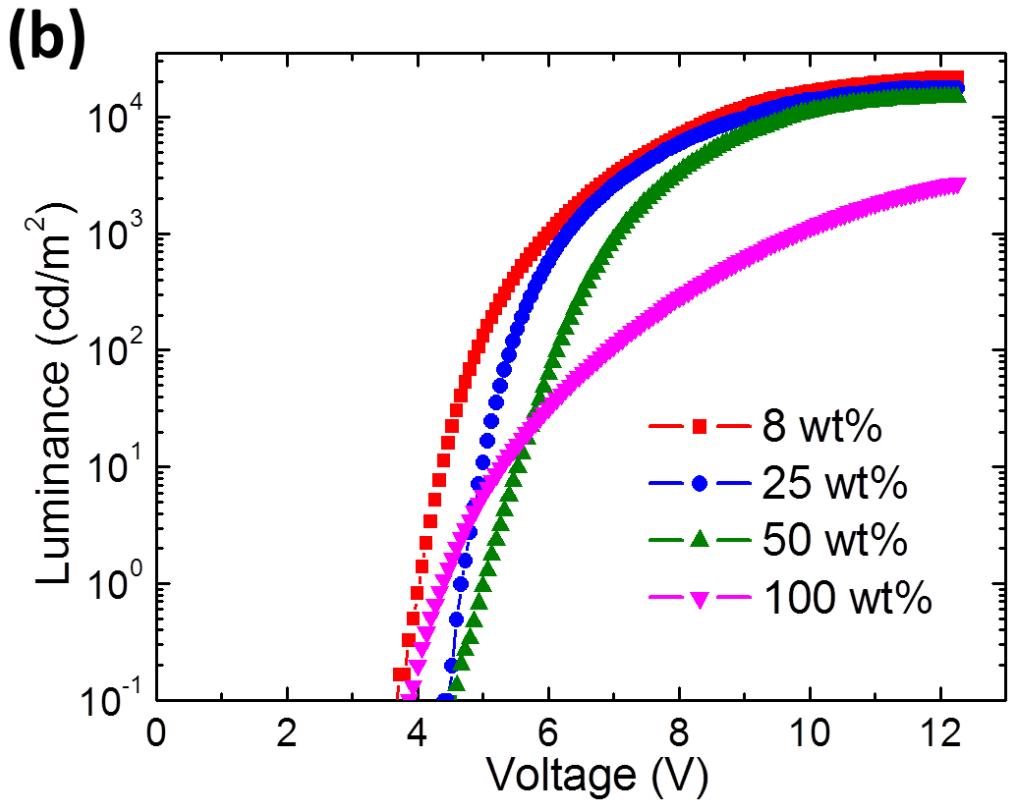

Figure 3-14 EL performance of ExOLEDs containing **HAP-3MF**:**mCP** systems with various weight ratios. (a) EL spectra at a current density of 10 mA/cm^2. The EL spectra for 8 wt%, 25 wt% and 50 wt% **HAP-3MF**:**mCP** systems are centered at 538 nm, 550 nm and 555 nm, respectively, which are highly consistent with their PL spectra. While for the OLED incorporating 100 wt% **HAP-3MF**:**mCP** system as an emitting layer, it should be noted that its EL spectrum (centered at 548 nm) was red-shifted as compared to the PL spectrum of 100 wt% **HAP-3MF**:**mCP** film (centered at 526 nm). This should be due to exciplex formation at the interface between TCTA and **HAP-3MF** in view of the OLED structure. (b) Luminance as a function of voltage. The maximum luminance follows the EQE trends, with 22000 cd/m^2 in 8 wt%, 17589 cd/m^2 in 25 wt%, 14866 cd/m^2 in 50 wt% and 2714 cd/m^2 in 100 wt% **HAP-3MF**:**mCP** systems. Therefore, the maximum luminance decreased as the weight ratio of **HAP-3MF** was increased. We believe that concentration quenching plays a very important role in the EL process based on planar molecular geometry of **HAP-3MF** and OLEDs performance.

3-5. Conclusion

We designed a highly efficient exciplex system of 8 wt% **HAP-3MF**:**mCP** with a very small ΔE_{ST}, resulting in efficient exciton up-conversion and a high PLQE of 66.1%. Using this exciplex system as an emitting layer in an ExOLED, a rather high EQE of 11.3% was obtained. These findings are of fundamental interest for the development of highly efficient OLEDs based on exciplex systems. Through elaborate molecular design and careful selection of electron donors and acceptors, we believe that ExOLEDs with enhanced efficiencies can be expected.

3-6. References

1. (a) C. W. Tang and S. A. VanSlyke, *Appl. Phys. Lett.*, 1987, **51**, 913; (b) J. H. Burroughes, D. D. C. Bradley, A. R. Brown, R. N. Marks, K. Mackay, R. H. Friend, P. L. Burns and A. B. Holmes, *Nature*, 1990, **347**, 539; (c) M. A. Baldo, D. F. O'Brien, Y. You, A. Shoustikov, S. Sibley, M. E. Thompson and S. R. Forrest, *Nature*, 1998, **395**, 151; (d) S. Reineke, F. Lindner, G. Schwartz, N. Seidler, K. Walzer, B. Lussem and K. Leo, *Nature*, 2009, **459**, 234.
2. (a) M. Cocchi, D. Virgili, V. Fattori, D. L. Rochester and J. A. G. Williams, *Adv. Func. Mater.*, 2007, **17**, 285; (b) Y.-C. Chiu, J.-Y. Hung, Y. Chi, C.-C. Chen, C.-H. Chang, C.-C. Wu, Y.-M. Cheng, Y.-C. Yu, G.-H. Lee and P.-T. Chou, *Adv. Mater.*, 2009, **21**, 2221; (c) Y.-S. Park, S. Lee, K.-H. Kim, S.-Y. Kim, J.-H. Lee and J.-J. Kim, *Adv. Funct. Mater.*, 2013, **23**, 4914.
3. (a) M. A. Baldo, M. E. Thompson and S. R. Forrest, *Nature*, 2000, **403**, 750; (b) W. C. Wu, H.-C. Yeh, L.-H. Chan and C.-T. Chen, *Adv. Mater.*, 2002, **14**, 1072.
4. (a) D. Y. Kondakov, T. D. Pawlik, T. K. Hatwar and P. Spindler, *J. Appl. Phys.*, 2009, **106**, 124510; (b) S. M. King, M. Cass, M. Pintani, C. Coward, F. B. Dias, A. P. Monkman and M. Roberts, *J. Appl. Phys.*, 2011, **109**, 074502.
5. (a) A. Endo, K. Sato, K. Yoshimura, T. Kai, A. Kawada, H. Miyazaki and C. Adachi, *Appl. Phys. Lett.*, 2011, **98**, 083302; (b) T. Nakagawa, S.-Y. Ku, K.-T. Wong and C. Adachi, *Chem. Commun.*, 2012, **48**, 9580; (c) G. Méhes, H. Nomura, Q. Zhang, T. Nakagawa and C. Adachi, *Angew. Chem. Int. Ed.*, 2012, **51**, 11311; (d) H. Tanaka, K. Shizu, H. Miyazaki and C. Adachi, *Chem. Commun.*, 2012, **48**, 11392; (e) Q. Zhang, J. Li, K. Shizu, S. Huang, S. Hirata, H. Miyazaki and C. Adachi, *J. Am. Chem. Soc.*, 2012, **134**, 14706; (f) H. Uoyama, K. Goushi, K. Shizu,

H. Nomura and C. Adachi, *Nature*, 2012, **492**, 234; (g) J. Li, T. Nakagawa, J. MacDonald, Q. Zhang, H. Nomura, H. Miyazaki and C. Adachi, *Adv. Mater.*, 2013, **25,** 3319.

6. (a) S. Iwata, J. Tanaka and S. Nagakura, *J. Chem. Phys.*, 1967, **47**, 2203; (b) K. Goushi, K. Yoshida, K. Sato and C. Adachi, *Nat. Photonics.*, 2012, **6**, 253.
7. (a) S. A. Jenekhe and J. A. Osaheni, *Science*, 1994, **265**, 765; (b) T. Noda, H. Ogawa and Y. Shirota, *Adv. Mater.*, 1999, **11**, 283; (c) Y. Shirota and H. Kageyama, *Chem. Rev.*, 2007**, 107**, 953; (d) S. L. Lai, M. Y. Chan, Q. X. Tong, M. K. Fung, P. F. Wang, C. S. Lee and S. T. Lee, *Appl. Phys. Lett.*, 2008, **93**, 143301; (e) W.-Y. Hung, G.-C. Fang, Y.-C. Chang, T.-Y. Kuo, P.-T. Chou, S.-W. Lin and K.-T. Wong, *ACS Appl. Mater. Inter.*, 2013, **5**, 6826; (f) D. Graves, V. Jankus, F. B. Dias and A. Monkman, *Adv. Funct. Mater.*, 2014, **24**, 2343.
8. K. Goushi and C. Adachi, *Appl. Phys. Lett.*, 2012, **101**, 023306.
9. Q. Wang, J. Ding, D. Ma, Y. Cheng, L. Wang, X. Jing and F. Wang, *Adv. Funct. Mater.*, 2009, **19**, 84.
10. B. Jürgens, E. Irran, J. Senker, P. Kroll, H. Müller and W. Schnick, *J. Am. Chem. Soc.*, 2003, **125**, 10288.
11. (a) R. S. Hosmane, M. A. Rossman and N. J. Leonard, *J. Am. Chem. Soc.*, 1982, **104**, 5497; (b) E. Kroke, M. Schwarz, E. Horath-Bordon, P. Kroll, B. Noll and A. D. Norman, *New J. Chem.*, 2002, **26**, 508.
12. W. Zheng, N.-B. Wong, W. Wang, G. Zhou and A. Tian, *J. Phys. Chem. A*, 2004, **108**, 97.
13. D. R. Miller, D. C. Swenson and E. G. Gillan, *J. Am. Chem. Soc.* 2004, **126**, 5372.

Chapter 4

Thermally Activated Delayed Fluorescence from ^{3}n-π^* to ^{1}n-π^* Up-Conversion and Its Application to Organic Light-Emitting Diodes

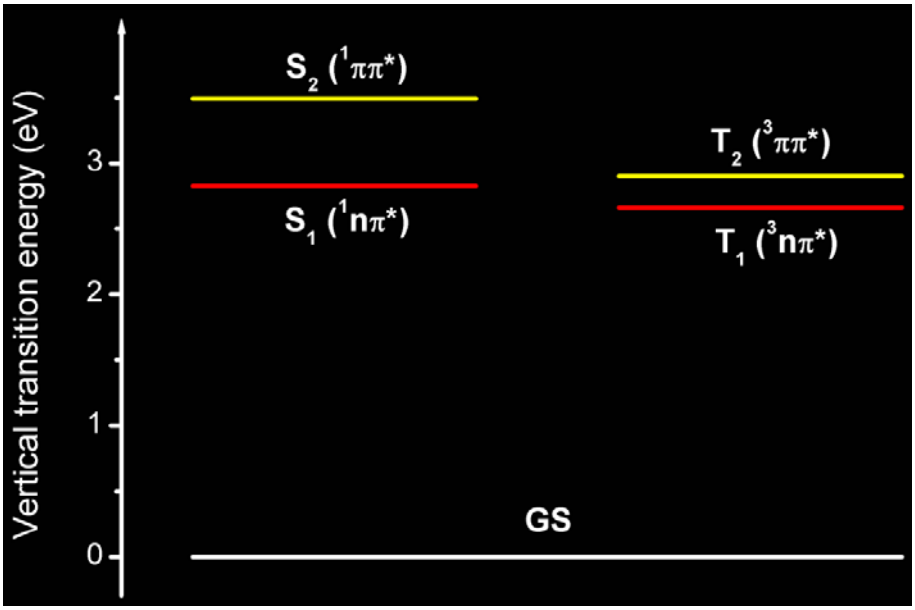

J. Li, Q. Zhang, H. Nomura, H. Miyazaki, and C. Adachi, *Appl. Phys. Lett.*, 2014, **105**, 013301.

4-1. Introduction

The most important design consideration of TADF molecules is to obtain a small energy gap between the S_1 and T_1 states (ΔE_{ST}). A molecule meets this requirement only when its lowest-energy transition has a small singlet–triplet exchange energy.[1] Current trends in the development of TADF emitters are focusing on intramolecular or intermolecular donor-acceptor (D-A)-type molecules, because charge-transfer (CT) transitions always have small singlet-triplet splitting owing to the small exchange integral between the involved wave functions.[2-13] Alternatively, more localized n-π* transitions are also overlap-forbidden and tend to have small singlet-triplet splitting. Although TADF has been observed from several aromatic ketones, these compounds emit weakly because of very slow radiative decay from the ^{1}n-π* state.[1] In our recent study, we reported an efficient CT-type TADF emitter (**HAP-3TPA**) with three triphenylamine units as donors and a heptazine core as an acceptor.[9] During the survey of heptazine derivatives, we observed bright green luminescence from **HAP-3MF** which has an acceptor-only structure, which can act as an intermediate in the synthesis of such kind of D-A-type compounds and an electron acceptor in exciplex systems.[13] In this study, an OLED employing **HAP-3MF** as the emitter achieved a maximum IQE exceeding the limit assuming that emission arises from conventional fluorescence alone, implying a hidden, efficient TADF pathway is operating in this n-π* emitter.

4-2. Molecular design

HAP-3MF, which is composed of a heptazine core and three 2-fluorotoluene groups, was chosen as an ideal n-π* emitter. This is because **HAP-3MF** contains a highly conjugated heterocyclic ring system and the n-π* electronic transition would easily take place involving the lone pairs of the nitrogen atoms.

The little spatial overlap between n and π* orbitals means that the singlet-triplet splitting of n-π* transitions is expected to be small in **HAP-3MF**. However, the precise nature of the T_1 state of **HAP-3MF** is unknown because **HAP-3MF** shows no phosphorescence (>10 ms delayed) in frozen solution at 77 K. To better understand the nature of the frontier orbitals of **HAP-3MF**, density functional theory (DFT) and time-dependent DFT (TD-DFT) calculations were carried out at the B3LYP/6-31G(d) level using the Gaussian 09 program.[14] Details of the quantum chemical calculations are as follows.

Optimized geometry data for **HAP-3MF** (unit: Å):

N	1.76384506	-1.81856122	-0.00000053
C	0.47625858	-1.48345137	-0.00000350
N	0.12138004	-0.12321647	-0.00001153
C	1.12178981	0.86419912	-0.00000774
N	2.39976560	0.49395024	-0.00000456
C	2.66873934	-0.82370679	-0.00000241
N	-0.48348614	-2.40508681	-0.00000028
C	-1.75892316	-1.97924496	-0.00000346
N	-2.16800006	-0.69809067	-0.00000851
C	-1.23380262	0.24927078	-0.00001064

N	-1.55231974	1.54132566	-0.00001169
C	-0.54573881	2.43300865	-0.00001060
N	0.76827037	2.14691225	-0.00000838
C	4.08975096	-1.21564084	-0.00000105
C	-2.80756116	-3.01528093	0.00000043
C	-0.91671338	3.85975578	-0.00000748
C	5.09531788	-0.23217646	0.00000312
C	6.44769891	-0.56838594	0.00000479
C	6.75536997	-1.93335769	-0.00000023
C	5.79207576	-2.93566443	-0.00000632
C	4.44995767	-2.57330071	-0.00000541
C	-4.16531741	-2.64806961	-0.00002063
C	-5.18131321	-3.60185327	-0.00001779
C	-4.78378655	-4.94336526	0.00000778
C	-3.45374556	-5.34768938	0.00002290
C	-2.45941818	-4.37606094	0.00002071
C	-2.27112690	4.23921810	-0.00000575
C	-2.65521327	5.57883316	0.00000160
C	-1.62669565	6.52748249	0.00000163
C	-0.27717876	6.19398133	-0.00000586
C	0.07914625	4.85026260	-0.00000765
F	8.05729793	-2.28935603	-0.00000018
F	-5.74661314	-5.88930346	0.00001639
F	-1.96908215	7.83311670	0.00000611

C	7.54874976	0.46122782	0.00002132
C	-4.09699622	6.01896575	0.00003220
C	-6.64490613	-3.24081292	-0.00001298
H	4.79811061	0.81103877	0.00000373
H	6.10509501	-3.97447250	-0.00001149
H	3.67072566	-3.32633917	-0.00000915
H	-4.41561280	-1.59264776	-0.00004482
H	-3.21954515	-6.40704916	0.00003660
H	-1.41174221	-4.65306520	0.00003236
H	-3.02659402	3.46083897	-0.00001252
H	0.46625246	6.98415325	-0.00000958
H	1.12069172	4.55122510	-0.00001166
H	7.13303944	1.47241791	-0.00012257
H	8.19347133	0.35524014	0.88030803
H	8.19366638	0.35506133	-0.88009865
H	-4.76592745	5.15418140	-0.00033243
H	-4.32680009	6.63050044	0.88039547
H	-4.32664221	6.63114456	-0.87991903
H	-6.77562280	-2.15535133	-0.00043320
H	-7.15593593	-3.64860518	-0.87998266
H	-7.15574723	-3.64788156	0.88040725

Excitation energies and oscillator strengths for **HAP-3MF**:

Excited State 1: Triplet-A 2.6604 eV 466.04 nm f=0.0000 <S**2>=2.000

128 ->129 0.69622

Excited State 2: Singlet-A 2.8256 eV 438.79 nm f=0.0002 <S**2>=0.000

128 ->129 0.69356

Excited State 3: Triplet-A 2.9027 eV 427.13 nm f=0.0000 <S**2>=2.000

125 ->131 0.20239

126 ->130 -0.13805

127 ->129 0.60219

127 ->131 0.12223

Excited State 4: Triplet-A 2.9133 eV 425.58 nm f=0.0000 <S**2>=2.000

125 ->130 0.18694

126 ->129 0.59877

126 ->131 -0.13889

127 ->130 -0.14100

Excited State 5: Triplet-A 2.9543 eV 419.68 nm f=0.0000 <S**2>=2.000

125 ->129 0.54832

126 ->130 0.24468

127 ->131 0.26421

Excited State 6: Triplet-A 3.2268 eV 384.23 nm f=0.0000 <S**2>=2.000

128 ->131 0.67681

Excited State 7: Triplet-A 3.2290 eV 383.97 nm f=0.0000 <S**2>=2.000

126 ->130 -0.11321

128 ->130 0.66783

128 ->136 0.10437

Excited State 8: Singlet-A 3.4924 eV 355.02 nm f=0.4590 <S**2>=0.000

127 ->129 0.69925

Excited State 9: Singlet-A 3.5145 eV 352.77 nm f=0.4793 <S**2>=0.000

126 ->129 0.69898

Excited State 10: Singlet-A 3.5513 eV 349.12 nm f=0.0000 <S**2>=0.000

119 ->130 -0.10024

120 ->131 0.10222

121 ->129 0.68880

Excited State 11: Singlet-A 3.5669 eV 347.59 nm f=0.0000 <S**2>=0.000

120 ->129 0.68191

121 ->131 0.13163

Excited State 12: Singlet-A 3.5840 eV 345.94 nm f=0.0000 <S**2>=0.000

119 ->129 0.68187

121 ->130 -0.12930

As shown in Fig. 4-1a, in the ground state, the HOMO is mainly associated with the sp^2-hybridized N atom in the heptazine core, while the calculated LUMO is distributed over the whole π-conjugated system. This distribution is consistent with our previous assumption that the lowest-energy transition has n-π^* character. On the basis of this ground-state electronic structure, the vertical energies of S_1 (HOMO→LUMO) and S_2 (HOMO-1→LUMO) transitions were calculated to be 2.8256 eV (439 nm) and 3.4924 eV (355 nm), respectively, with oscillator strengths (*f*) of 0.0002 and 0.4590, respectively. Both the transition energies and relative intensities of *f* are in accordance with the experimental results in toluene. Because the orbitals involved in the T_1 transition are similar to those involved in the S_1 transition, the T_1 state of **HAP-3MF** can be assigned to a ^{3}n-π^* state. The energy difference between S_1 (^{1}n-π^*) and T_1

(^{3}n-π*) states is calculated to be as small as 0.165 eV. Although the singlet-triplet splitting of a localized π-π* transition is always much larger than that of an n-π* transition, the $^3\pi$-π* state (T_2) was calculated to be higher than the ^{3}n-π* state (T_1) by just 0.24 eV (Fig. 4-1b) because of the short conjugation length of **HAP-3MF**.

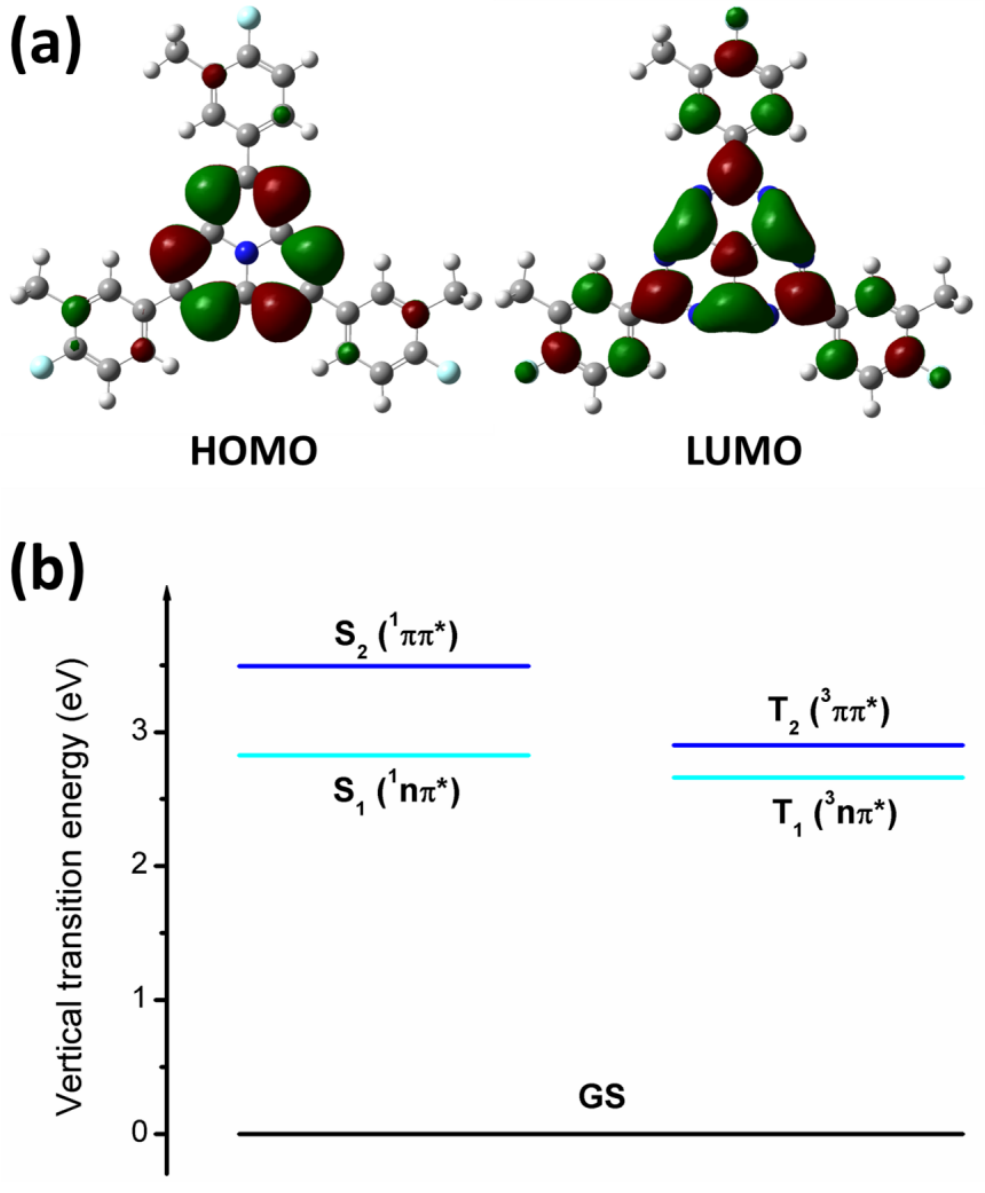

Figure 4-1. (a) HOMO and LUMO and (b) singlet and triplet energy levels of **HAP-3MF** calculated at the B3LYP/6-31G(d) level.

4-3. Optical properties

4-3-1. Solution

The UV-vis absorption and PL spectra of **HAP-3MF** in toluene at room temperature (RT) are presented in Fig. 4-2. Both the low-energy absorption band centered around 450 nm and the emission band centered around 520 nm exhibit well-resolved vibronic structure, indicating a narrow conformational distribution in both ground and excited states as a result of the rigid molecular structure of **HAP-3MF**. The intense absorption with a maximum at 327 nm is assigned to the π-π* transition of this π-conjugated system, while the low-intensity absorption band with a maximum at 450 nm (ε ~200 $M^{-1}\cdot cm^{-1}$) is attributed to the n-π* transition involving the lone pairs of N heteroatoms and a π anti-bonding molecular orbital by reference to other nitrogen heterocycles.[15-17] To confirm the n-π* character of the S_1 transition of **HAP-3MF**, its UV-vis absorption spectrum was also recorded in a more polar solvent, acetonitrile (Fig. 4-2). As expected, a typical blue shift of the S_1 transition band was observed, which is caused by the ability of polar solvents to stabilize lone electron pairs.[18] The PLQY of **HAP-3MF** in toluene at RT was Φ_F = 0.26, and it exhibited a rather long fluorescence lifetime (τ_F) of 252 ns. The radiative rate constant of fluorescence (k_F) of **HAP-3MF** was calculated to be 1.0×10^{-6} s^{-1} according to the equation $k_F = \Phi_F/\tau_F$. The extremely low fluorescence rate and absorption coefficient of **HAP-3MF** are typical characteristics of n-π* transitions, and are directly related to their small transition dipole moment. However, the rigid, extended π-conjugated backbone of **HAP-3MF** suppresses non-radiative decay, leading to a relatively high PLQY among molecules exhibiting n-π* transitions.[1]

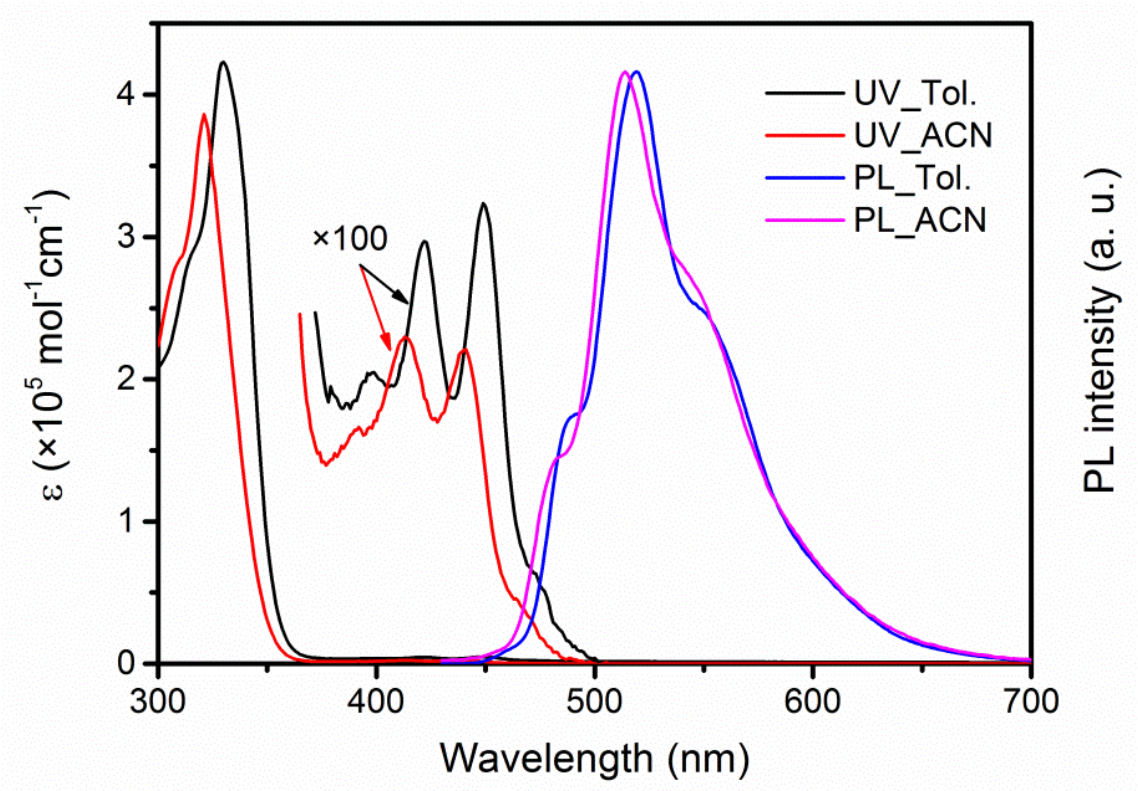

Figure 4-2. UV-vis absorption and PL spectra of **HAP-3MF** in toluene (Tol.) and acetonitrile (ACN).

Although ΔE_{ST} predicted by the TD-DFT calculation is small enough for thermal repopulation of the S_1 state *via* $T_1 \rightarrow S_1$ reverse intersystem crossing at RT, it is difficult to observe TADF from **HAP-3MF**. As shown in Fig. 4-3, in air-equilibrated toluene, the emission decay of **HAP-3MF** can be well fitted by a single exponential with a lifetime of 252 ns. In oxygen-free toluene, the emission intensity of the long-lived component increases slightly, which is consistent with TADF.

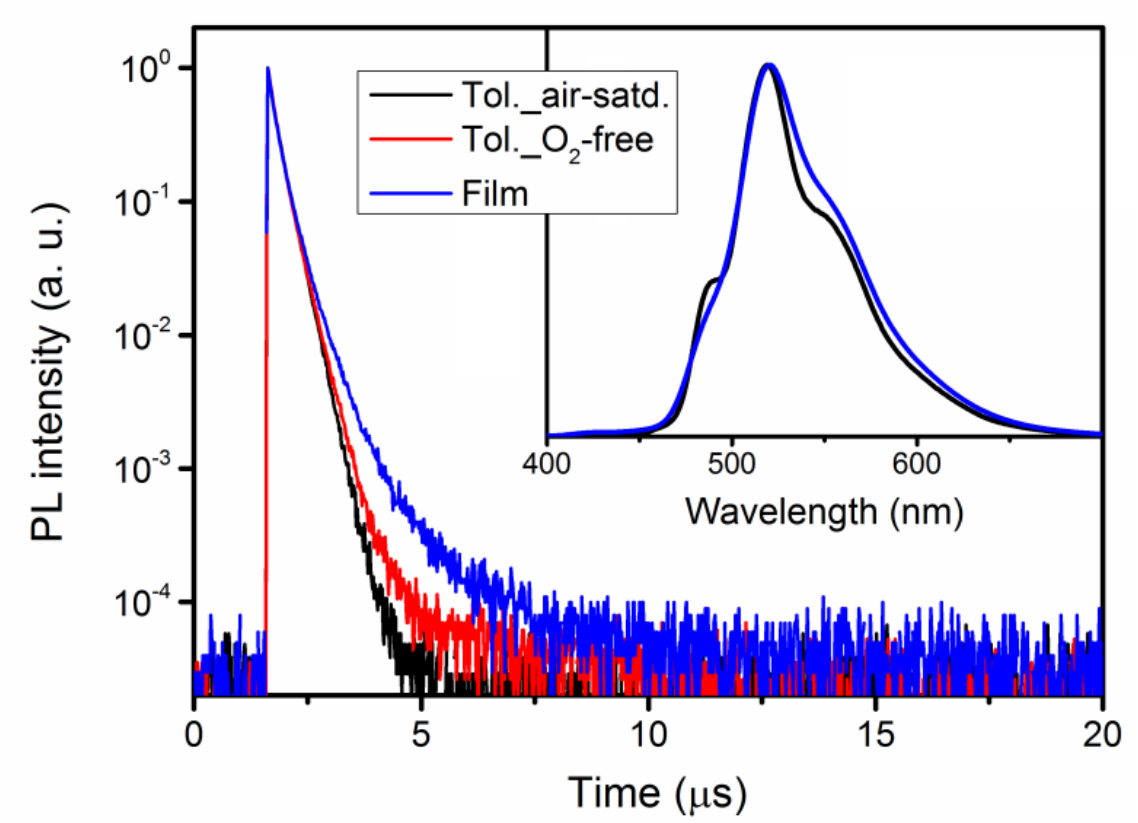

Figure 4-3. Transient PL decay of **HAP-3MF** in toluene and DPEPO film (6 wt%) at RT. Inset: PL spectra of **HAP-3MF** in toluene and DPEPO film (6 wt%).

4-3-2. Doped film

The transient PL decay characteristics of **HAP-3MF** were also measured in a 6 wt%-doped bis(2-(diphenylphosphino)phenyl) ether oxide (DPEPO) film under vacuum.[19] A more intense delayed component is observed in the transient decay spectrum of **HAP-3MF** in the solid film, probably because the rigid matrix suppresses non-radiative processes in the ^{3}n-π* state and allows more energy to up-convert to the emissive ^{1}n-π* state. However, even in the solid film, the percentage of the delayed component in the total emission is still less than 4%, as estimated from Fig. 4-3. The low intensity of both TADF and phosphorescence of HAP-3MF can be a result of the

El-Sayed rule,[20] which indicates a forbidden nature of the intersystem crossing (ISC) from ^{1}n-π* to ^{3}n-π* state. The ISC rate is therefore considerably lower than the sum of the radiative and non-radiative decay rates of ^{1}n-π* to ground state. However, the excitons formed directly in the T_1 state of HAP-3MF can efficiently up-convert to the S_1 state in the case of EL, because the ISC rate of $T_1 \rightarrow S_1$ is low but more competitive than that of $T_1 \rightarrow S_0$ according to the energy-gap law. In addition, a nearby T_2 state (0.24 eV above the T_1 state) revealed by TD-DFT may be involved in the TADF process and provide a fast symmetry-allowed transition from it ($^3\pi$-π*) to S_1 (^{1}n-π*) state. The schematic representation of PL and EL decay processes in HAP-3MF are illustrated in Fig. 4-4.

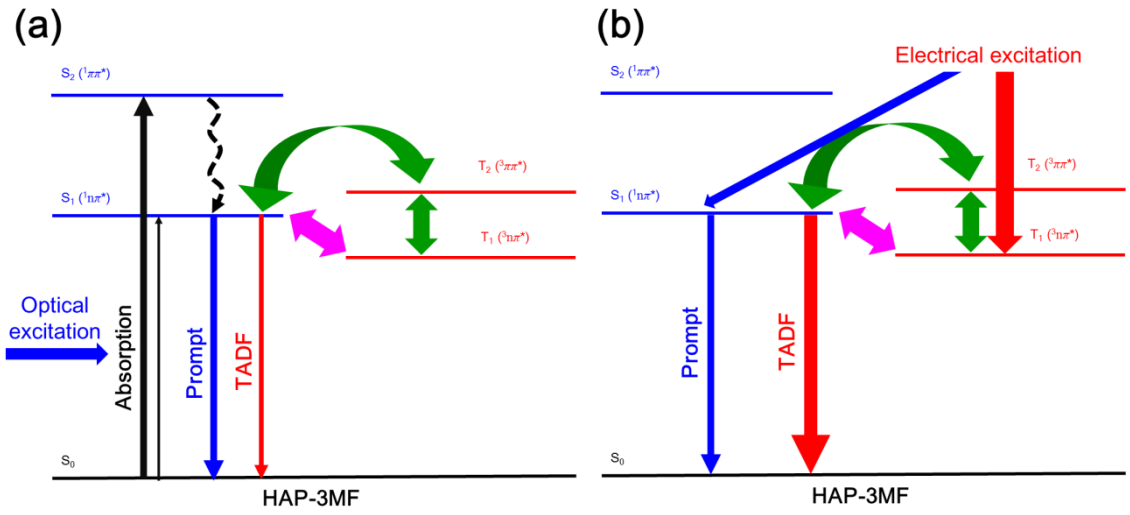

Figure 4-4. Schematic representation of (a) PL and (b) EL decay processes in HAP-3MF.

4-4. OLED characteristics

4-4-1. OLED performance

To verify the unique EL characteristics of **HAP-3MF**, an OLED containing an emitting layer of 6 wt% **HAP-3MF**:DPEPO was fabricated. The OLED structure and energy diagram are presented in Fig. 4-5a. ITO was used as an anode, α-NPD as a hole transport layer, TPBI as an electron transport layer, and LiF and Al acted as the cathode. Thin layers of mCP and DPEPO with high triplet energies were inserted to confine the triplet excitons in the emitting layer. The EL spectra of this device measured at 1, 10, and 100 mA/cm^2 (inset of Fig. 4-5b) are similar, and in good accordance with the PL of the emitting layer. Importantly, the OLED showed a rather high maximum EQE of 6.0% (Fig. 4-5b) without any light out-coupling enhancement architecture. This EQE exceeds the theoretical maximum assuming that the emitter is a conventional fluorescent material. The theoretical maximum EQE can be calculated from the following formula, EQE = $\gamma \times \eta_r \times$ PLQY $\times \eta_{out}$, where γ is the electron/hole recombination ratio, η_r is the exciton formation ratio for radiative transitions (η_r = 0.25 for conventional fluorescent emitters), and η_{out} is the light out-coupling efficiency. According to this formula, the theoretical maximum EQE should be limited to 1.3–2.0% when γ = 1.0, η_r = 0.25, PLQY = 0.26 and η_{out} = 0.2–0.3. Thus, the high efficiency of this device should be ascribed to the TADF pathway in **HAP-3MF**, which harvests emissive singlet excitons from the long-lived triplet excitons by efficient up-conversion.

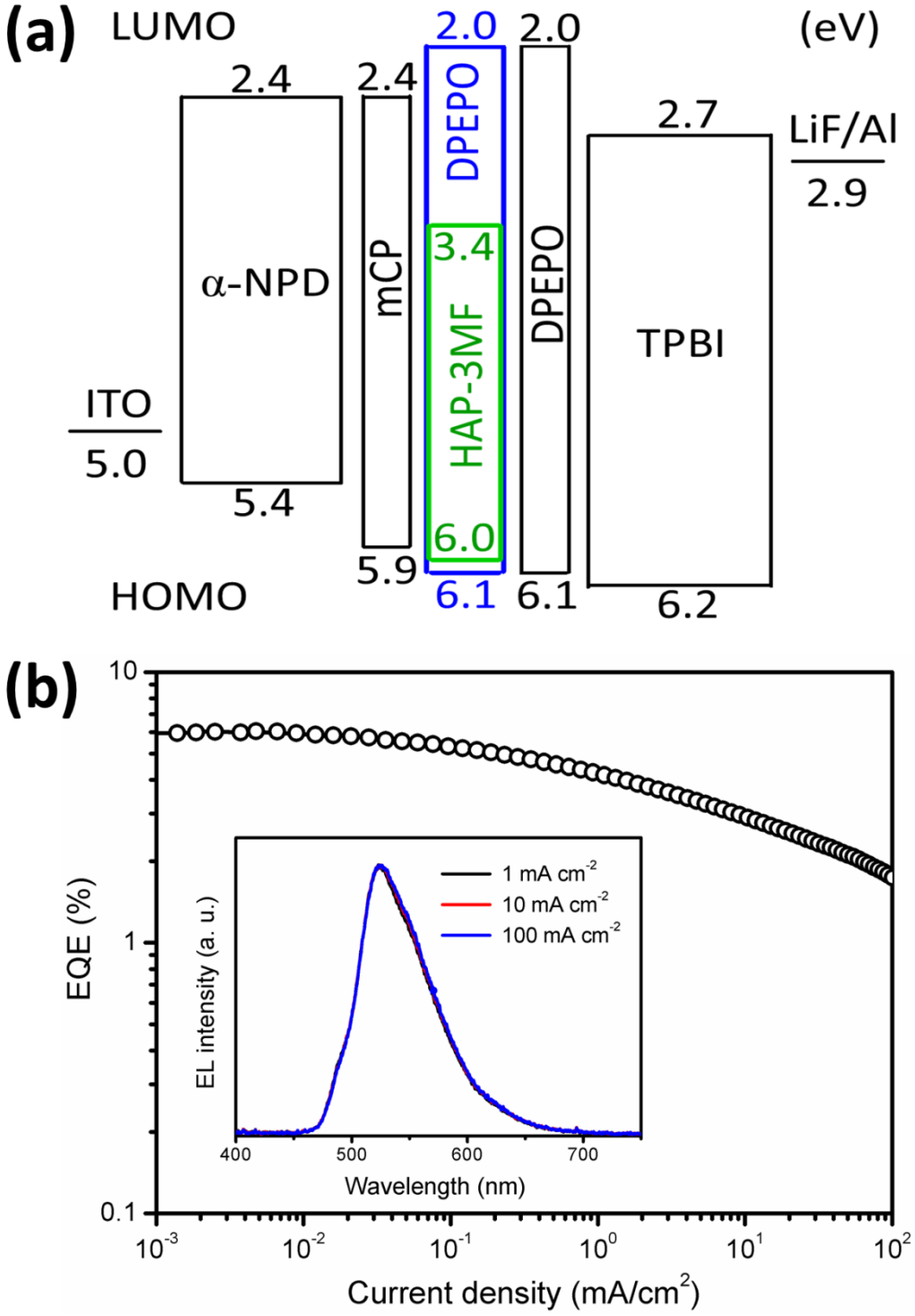

Figure 4-5. EL performance of an OLED containing 6 wt% **HAP-3MF**:DPEPO as an emitting layer. (a) Device structure and energy diagram. (b) EQE as a function of current density. Inset: EL spectra recorded at various current densities.

4-4-2. Transient electroluminescence

To obtain definitive evidence of the contribution of triplet excitons from the TADF pathway, time-resolved EL measurements in the time range of 100 μs and 10 ms were performed with an electrical excitation pulse of 500 ns at RT. As expected, long-lifetime delayed components which can be attributed to TADF were clearly observed from the transient EL spectra (Fig. 4-6). On the basis of the integrals of prompt and delayed components, the percentage of the delayed one was calculated to be as high as 71% which is much higher than that in the PL process, confirming an efficient conversion of triplet excitons to singlet ones in this HAP-3MF based OLEDs.

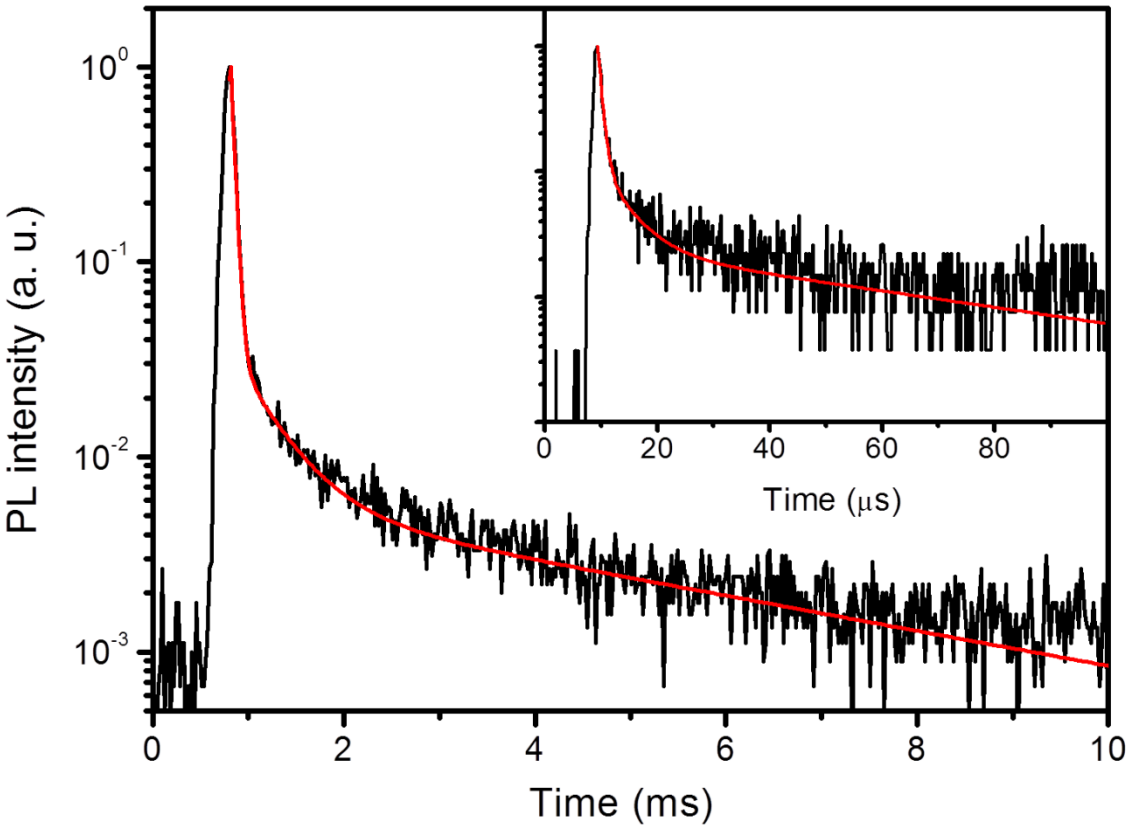

Figure 4-6. Transient EL decay (black) and fitting (red) in the time range of 10 ms and 100 μs (inset) for an OLED containing 6 wt% **HAP-3MF**:DPEPO as an emitting layer.

4-5. Conclusion

Intense n-π* fluorescence from a nitrogen-rich heterocyclic compound, 2,5,8-tris(4-fluoro-3-methylphenyl)-1,3,4,6,7,9,9b-heptaazaphenalene (HAP-3MF), is demonstrated. The overlap-forbidden nature of the n-π* transition and the higher energy of the $^3\pi$-π* state than the ^{3}n-π* one lead to a small energy difference between the S_1 and T_1 excited states of HAP-3MF. Green-emitting HAP-3MF has a moderate Φ_F = 0.26 in both toluene and doped film. However, an OLED containing HAP-3MF achieved a high EQE = 6.0%, indicating that HAP-3MF harvests singlet excitons through a thermally activated $T_1 \rightarrow S_1$ pathway in the EL process. These results reveal that n-π* emitters are a type of TADF materials and are suitable for OLED applications. We believe that further design and synthesis of TADF emitters based on n-π* transitions will realize unique light-emitting materials.

4-6. References

1. N. J. Turro, *Modern Molecular Photochemistry*. (University Science Books, 1991).
2. A. Endo, M. Ogasawara, A. Takahashi, D. Yokoyama, Y. Kato, and C. Adachi, *Adv. Mater.* **21**, 4802 (2009).
3. A. Endo, K. Sato, K. Yoshimura, T. Kai, A. Kawada, H. Miyazaki, and C. Adachi, *Appl. Phys. Lett.* **98**, 083302 (2011).
4. K. Goushi, K. Yoshida, K. Sato, and C. Adachi, *Nat. Photon.* **6**, 253 (2012).
5. T. Nakagawa, S. Y. Ku, K. T. Wong, and C. Adachi, *Chem. Commun.* **48**, 9580 (2012).
6. G. Méhes, H. Nomura, Q. Zhang, T. Nakagawa, and C. Adachi, *Angew. Chem. Int. Ed.* **51**, 11311 (2012).
7. Q. Zhang, J. Li, K. Shizu, S. P. Huang, S. Hirata, H. Miyazaki, and C. Adachi, *J. Am. Chem. Soc.* **134**, 14706 (2012).
8. H. Uoyama, K. Goushi, K. Shizu, H. Nomura, and C. Adachi, *Nature* **492**, 234 (2012).
9. J. Li, T. Nakagawa, J. MacDonald, Q. Zhang, H. Nomura, H. Miyazaki, and C. Adachi, *Adv. Mater.* **25**, 3319 (2013).
10. Q. Zhang, B. Li, S. P. Huang, H. Nomura, H. Tanaka, and C. Adachi, *Nat. Photon.* **8**, 326 (2014).
11. W. Y. Hung, G. C. Fang, Y. C. Chang, T. Y. Kuo, P. T. Chou, S. W. Lin, and K. T. Wong, *ACS Appl. Mater. Inter.* **5**, 6826 (2013).
12. D. Graves, V. Jankus, F. B. Dias, and A. Monkman, *Adv. Funct. Mater.* **24**, 2343 (2014).
13. J. Li, H. Nomura, H. Miyazaki, and C. Adachi, *Chem. Commun.* **50**, 6174 (2014).

14. M. J. Frisch, G. W. Trucks, H. B. Schlegel, G. E. Scuseria, M. A. Robb, J. R. Cheeseman, G. Scalmani, V. Barone, B. Mennucci, G. A. Petersson, H. Nakatsuji, M. Caricato, X. Li, H. P. Hratchian, A. F. Izmaylov, J. Bloino, G. Zheng, J. L. Sonnenberg, M. Hada, M. Ehara, K. Toyota, R. Fukuda, J. Hasegawa, M. Ishida, T. Nakajima, Y. Honda, O. Kitao, H. Nakai, T. Vreven, J. A. Montgomery, Jr., J. E. Peralta, F. Ogliaro, M. Bearpark, J. J. Heyd, E. Brothers, K. N. Kudin, V. N. Staroverov, R. Kobayashi, J. Normand, K. Raghavachari, A. Rendell, J. C. Burant, S. S. Iyengar, J. Tomasi, M. Cossi, N. Rega, J. M. Millam, M. Klene, J. E. Knox, J. B. Cross, V. Bakken, C. Adamo, J. Jaramillo, R. Gomperts, R. E. Stratmann, O. Yazyev, A. J. Austin, R. Cammi, C. Pomelli, J. W. Ochterski, R. L. Martin, K. Morokuma, V. G. Zakrzewski, G. A. Voth, P. Salvador, J. J. Dannenberg, S. Dapprich, A. D. Daniels, Ö. Farkas, J. B. Foresman, J. V. Ortiz, J. Cioslowski, and D. J. Fox, *Gaussian 09, Revision C.01*. (Gaussian, Inc., 2009).
15. J. R. Platt, *J. Chem. Phys.* **19**, 101 (1951).
16. J. W. Sidman, *Chem. Rev.* **58**, 689 (1958).
17. L. Goodman, *J. Mol. Spectrosc.* **6**, 109 (1961).
18. H. McConnell, *J. Chem. Phys.* **20**, 700 (1952).
19. Q. Zhang, T. Komino, S. P. Huang, S. Matsunami, K. Goushi, and C. Adachi, *Adv. Funct. Mater.* **22**, 2327 (2012).
20. M. A. El-Sayed, *J. Chem. Phys.* **38**, 2834 (1963).

Chapter 5

Summary

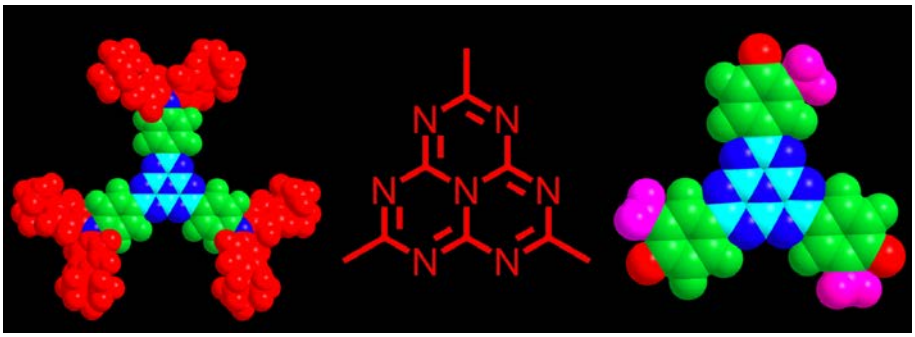

In this thesis, TADF based on heptazine derivatives and its application to OLEDs have been investigated.

In Chapter 2, a highly efficient orange-red TADF emitter based on a starburst-type heptazine derivative, 4,4',4''-(1,3,4,6,7,9,9b-heptaazaphenalene-2,5,8-triyl)tris(*N*,*N*-bis (4-(*tert*-butyl)phenyl)aniline) (**HAP-3TPA**), has been designed and synthesized. An OLED incorporating **HAP-3TPA** exhibits rather high EL performance with a maximum EQE of 17.5%, a maximum power efficiency of 22.1 lm W^{-1}, a maximum current efficiency of 25.9 cd A^{-1}, a turn-on voltage of 4.4 V at a luminance of 100 cd m^{-2}, and a peak luminance of 17000 cd m^{-2} without any light out-coupling enhancement. Even though **HAP-3TPA** shows weak TADF in both solution and a doped film, a significant delayed fluorescence has been demonstrated in transient EL, indicating that efficient RISC from the T_1 to the S_1 leads to highly efficient OLED under electrical excitation.

In Chapter 3, highly efficient exciplex systems with blended structures containing 1,3-di(9H-carbazol-9-yl)benzene (**mCP**) as an electron donor, and 2,5,8-tris(4-fluoro-3-methylphenyl)-1,3,4,6,7,9,9b-heptaazaphenalene (**HAP- 3MF**) as an electron acceptor have been developed. The exciplex system of 8 wt% **HAP-3MF**:**mCP** shows a very small ΔE_{ST}, resulting in efficient exciton up-conversion and a relatively high PLQE of 66.1%. Using the exciplex-based TADF characteristics, an exciplex-based OLED containing 8 wt% **HAP-3MF**:**mCP** as an emitting layer exhibits a rather high EQE of 11.3% along with rather low roll-off characteristics, a low turn-on voltage of 4.0 V and quite high peak luminance of 22000 cd m^{-2} at 12.2 V.

In Chapter 4, TADF were found in an emissive heptazine derivative whose S_1 and T_1 states have mainly n-π* character. The overlap-forbidden nature of the n-π* transition and the higher energy of the $^3\pi$-π* state than the ^{3}n-π* one lead to a small energy

difference between the S_1 and T_1 excited states of HAP-3MF. An OLED containing HAP-3MF achieved a rather high EQE of 6.0% in consideration of a rather low PLQE of 0.26, indicating that HAP-3MF harvests singlet excitons through a thermally activated $T_1 \rightarrow S_1$ pathway in the EL process.

The development of this study for further understanding and improving device performance will be conducted. The future study of TADF based on heptazine derivatives can be divided into three main themes, molecular orientation, non-doped OLEDs and application extension.

First, it has been found that molecular orientation has an important effect on optical and electrical properties of organic semiconducting materials. Therefore, it is worth investigating the effect of molecular orientation of heptazine derivatives on charge-transport characteristics and optoelectronic properties in order to design highly efficient TADF molecules and achieve high-performance OLEDs.

Second, non-doped OLEDs have attracted numerous attentions because they could be the solution to solve hard-to-control doping problem in the device fabrication process. TADF molecules are prone to aggregation and concentration quenching in the solid state due to extended π-conjugation structures and strong intermolecular π-π interactions. To reduce concentration quenching of TADF molecules and achieve non-doped OLEDs, it is possible to introduce non-planar substituents into the molecular structure.

Third, heptazine derivatives have exhibited a number of intriguing thermal, optical and electrical properties. Consequently, it is promising to extend the application of heptazine derivatives from OLEDs to other optoelectronic devices, such as organic solar cells based on the strong absorption in the visible range, or organic laser diodes based on their high quantum efficiencies.

List of Publications

Original papers

[1] Jie Li, Tetsuya Nakagawa, James MacDonald, Qisheng Zhang, Hiroko Nomura, Hiroshi Miyazaki, and Chihaya Adachi, *Adv. Mater.*, 2013, **25**, 3319–3323.

[2] Jie Li, Hiroko Nomura, Hiroshi Miyazaki, and Chihaya Adachi, *Chem. Commun.*, 2014, **50**, 6174–6176.

[3] Jie Li, Qisheng Zhang, Hiroko Nomura, Hiroshi Miyazaki, and Chihaya Adachi, *Appl. Phys. Lett.*, 2014, **105**, 013301.

Joint papers

[1] Qisheng Zhang, Jie Li, Katsuyuki Shizu, Shuping Huang, Shuzo Hirata, Hiroshi Miyazaki, and Chihaya Adachi, *J. Am. Chem. Soc.*, 2012, **134**, 14706–14709.

Symposium

[1] Jie Li, Tetsuya Nakagawa, James MacDonald, Qisheng Zhang, Hiroko Nomura, Hiroshi Miyazaki, Chihaya Adachi, *TADF International Workshop*, Fukuoka, Japan (March 14, 2014).

[2] Jie Li, Tetsuya Nakagawa, James MacDonald, Qisheng Zhang, Hiroko Nomura, Hiroshi Miyazaki, Chihaya Adachi, *Solid State and Organic Lighting* (SOLED), Tucson, USA (November 03, 2013).

[3] Jie Li, Tetsuya Nakagawa, James MacDonald, Qisheng Zhang, Hiroko Nomura, Hiroshi Miyazaki, Chihaya Adachi, *The 74th Japan Society of Applied Physics* (JSAP) *Autumn Meeting 2013*, Kyoto, Japan (September 16, 2013).

[4] Jie Li, Tetsuya Nakagawa, James MacDonald, Qisheng Zhang, Hiroko Nomura, Hiroshi Miyazaki, Chihaya Adachi, *The 9th International Polymer Conference* (IPC2012), Kobe, Japan (December 11, 2012).

Acknowledgements

First of all, the author would like to express his deepest appreciation to Professor Chihaya Adachi for continuous guidance and encouragement throughout the present research.

Meanwhile, the author is grateful to Professor Toshihiko Imato and Professor Yoshio Hisaeda for helpful discussions and suggestions regarding to this work.

Special gratitude is dedicated to Professor Katsumi Tokumaru for fruitful and enlightening discussions.

Furthermore, the author has profited greatly by a number of conversations with Associate Professor Takuma Yasuda and Assistant Professor Kenichi Goushi. Sincere thanks are expressed to Tetsuya Nakagawa, Qisheng Zhang, Hiroko Nomura and Hiroshi Miyazaki for numerous help on not only experiments but also daily life over the years.

The author would like to acknowledge all members in Adachi laboratory and all persons whom I met. Especially, the author would like to thank Katsuyuki Shizu, William Potscavage, Masatsugu Taneda, Yanqiong Zheng, Takeshi Komino, Shuanghong Wu, Tetsuji Hayano, Hajime Nakanotani, Kohei Tsugita, Yoshitake Suzuki, Yumi Sakai, Ryota Kabe, Masaya Hirade, Le Zhang, Yu Seok Yang, Jun Yun Kim, Bo Li, Ko Inada, Shin Woong, Méhes Gábor, Hiroshi Fujimoto, Sae Youn Lee, Kou Yoshida, Munetomo Inoue, Li Zhao, Jingyu Wang, Sun Bin Hwang, Dae Hyun Kim, Hossain Shihab, Ji Young Lee, Yasuhiro Hatae, Keigo Sato, Keiro Nasu, Yuta Sagara, Fei Zhao, Ryosuke Kondo, Chao-Jen Tsou, Hin Wai Mo, Daniel Tsang, Takahiro Higuchi, Yuta Hirayama, Hiroyuki Mieno, Hiroki Noda and Naoto Noutsuka for their kind supports and friendship.

The author is greatly indebted to his family for their continuous moral supports and warm encouragements.

Moreover, the author would like to thank the Japan Society for the Promotion of Science (JSPS) for the Funding Program for World-Leading Innovative R&D on Science and Technology (FIRST) and the International Institute for Carbon Neutral Energy Research (WPI-I2CNER) sponsored by MEXT.

Finally, the author is also thankful to China Scholarship Council (CSC) and Kyushu University for the scholarship which allows the author to focus on the research.